ABSTRACT

Title of Thesis: Underwater Movement of Obstacles Due to Explosive Detonation

Alexander Sergeevich Tsarev, Master of Science, 2007

Thesis Directed By: Professor William Fourney
                      Department of Mechanical Engineering

The U.S. Navy has an interest in researching the movement of obstacles in shallow water due to an explosive detonation. Obstacles that are placed in shallow water on a shoreline can damage vehicles that are attempting to land on shore. The U.S. Navy believes that explosives can be used to clear the obstacles out of the way and create a safe path for vehicles. Conducting tests on small scale is a cheap and relatively safe, but it would normally require reducing atmospheric pressure by the scale factor which cannot be easily achieved. The Naval Surface Warfare Center, Indian Head Division, is investigating a "Low Pressure" scaling method that should work for small scales in normal atmospheric pressure. The method alters the depth and size of charge in order to create the same gas bubble growth as measured in full scale conditions. This study examines the validity of the Low Pressure scaling method by comparing the results to other similar studies. This study also makes some independent analysis of factors such as depth of water, size of charge, obstacle orientation and obstacle stand off distance from the charge.

UNDERWATER MOVEMENT OF OBSTACLES DUE TO EXPLOSIVE
DETONATION

by

Alexander Sergeevich Tsarev

Thesis submitted to the Faculty of the Graduate School of the
University of Maryland, College Park in partial fulfillment
of the requirements for the degree of
Master of Science
2007

Advisory Committee:

Professor William Fourney, Chair
Professor Henry Haslach, Jr.
Professor Deborah J. Goodings

Acknowledgments

I would like to thank everyone who has helped me to complete this research. I could not have been successful without the help of the following individuals:

Dr. William Fourney, thank you for your guidance, understanding, encouragement and kindness throughout the course of my research. It was truly a pleasure to work for you.

Dr. Robert Bonenberger, Uli Leiste, and Les Taylor, thank you for providing assistance with my work in the lab. Your knowledge of explosive effects and scientific methods was a great asset to me.

Thanks to all of the graduate, undergraduate, and German students who worked in the lab for helping with the every day tasks and helping to provide a great work environment.

Last but not least, I would like to thank my family and friends for their support and encouragement throughout my education. I could not have made it out of college in one piece without the backbone of support that my family and friends have provided.

Table of Contents

List of Tables

List of Figures

Chapter 1 – Introduction and Background

1.1   Overview

This thesis describes research conducted at the University of Maryland (UMD), College Park, within the Mechanical Engineering Department and Dynamic Effects Laboratory in the A. James Clark School of Engineering. The research focuses on the movement of obstacles in shallow underwater explosions. This subject is of interest to the U.S. Navy because obstacles are sometimes deliberately placed into the shallow water area on a beach to prevent amphibious vehicles from landing safely on shore. The Naval Surface Warfare Center (NSWC) in Indian Head, Maryland, has devised a method of clearing these obstacles by dropping bombs into the water and using the energy of the explosive to move the obstacles out of the projected path of the vehicle.

The NSWC has supported several studies on the subject using Mk-82 and Mk-84 bombs to determine the motion of the obstacles when they are in proximity of a detonated explosive.   Studies were performed by SRI International at a $1/12^{th}$ scale in an attempt to verify the full-scale results with a more cost efficient testing process. SRI International used two different scaling theories, Hopkinson's and Low Pressure scaling, in order to recreate the full-scale setup.

The primary goal of this research study was to further investigate the validity of the Low Pressure scaling theory proposed by William McDonald [3] of the NSWC. The UMD

tests were performed on an even smaller scale than the SRI tests, ranging from 1/26th scale to 1/42nd scale.

1.2   *Mk-82 and Mk-84 Bombs*

The Mk-80 series of bombs are designed to be aerodynamically streamlined and are often referred to as Low Drag General Purpose bombs [7]. They are most often used in applications where maximum blast and explosive effects are desired. The bombs are unguided and travel to the target by free fall. About 45% of the weight of the bomb is comprised of explosive material. The differences between the Mk-82 and Mk-84 bomb are highlighted in Table 1.1.

	Weight	**Length**	**Diameter**	**Explosive**
Mk-82	500 lbs	66.15 in	10.75 in	192 lbs Tritonal, Minol II, or H-6
Mk-84	2000 lbs	129 in	18 in	945 lbs Tritonal or H-6

Table 1.1 - Specifications of the Mk-82 and Mk-84 bombs

The tests conducted by SRI International used different amounts of explosive while keeping the scale factor constant at 1/12th in order to model the two bombs. However, the UMD tests used the same charge for all tests, but the scale factor was reduced for tests that simulate the Mk-84 instead of increasing the weight of the explosive.

1.3 Mechanics of Underwater Explosions

Since this study deals with underwater explosions it is important to describe the sequence of events that occur when an explosive is detonated underwater. Robert H. Cole describes these events in great detail in *Underwater Explosions* [9]. This section summarizes certain parts of Cole's work that are applicable to obstacle movement due to shallow underwater explosions.

An explosion occurs when an explosive compound is subjected to some energy that is great enough to start a chemical reaction. The chemical reaction converts the explosive material into a gas at a very high temperature and pressure. The reaction begins in a small section of the material where the initiating energy was applied. The heat and pressure emitted from this small section of explosive then causes adjacent material to go through the same reaction, and thus the reaction propagates through the material.

The first effect of the detonation that can be observed is the shock wave. When the chemical reaction in the explosive material is completed and the pressure of the gas reaches the boundary of water a compression wave that travels at the rate of several thousand feet per second is formed. This shock wave can have destructive effects in some cases, however it was found to have little or no effect on the motion of obstacles in this study. High speed videos of the experiments conducted in this study reveal that obstacles do not begin moving until they are approached by the gas bubble described in the next paragraph.

The pressure of the gas drops after the shock wave has been emitted, but it is still significantly higher than the hydrostatic pressure of the water around the explosion. The high pressure of the gas pushes the water out and causes an expansion of volume that can be described as a gas bubble. In deep water conditions where the gas bubble is completely surrounded by water an oscillation of bubble size can be observed. This oscillation of the bubble size can be attributed to the constantly changing pressure in the gas. As the gas bubble expands, the pressure drops, but the water continues to move outward due to inertial effects. The gas bubble eventually stops expanding, but by this time the pressure of the gas has dropped below the value of the hydrostatic pressure around the gas. The bubble then collapses until it reaches a high pressure again and expands. As the bubble oscillates in volume, it travels upward towards the surface of the water. When the bubble reaches the surface of the water, the gasses escape into the atmosphere.

This study deals with shallow water conditions and the growth of the gas bubble is different from what has been observed in deep water. Once the explosive is detonated, there is a shock wave and an expansion of gas that forms a bubble, but since the water is shallow the gas bubble breaks the surface of the water before the bubble can begin to collapse under hydrostatic pressure. This phenomenon is described as a bubble that vents. When the gas escapes into the atmosphere, the water that was displaced flows back towards the location from which the charge was detonated. The flow of water back towards the location of the charge could play a significant role in the motion of obstacles. The observations of these effects are described in Chapter 4.

1.4   *Cavitation*

One other effect that can be observed in underwater explosions is the cavitation of water due to the shock wave. Cavitation is the creation of vapor bubbles in a liquid and it occurs when the pressure of the liquid falls below the vapor pressure [10]. Cavitation can also be attributed to temperature effects and would occur when the temperature of the liquid reaches or exceeds the saturated vapor/liquid temperature [10]. In an underwater explosion, this pressure drop likely results from the travel of the shock wave through the water [11]. As the wave travels through the water, localized regions undergo a cycle of compression and tension due to the passing of the wave. A bubble can be nucleated from a microscopic void created by the pressure and temperature changes in the water. These voids usually occur in areas of weakness such as a boundary between the liquid and the solid wall of the container or particles in the water [10]. Other weaknesses are the micro-bubbles of contaminant gas suspended in the water.

These microscopic voids grow into small bubbles and this phenomenon can be observed in the high speed videos taken during this study. Figure 1.1 shows a sequence of frames from one of the tests where the region of cavitation can be clearly seen. The cavitation bubbles are only seen near the bottom surface of the container. This can most likely be attributed to the fact that the largest surface of contact between the liquid and solid boundary is the bottom surface of the container. It has also been observed that small bubbles of contaminant air are present on the bottom surface of the container before a test is conducted. Cavitation did not appear to cause any motion of obstacles.
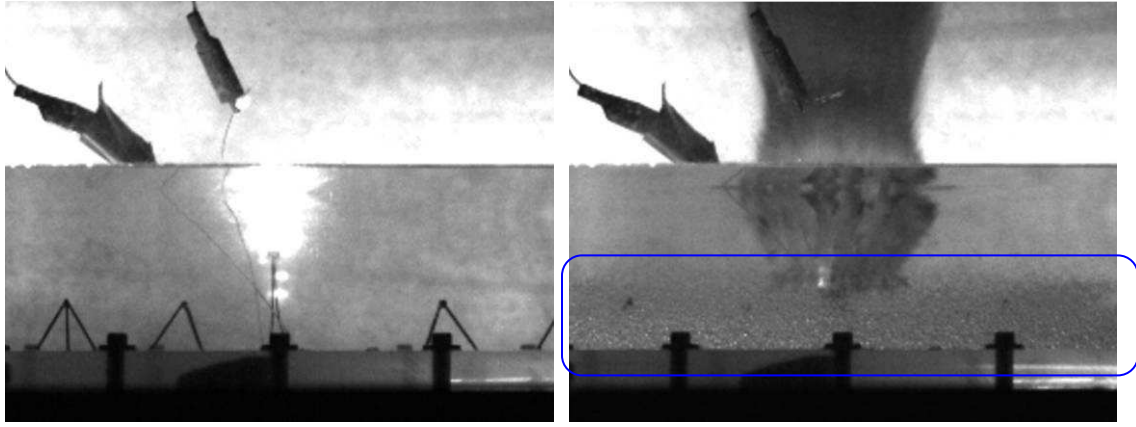
**Figure 1.1 - Left: Light emitted as explosive detonates.
Right: Cavitation bubbles can be seen near the bottom surface of the container**

1.5 Low Pressure Scaling

Low Pressure scaling, as defined in this section, is a theory devised by William

McDonald of the NSWC, Indian Head Division [3]. The theory is a modification of

Vacuum Tank scaling, which is attributed to Snay [16]. McDonald states that Vacuum

Tank scaling and Low Pressure scaling are two names for the same method that was

originally described by Snay. However, McDonald does not give a new name for his

modified scaling theory. For the sake of clarity, McDonald's theory will be referred to as

Low Pressure scaling throughout this thesis and Snay's original theory will be referred to

as Vacuum Tank scaling.

The motivation behind the development of the Vacuum Tank scaling theory is to be able

to use relatively inexpensive small scale tests to obtain the same information provided by

full scale tests. The research of scaling the effects of underwater explosions dates back to

World War II. Snay showed that while the explosion shock wave can be scaled for

analysis of small-scale field tests, the scaling of bubble-induced flow phenomena requires the use of special equipment such as centrifuges and vacuum tanks.

The following paragraphs show the derivation for Snay's scaling theories. Several different scaling possibilities can be derived from the basic equations governing fluid flow [3]. The equations for conservation of mass (1) and conservation of momentum (2) of inviscid flows are written below. For flows with a high Reynolds number the assumption of inviscid flow is justifiable [15]. Normally, conservation of energy would also have to be considered, but in the case of incompressible inviscid flows it is not necessary [15]. The mass and momentum conservation equations are sufficient to relate the three velocity components and pressure [8].

$$\frac{\partial \rho}{\partial t} + \nabla \cdot (\rho \mathbf{u}) = 0 \tag{1}$$

$$\frac{\partial \rho \mathbf{u}}{\partial t} + \nabla \cdot (\rho \mathbf{u}) \mathbf{u} + \nabla p = -\rho g \hat{\mathbf{k}} \tag{2}$$

In equations (1) and (2) ρ is the density, p is the pressure, $\mathbf{u}$ is the velocity vector, g is gravity, and $\hat{\mathbf{k}}$ is the unit vector in the vertical direction. For bubble-induced flow phenomena, water can be treated as an incompressible fluid so the density of an element will not change as it travels [8, 15]. Therefore, equations (1) and (2) reduce to:

$$\nabla \cdot (\mathbf{u}) = 0 \tag{3}$$

$$\rho \frac{\partial \mathbf{u}}{\partial t} + \rho \nabla \cdot (\mathbf{u}) \mathbf{u} + \nabla p = -\rho g \hat{\mathbf{k}} \tag{4}$$

It is convenient to use a cylindrical coordinate system for underwater explosions. The gas bubble expands in the radial and vertical directions, so there is no significant flow expected in the tangential direction. Equations (3) and (4) are written in terms of cylindrical coordinates below [8].

(Continuity)
$$\frac{1}{r}\frac{\partial}{\partial r}(ru) + \frac{1}{r}\frac{\partial v}{\partial \theta} + \frac{\partial w}{\partial z} = 0 \qquad (5)$$

(Radial Momentum)
$$\frac{Du}{Dt} - \frac{v^2}{r} = -\frac{1}{\rho}\frac{\partial p}{\partial r} \qquad (6)$$

(Tangential Momentum)
$$\frac{Dv}{Dt} + \frac{uv}{r} = -\frac{1}{\rho r}\frac{\partial p}{\partial \theta} \qquad (7)$$

(Vertical Momentum)
$$\frac{Dw}{Dt} = -\frac{1}{\rho}\frac{\partial p}{\partial z} + g \qquad (8)$$

where r, θ, and z are the cylindrical directions. The symbols u, v, and w are the components of velocity in the radial, tangential and vertical directions. In cylindrical coordinates $\frac{D}{Dt} = \frac{\partial}{\partial t} + u\frac{\partial}{\partial r} + \frac{v}{r}\frac{\partial}{\partial \theta} + w\frac{\partial}{\partial z}$.

It can be assumed that the underwater explosion phenomena are axisymmetric in the cylindrical coordinates ($v = 0$) and therefore equations (5) through (8) reduce to the following [3]:

(Continuity)
$$\frac{1}{r}\frac{\partial}{\partial r}(ru) + \frac{\partial w}{\partial z} = 0 \qquad (9)$$

(Radial Momentum) $$\frac{\partial u}{\partial t} + u\frac{\partial u}{\partial r} + w\frac{\partial u}{\partial z} = -\frac{1}{\rho}\frac{\partial p}{\partial r}$$ (10)

(Vertical Momentum) $$\frac{\partial w}{\partial t} + u\frac{\partial w}{\partial r} + w\frac{\partial w}{\partial z} = g - \frac{1}{\rho}\frac{\partial p}{\partial z}$$ (11)

In order to determine the scaling conditions, equations (9) – (11) must be written in terms of dimensionless variables. The radial and vertical characteristic lengths are defined as L_r and L_z, respectively, and the characteristic time as T. The velocity components, directions and time are rewritten in terms of characteristic values and dimensionless variables (indicated with a star).

$$u = \frac{L_r}{T}u^* \; , \;\; w = \frac{L_z}{T}w^* \; , \;\; r = L_r r^* \; , \;\; z = L_z z^* \; , \;\; t = Tt^*$$ (12)

When (12) is substituted into (9) – (11) the following equations result:

(Continuity) $$\frac{1}{r^*}\frac{\partial}{\partial r^*}(r^* u^*) + \frac{\partial w^*}{\partial z^*} = 0$$ (13)

(Radial Momentum) $$\frac{\partial u^*}{\partial t^*} + u^*\frac{\partial u^*}{\partial r^*} + w^*\frac{\partial u^*}{\partial z^*} = -\frac{T^2}{L_r}\frac{1}{\rho}\frac{\partial p}{\partial r}$$ (14)

(Vertical Momentum) $$\frac{\partial w^*}{\partial t^*} + u^*\frac{\partial w^*}{\partial r^*} + w^*\frac{\partial w^*}{\partial z^*} = \frac{T^2}{L_z}g_0 g' - \frac{T^2}{L_z}\frac{1}{\rho}\frac{\partial p}{\partial z}$$ (15)

In equation (15) g has been replaced by $g_0 g'$, where the characteristic gravity, g_0, is the acceleration of gravity at sea level. Here, g' is the gravity scale factor and has been written with a prime instead of a star because the scale factors are later written with primes.

In order to complete the transformation of the governing equations into non-dimensional variables, the right side of equations (14) and (15) must be converted. In order to do this, the characteristic pressure, P, must be introduced.

$$P = \frac{L_r L_z}{\rho T^2} \quad \text{so that} \quad p = Pp^* \tag{16}$$

Substituting r^*, z^* and p^* into equations (14) and (15) gives the following result:

(Radial Momentum) $\quad \dfrac{\partial u^*}{\partial t^*} + u^* \dfrac{\partial u^*}{\partial r^*} + w^* \dfrac{\partial u^*}{\partial z^*} = -N_r^{-1} \dfrac{\partial p^*}{\partial r^*}$ (17)

(Vertical Momentum) $\quad \dfrac{\partial w^*}{\partial t^*} + u^* \dfrac{\partial w^*}{\partial r^*} + w^* \dfrac{\partial w^*}{\partial z^*} = F^{-1} - N_z^{-1} \dfrac{\partial p^*}{\partial z^*}$ (18)

where F, N_r, and N_z are known as the Froude (F) and Newton (N_r, N_z) numbers.

$$F = \frac{L_z}{g_0 g' T^2} \qquad N_r = \frac{\rho L_r^{\,2}}{T^2 P} \qquad N_z = \frac{\rho L_z^{\,2}}{T^2 P} \tag{19}$$

The Froude number is associated with gravitational effects and the Newton numbers are related to dynamic inertial effects [3]. If the Froude and Newton numbers are the same for full-scale and small-scale conditions then they will be governed by the same equations and should produce similar results. The previous statement can be written by: $F = F'$, $N_r = N'_r$, $N_z = N'_z$, where the primed terms denote the small-scale values. The Froude number includes the gravity term. In full scale conditions (F) the gravity scale factor (g') is equal to one. Therefore, when rearranging terms in $F = F'$, the g_0

10

terms cancel out and only one g' term remains. Using equation (19) and rearranging terms so that the primed terms are in the numerator and unprimed terms are in the denominator gives the following equations:

$$\left(\frac{T'}{T}\right)^2 g' = \frac{L'_z}{L_z} \tag{20}$$

$$\left(\frac{T'}{T}\right)^2 \frac{P'}{P} = \left(\frac{L'_r}{L_r}\right)^2 \frac{\rho'}{\rho} \tag{21}$$

$$\left(\frac{T'}{T}\right)^2 \frac{P'}{P} = \left(\frac{L'_z}{L_z}\right)^2 \frac{\rho'}{\rho} \tag{22}$$

Equations (20) – (22) can be rewritten in terms of $\tau, \varphi, \lambda_r, \lambda_z$ and π, where the scale factors are written as $\tau = \frac{T'}{T'}$, $\varphi = \frac{P'}{P}$, $\lambda_r = \frac{L'_r}{L_r}$, $\lambda_z = \frac{L'_z}{L_z}$ and $\pi = \frac{\rho'}{\rho}$. This gives the following relations:

$$\tau^2 g' = \lambda_z \tag{23}$$

$$\tau^2 \varphi = \pi \lambda_r^2 \tag{24}$$

$$\tau^2 \varphi = \pi \lambda_z^2 \tag{25}$$

In order to have geometric similarity set $\lambda_r = \lambda_z = \lambda$. This means that $N_r = N_z = N$. Finally, there are two equations remaining which are used to determine the possible scaling conditions.

$$\tau^2 g' = \lambda \qquad\qquad (26)$$

$$\tau^2 \varphi = \pi\lambda^2 \qquad\qquad (27)$$

The different ways in which the above equations can be satisfied are expressed in Table

1.2. The scale factor values are expressed in terms of the length scale factor, λ, except

for the case of Mixed Type scaling in which the pressure scale factor, φ, was also used.

Scaling Description	Length λ	Time τ	Pressure φ	Density π	Gravity g'
Full-Scale	1	1	1	1	1
Centrifuge	λ	λ	1	1	$1/\lambda$
Vacuum Tank	λ	$\sqrt{\lambda}$	λ	1	1
High Density	λ	$\sqrt{\lambda}$	1	$1/\lambda$	1
Mixed Type	λ	$\sqrt{\lambda}$	φ	φ/λ	1

Table 1.2 - Possibilities for Scaling Incompressible Inviscid Flow

Each of the different types of scaling has certain difficulties that must be overcome when

testing on a small scale. In the case of Centrifuge scaling, it is necessary to change the

gravity in area of testing which cannot be easily or cheaply done. For the purpose of this

study, it would not be feasible to conduct tests in a centrifuge since this would require a

very large centrifuge and it would be difficult to film the motion of obstacles. High

Density scaling would require the use of an inviscid fluid that has a higher density than

water. For the scales used in the study ranging from $1/26^{th}$ to $1/42^{nd}$ the density of the

fluid would have to be up to forty-two times greater than the density of water. Mixed

Type scaling requires scaling both the pressure and density and could not possibly be any easier to set up in an experiment than one of the other methods.

Equality of the full scale and small scale equations of continuity and conservation of momentum alone are not enough to achieve similarity. The initial and boundary conditions must also be similar. In his paper, McDonald briefly describes how conditions such as initial velocity, geometric boundaries, and pressure changes between air and water can be accounted for in small scale tests [3].

Perhaps the most complex value to scale is the necessary weight of the explosive in a small scale test. The energy of the explosive, E, can be used to determine the scaling factor. Relating the characteristic length, L, to the energy of the explosive yields:

$$L = \left(\frac{E}{\rho g_0 g'} \right)^{1/4} \tag{28}$$

Equation (28) can be used to define the energy scale factor ε in terms of the scale factors for density, length and gravity.

$$\varepsilon = \frac{E'}{E} = \frac{\rho'}{\rho} \left(\frac{L'}{L} \right)^4 g' = \pi \lambda^4 g' \tag{29}$$

It is usually assumed that the bubble energy, E, is proportional to the weight of the explosive charge, W. The constant of proportionality between energy and weight, Q, is

dependant on a term, J_∞, where J_∞ is a relation between the bubble radius and specific

heats of the bubble gas. Explosive handbooks and test results often provide tables from

which the values of J_∞ can be derived.

$$Q = \frac{4\pi}{3} J_\infty^3 \tag{30}$$

$$E = QW \tag{31}$$

$$\varepsilon = \frac{E'}{E} = \left(\frac{J_\infty'}{J_\infty}\right)^3 \frac{W'}{W} \tag{32}$$

Combining equations (29) and (32) gives the relationship between scaling factors for

density, length, gravity and the weight of the explosive charge. The relationship between

scaling factors and the weight of the explosive will be shown for Vacuum Tank scaling in

equation (33). The reasons for choosing this method will be explained in the rest of this

section. In Vacuum Tank scaling, density and gravity are held constant between full

scale and small scale experiments. Therefore, when equations (29) and (32) are

combined the result is the following:

$$\lambda = \left[\left(\frac{J_\infty'}{J_\infty}\right)^3 \frac{W'}{W}\right]^{1/4} \tag{33}$$

As hinted at before, the most promising of the scaling methods in Table 1.2 is Vacuum

Tank scaling. The pressures that affect the expansion of the gas bubble in water are the

pressure due to the weight of the water and the atmospheric pressure. The pressure due

to the weight of the water is properly scaled if the geometry is scaled since the pressure depends only on the depth of water. However, it is difficult to change the atmospheric pressure. One possible method would be to build some kind of pressurized vessel around the body of water to alter the atmospheric pressure.

McDonald has proposed a much simpler method that is investigated in this study. When small scale tests are performed in the field using Vacuum Tank scaling, the atmospheric pressure would suppress the growth of the gas bubble in the water. McDonald suggests that if the depth of charge and weight of charge used can be altered slightly in order to produce the same bubble growth as in a full scale test, then all other conditions of Vacuum Tank scaling can be used. The alteration of charge size and depth is the identifying factor of Low Pressure scaling. Low Pressure scaling has the same rules as Vacuum Tank scaling, but Low Pressure scaling modifies the size of the charge and depth of the charge from the values that are determined by Vacuum Tank scaling. The exact size and depth of charge for Low Pressure scaling is determined by computational simulations of gas bubble growth. The original investigatory computations were performed by William Szymczak (Naval Research Lab) and Andrew Wardlaw (NSWC) [3]. The investigatory simulations show that it is possible to use Low Pressure scaling to closely match full scale bubble growth. The gas bubble growth on the small scale should have the same radius-time curve for the growth of the bubble as measured in full scale tests. The bubble radius that is measured in the curve is the maximum radius of the bubble for each point in time. In shallow water, this maximum radius is usually on the bottom surface.

As mentioned earlier, some tests were performed by SRI International at the $1/12^{th}$ scale using the Low Pressure scaling method. Scientists at the NSWC computed the necessary charge weights and charge depths for properly modeling the growth of the gas bubble. The conditions for the tests at SRI International called for the use of the different weights of explosives to model the Mk-82 and Mk-84 bombs while the scale factor was held constant to 1/12th.

The scaling conditions for this study at the University of Maryland were computed using the same methods, but the weight of the charge was held constant instead of the scale factor. The RP-80 charge used in this study is described in detail in Section 2.1. The RP-80 charge was used because it is readily available to the Dynamic Effects Lab and is manufactured with a water-tight enclosure so that it can be easily placed underwater. Andrew Warldaw of the NSWC used computational methods to determine the necessary scale factor and depth of charge necessary for use with the RP-80. These test conditions are described in detail in Section 3.5.

Chapter 2 – Research Equipment

2.1   RP-80 Exploding Bridge Wire Detonator

The RP-80 Exploding Bridge Wire (EBW) Detonator was the only explosive charge used in this study. The RP-80 EBW is one of several general use EBW detonators manufactured by Teledyne RISI, Inc. The RP-80 consists of 80mg PETN initiating explosive, 123 mg RDX output explosive and other parts as shown in Figure 2.1 [1].

1. Plastic molded head
2. Brass sleeve
3. Bridgewire (Gold)
4. Initiating explosive: 80 mg PETN
5. Output explosive: 123 mg RDX
6. Aluminum cup 0.007" thick
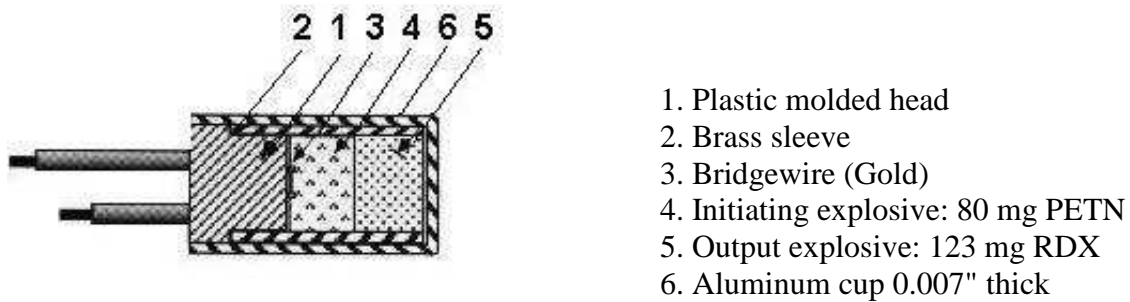
Figure 2.1- Cross-Sectional View of RP-80 EBW Detonator

Figure 2.2 shows the external dimensions of the detonator.
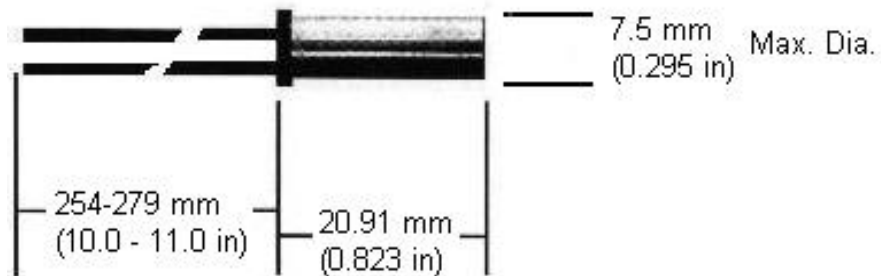
Figure 2.2 - External Dimensions of RP-80 EBW Detonator

Table 2.1 lists the firing parameters for the RP-80 detonator as provided by the

manufacturer [1].

Threshold Burst Current	180 amps
Threshold Voltage	Approx. 500 volts
Threshold Voltage Std. Deviation	75 volts maximum
Function Time	2.65 uS typical
Function Time Simultaneity Standard Deviation	0.125 uS maximum

Table 2.1 - Firing Parameters of the RP-80 EBW Detonator

The RP-80 was convenient to use in this study because of its size and the rubber o-ring

inside the aluminum cup provides a seal for shallow underwater use. The rubber o-ring is

not included in the diagram provided by Teledyne RISI, Inc. (Figure 2.1), but when the

aluminum cup is taken off the RP-80 the o-ring can be seen among the other components

of the detonator. Figure 2.3 shows the disassembled RP-80 with the aluminum cup,

plastic head, brass sleeve, o-ring, PETN powder, and RDX pellet. The units on the ruler

are centimeters.

Figure 2.3 - Disassembled View of the RP-80 and Its Internal Components

2.2   The FS-17 Explosive Bridge Wire Firing System

Teledyne RISI, Inc. provides several different kinds of firing systems for EBW

detonators. Some advantages of the FS-17 system are that it is battery powered and

provides a signal that can trigger a camera to begin recording. The battery can be

charged easily by plugging the control unit into a standard 110 VAC socket.

The FS-17 system consists of two parts: the firing module and control unit. The firing

module sends a high voltage pulse to the EBW detonator which causes the detonator to

go off. The control unit contains most of the safety features in the firing system. A

diagram of the FS-17 system and its components can be seen in Figure 2.4. The

numbered components are listed on the next page.
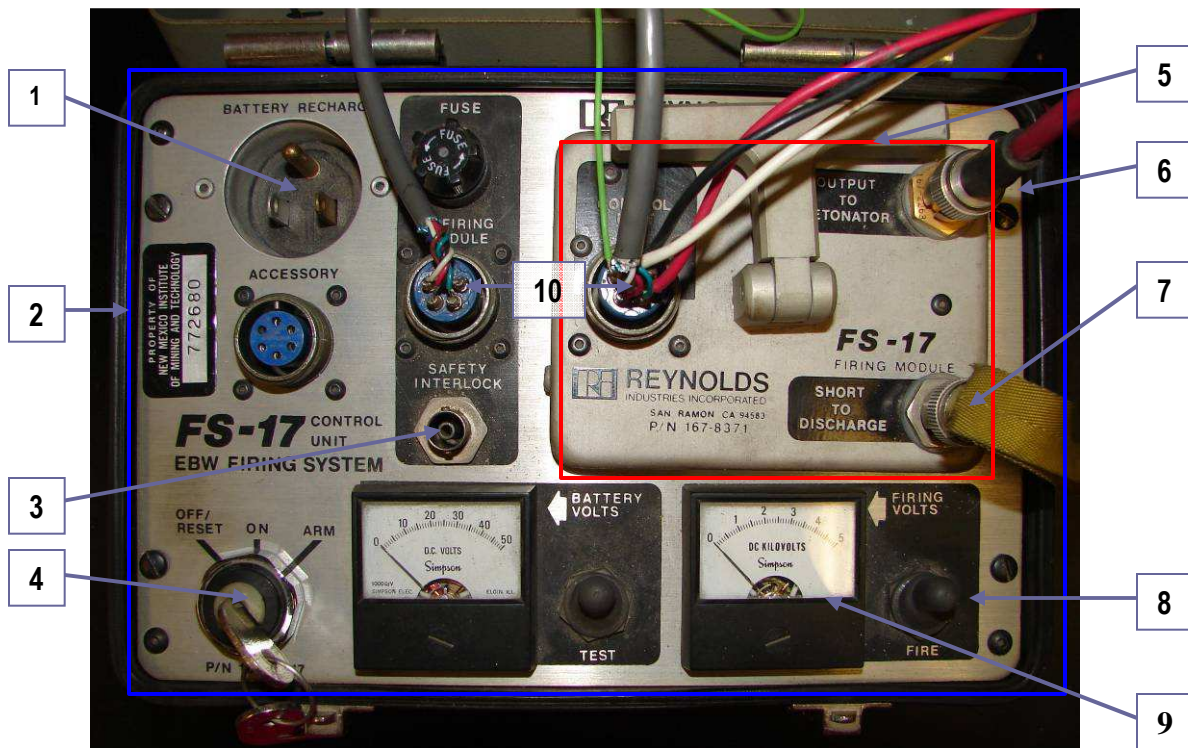
Figure 2.4 - The FS-17 Firing System and Components

List of Components in the FS-17 Firing System

1. Battery Recharge Plug
2. Control Unit (Blue Outline)
3. Safety Interlock
4. Arm Key
5. Firing Module (Red Outline)
6. Coaxial Output to Detonator
7. Discharge Connector
8. Firing Switch
9. Firing Module Voltage Gauge
10. Control Unit to Firing Module Connection

In order to operate the firing system, an exact procedure must be followed. First, the shorting plug must be removed from the discharge connector on the firing module and mated with the safety interlock on the control unit. The control unit has a second safety feature that requires a key to turn into the "arm" position before the firing module can be charged. The key must be held in the "arm" position while the control unit sends a low 32-40 volt input to the firing module. A one microfarad capacitor in the firing module charges up to 3500-4000 volts [2]. The control unit has a display gauge that indicates the high voltage in the firing module. Once the operator sees that the module is charged to at least 3500 volts, he can give a countdown and press the "fire" switch. Pressing the "fire" switch causes the control unit to send a 30 volt pulse over a spark gap to the firing module. The capacitor in the firing module is then discharged into a cable that sends a trigger signal to the camera and then a coaxial cable that sets off the explosive. In order to ensure safety at all times when not operating the firing system, the key must be turned to the "off" position and the shorting plug must be mated with the discharge connector.

An FS-10 firing system was used for some tests. The FS-10 is an older model and provides the same function as the FS-17 firing system. The operation was slightly

different because the FS-10 has an arm switch that must be held down instead of key that must be turned. The FS-10 also does not have a dial to display the firing module voltage, but has an indicator that lights up when a suitable voltage has been attained.

2.3   Trigger Mechanism

The ability to time the response of the high speed cameras to record the explosion and the following effects is an important aspect of the research conducted in this study. The red and white wires coming out of the firing module connection (component #10) seen in Figure 2.4 on page 19 lead to the trigger mechanism. The trigger mechanism, shown in Figure 2.5, sends a five volt pulse to the camera. The camera can be set up to record when it receives the pulse or a short time after the pulse. The firing system is set up to send a signal to the camera and then detonate the explosive after a short delay. Two cameras were used for most of the tests conducted in this study. The trigger mechanism is shown with a split coaxial output in order to send a signal to each of the two cameras.
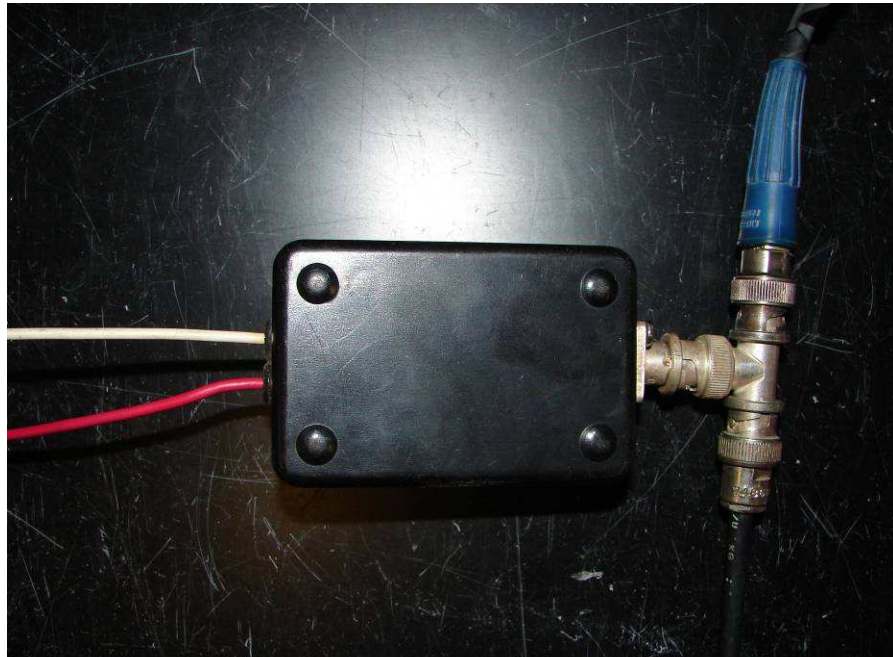
Figure 2.5 - Trigger Mechanism with Split Coaxial Output

2.4   Dummy Charge

A dummy charge was used in order to test equipment functionality before setting off the explosive. The dummy charge, shown in Figure 2.6, is simply a bridge wire without any explosive material. The two leads from the firing module are held in close proximity to each other inside a cylindrical aluminum case. When the firing module sends current through the positive lead, the current jumps the gap between the wires to the negative lead. The arc of current creates a flash of light and an audible bang that confirms the proper function of the firing system.
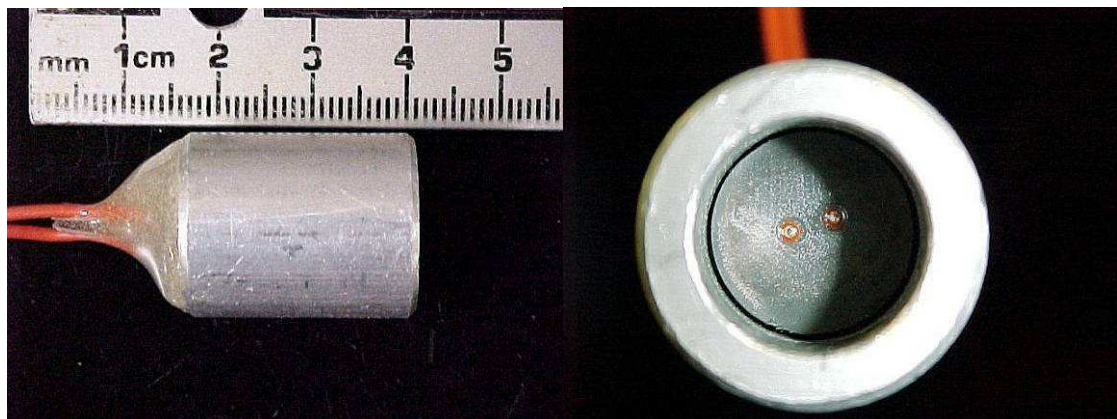
Figure 2.6 - Side View and Interior View of the Dummy Charge

2.5   Tetrahedron-Shaped Obstacles

Even though the Navy has done work with a variety of obstacles in the past, this study focused on the tetrahedron-shaped obstacles. The full scale tetrahedron obstacles were made from L-shaped angle iron that measured four inches wide in both directions and had a 5/8 inch thickness [12]. Figure 2.7 shows a cross-sectional view of a piece of angle iron used to make the full scale obstacles. Each leg of a tetrahedron measured 56 inches from vertex to vertex. Using a steel density of 0.284 pounds per cubic inch, the idealized

weight of a full scale tetrahedron is about 418 pounds (190 kg). The full scale

tetrahedrons were assembled by welding the legs together at the four corners.
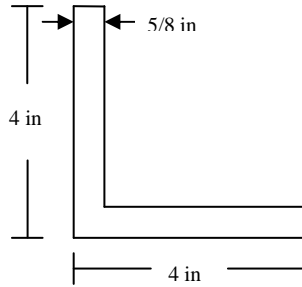
Figure 2.7 - Cross-Sectional View of Angle-Iron Used in Fabrication of Full-Scale Tetrahedrons

Since angle iron of a very small size is not easily obtainable, the obstacles used in this

study were made out of cylindrical rods brazed together at the four vertices. The rods

were chosen based on a search of readily available materials. Each available rod was

weighed and measured to obtain a weight per length value. The weight and leg length of

the obstacles for each scaling condition is summarized in Table 2.2. The weight per

length value was calculated by dividing the weight of the obstacle by the leg length and

number of legs in the obstacle (which was always six). Rods that had a weight per length

value slightly lower than the calculated value for the obstacles were usually used because

brazing filler and spray paint added weight to the obstacle. The average measured weight

of the obstacles listed in the table is based on four obstacles weighed before the first test

in which they were used.

	Full Scale	**1/26th**	**1/28th**	**1/36th**	**1/42nd**
Scaled Weight (grams)	190,000	10.81	8.66	4.07	2.56
Scaled Leg Length (inches)	56	2.15	2.00	1.56	1.33
Calculated Weight per Length (grams/inch)	N/A	0.838	0.722	0.435	0.320
Material Used (Diameter)	4" Angle Iron	Steel Rod (3/32")	Brass Rod (0.072")	Steel Rod (1/16")	Brass Rod (3/64")
Material Weight Per Length (grams/inch)	N/A	0.875	0.588	0.385	0.229
Average Measured Weight (grams)	N/A	10.78	8.47	4.14	2.43
Diameter to Length Ratio	N/A	0.436	0.360	0.401	0.352

Table 2.2 - Obstacle Properties for Various Scales

Using a weight per length value does not take the diameter of the rod and the density of the material into account. However, brass and steel have similar values for density, 0.318 and 0.284 pounds per cubic inch [4], respectively, and those metals were the only two materials used in the construction of the small-scale obstacles. Therefore, the diameter to length ratio was nearly the same for all the obstacles. Since the full-scale obstacles were made out of steel they also had a similar density. However, it is important to note that the rods used in the small-scale tests would not behave in the same way as the full-scale obstacles since they have a different shape and therefore have a different drag coefficient than the angle iron.

Each obstacle was manufactured by the same process. Calipers were used to etch a line into a rod marking the length of a single leg of the tetrahedron. The leg was then cut using shear scissors and filed down at the ends to make a smooth surface for brazing. Six

legs were cut for each obstacle and they were held together during brazing using a block of clay. Figure 2.8 outlines the process for obstacle manufacturing. First, a glob of clay was flattened by pressing the clay onto a table or other flat surface. Three legs were pressed into the clay to form an equilateral triangle. Three small pieces of clay were then placed on top of each vertex of the equilateral triangle. The remaining three legs were connected to the equilateral triangle base and aligned to create a tetrahedron shape. Once the shape of the obstacle was created and temporarily secured using the clay, the top vertex could be brazed using a MAPP gas torch and a flux-coated 1/16" bronze brazing rod. The other vertices were then brazed together using a similar process after some rearranging of the tetrahedron legs. Upon completion of brazing, the obstacles were spray painted black to provide contrast against the white background of the testing chamber used in the experiments. Finally, the obstacles were numbered using white paint lines, shown in Figure 2.9, to be able to distinguish between each obstacle.
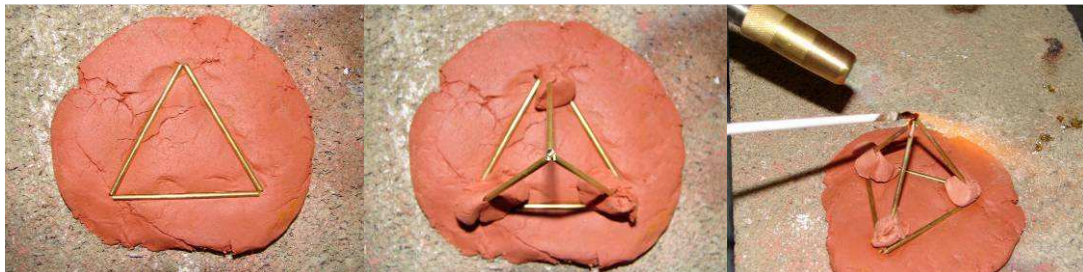
Figure 2.8 - Schematic of the Obstacle Manufacturing Process
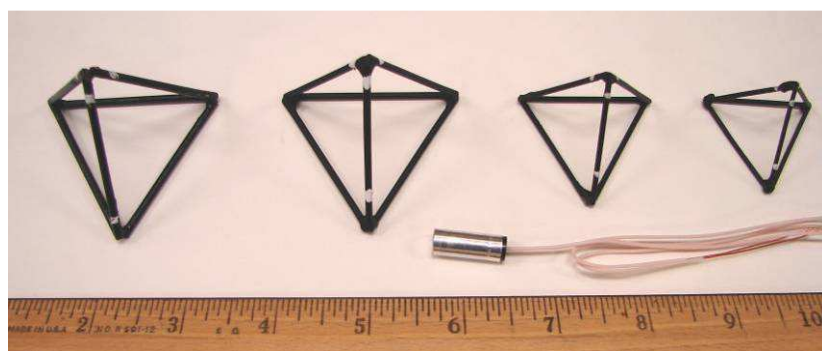
Figure 2.9 - Obstacles Arranged in Order from Largest to Smallest Scale Next to an RP-80

2.6   Testing Chamber Design and Assembly

One of the first issues during the study was determining the location for testing. At the
beginning of the study, the Dynamic Effects Laboratory had two possible locations for
detonating explosives. One was in a 5'x5'x2' steel container with an open top and the
other was a similar steel container that measured 4'x2'x2'. The larger container was
unavailable because it is filled with sand and used daily for other research conducted in
the lab.

The smaller of the two containers had two drawbacks. The first problem was that the
container was not wide enough to allow for the growth of the gas bubble created by the
explosive. Figure 2.10 shows that the gas bubble was measured to grow to almost eight
inches radius.   The two foot wide tub only allowed for four inches of clearance on either
side of the bubble. The proximity of the wall to the gas bubble would greatly affect the
flow of the water.
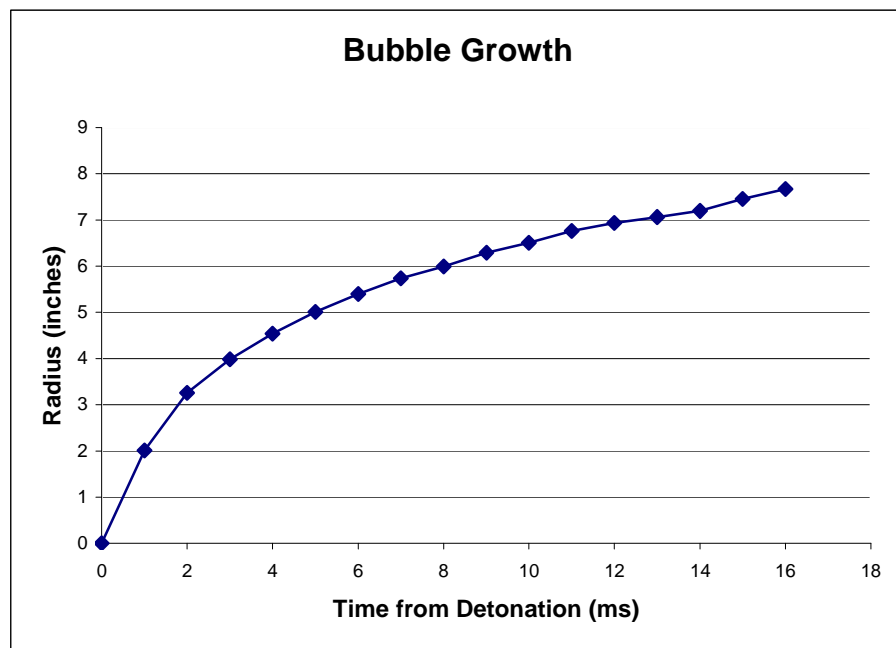
Figure 2.10 - Gas Bubble Growth Measured in Test 1

The second problem was that the only way to film the motion of the obstacles was by setting up a camera looking down into the tub. However, when the explosive was detonated, the water surface became distorted and it was nearly impossible to see any obstacles underneath the surface of the water. Figure 2.11 shows the overhead view from Test 1. It can be seen that the obstacles are hidden from view and would be nearly impossible to track using the overhead camera angle.

| 0 ms | 100 ms | 200 ms |
| 300 ms | 400 ms | 500 ms |
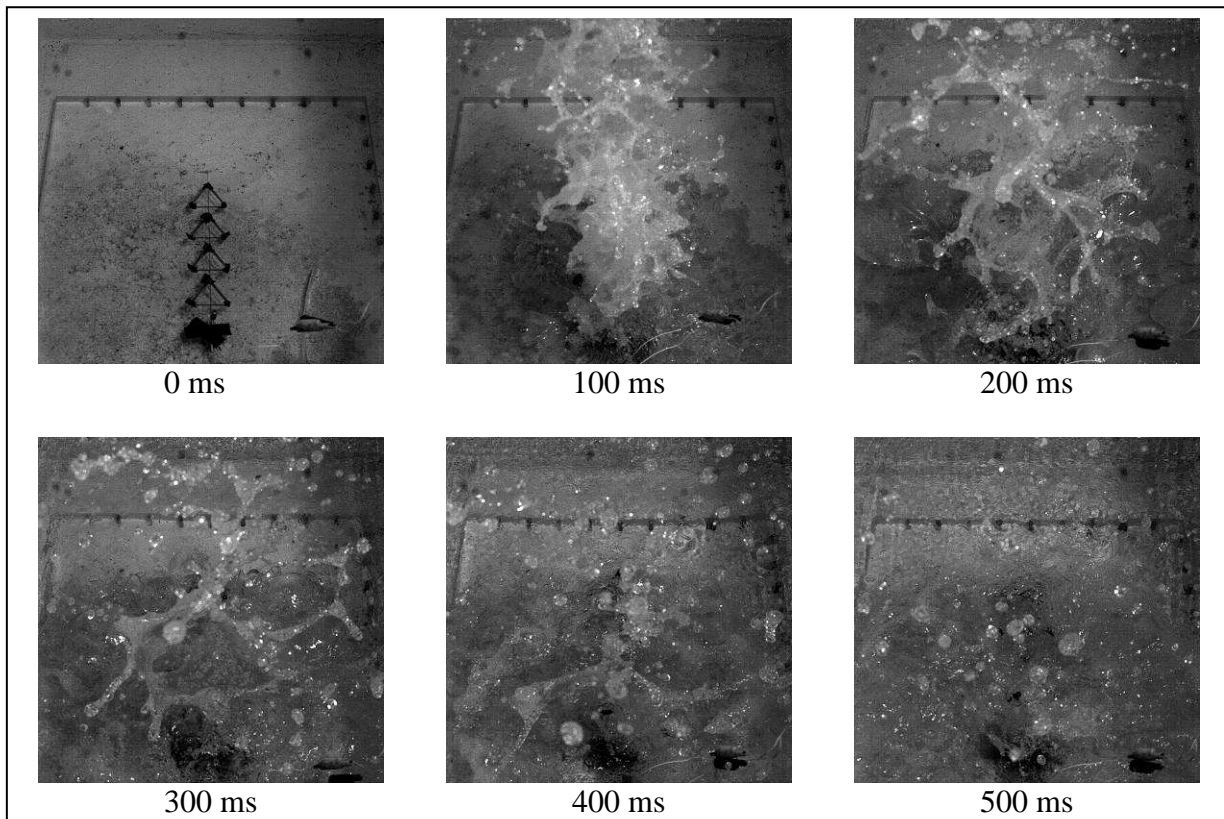
Figure 2.11 - Images from Test 1 Reveal that Obstacles are Difficult to Track from Above

The proposed solution was to build a container with transparent side walls and bottom. The container would allow for the use of two camera angles; one from the side of the container and one from underneath. The use of two cameras allows for tracking the obstacle motion in three dimensions, as opposed to a single camera view which only

provides data for two dimensions. The transparent walls and bottom also allow for light to pass through and illuminate the obstacles underneath the surface of the water. This is a great benefit since the high-speed cameras require a lot of light to capture a clear video.

The planned dimensions of the container were greatly affected by the amount of space available in the lab and the availability of transparent material. A container with a square bottom was the most logical because of the symmetry and ease of assembly. Ideally, the container would have had the walls as far from the center as possible to eliminate any effect that the walls have on the flow of water inside the container. However, this was not feasible, and the best option was to build a container that is as large as possible and consider the effects of the walls when making conclusions about the data. Since the container was going to be placed in a blast chamber where the floor is only five feet wide, it was clear that the container width would have to be less than five feet. In order to provide some clearance for moving around the container and placing equipment such as lights around the container, the necessary width for the container was determined to be three feet. The side walls of the container were two feet tall which was more than adequate since the depth of the water used in this study never exceeded four inches.

The container was built on a frame that has 30" tall legs in order to provide room for equipment to be placed underneath the container. Instead of placing a camera directly underneath the container, a mirror was used in combination with the camera to protect the camera in case the acrylic plate on bottom ever failed. Details of the experimental setup can be found in Chapter 3. The frame was assembled using extruded aluminum bars

from 80/20 Inc. This product is much like an erector set in that it allows for a variety of ways to connect parts and reinforce structures. The cross section of the bar is a square with t-shaped slots on all four sides. Specially shaped nuts fit into the slot and a bolt can be turned into the nut to fix a part to the bar. Figure 2.12 shows a view of the cross section of the 80/20 1010 model aluminum rod. The figure also shows how a bolt and nut are used to clamp a closed-cell foam and ¼" thick polycarbonate sheet to the aluminum rod. The black-colored foam acts as a seal on one side of the polycarbonate sheet and the red silicone washer seals the gap between the bolt and the hole on the other side of the sheet. The container did not leak even after withstanding the explosive detonation.
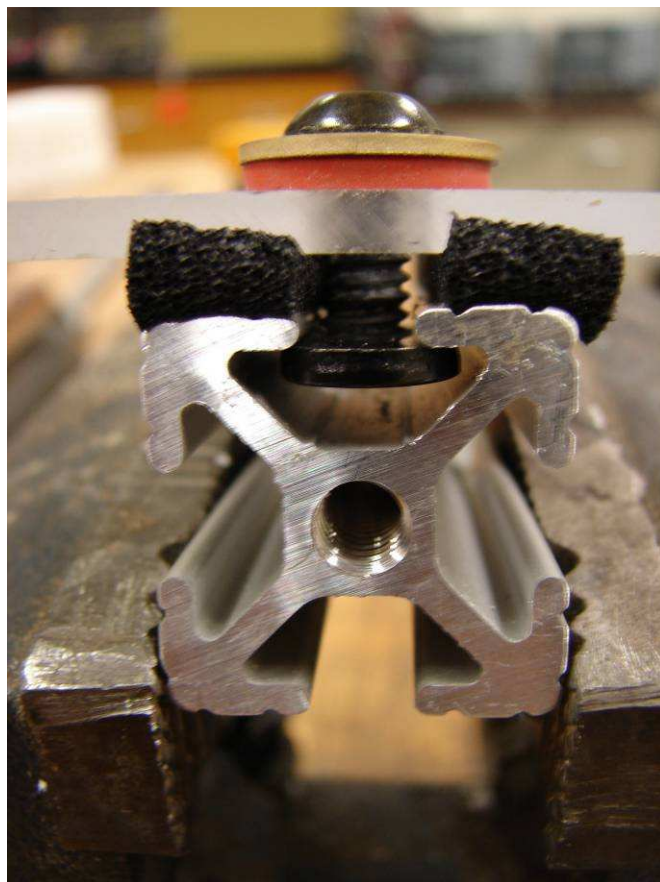
Figure 2.12 - Cross Section of 80/20 1010 Aluminum Rod and Bolted Polycarbonate Window

The bottom half of the frame, Figure 2.13, was built first.
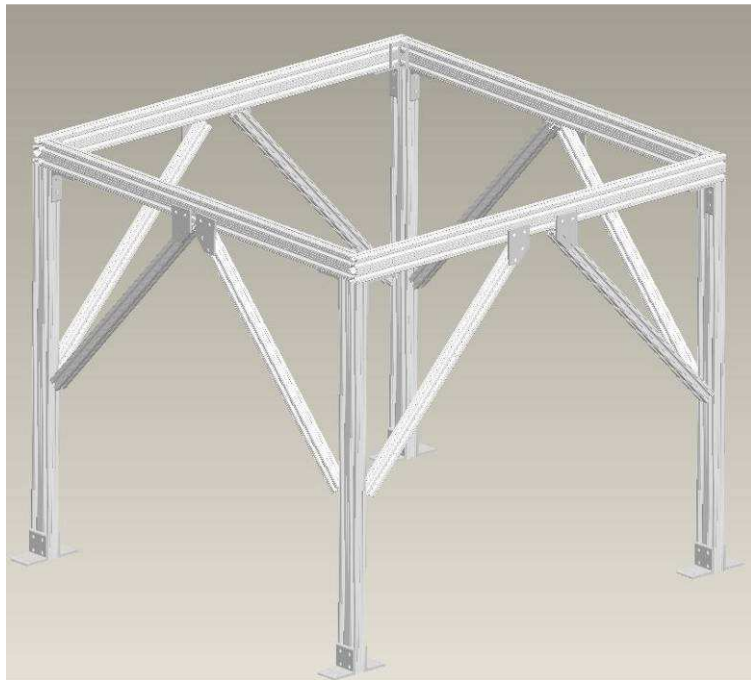
Figure 2.13 - Bottom Half of the Frame for the Testing Container

A one inch thick 3'x3' sheet of acrylic was then bolted on top of the frame. A closed-cell foam was placed between the aluminum frame and acrylic sheet to create a water-tight seal. The acrylic sheet had to be drilled with 5/16" holes around the perimeter to allow for ¼" diameter bolts to be used in holding the plate down. Since the aluminum bars are one inch wide, the holes were drilled on each side ½" from the edge of the acrylic sheet and three inches apart from each other. This allows for the bolts to fit into the center of the t-shaped slot on the aluminum frame and the distance between bolts was estimated to be close enough to create enough pressure on the foam to keep a water-tight seal. The bolts were used in combination with a silicone rubber washer and brass washer as seen in Figure 2.12. The brass washer was placed on top of the rubber washer in order to distribute the load on the rubber washer. The compressed rubber washer sealed any gaps

between the bolts and holes in the acrylic. Figure 2.14 shows the bottom half of the frame with the acrylic sheet (pink) placed on top of the frame.
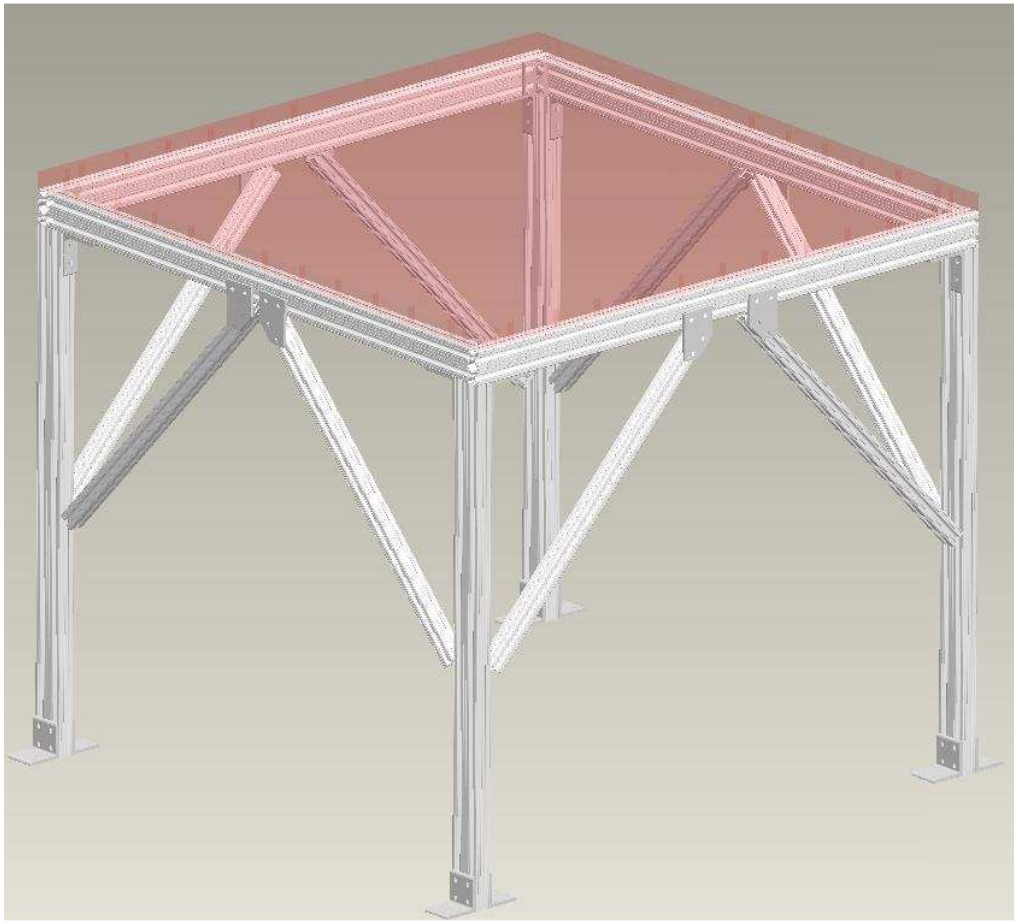
Figure 2.14 - Bottom Half of Frame with Acrylic Sheet

Once the acrylic plate was bolted down on top of the aluminum frame, four 22" long rods (red rods in Figure 2.15) were erected at the four corners of the plate.

Figure 2.15 - Top Half of Frame Assembly with Vertical Rods

The top of the rods were connected with four other rods (red rods in Figure 2.16) to create a box frame.
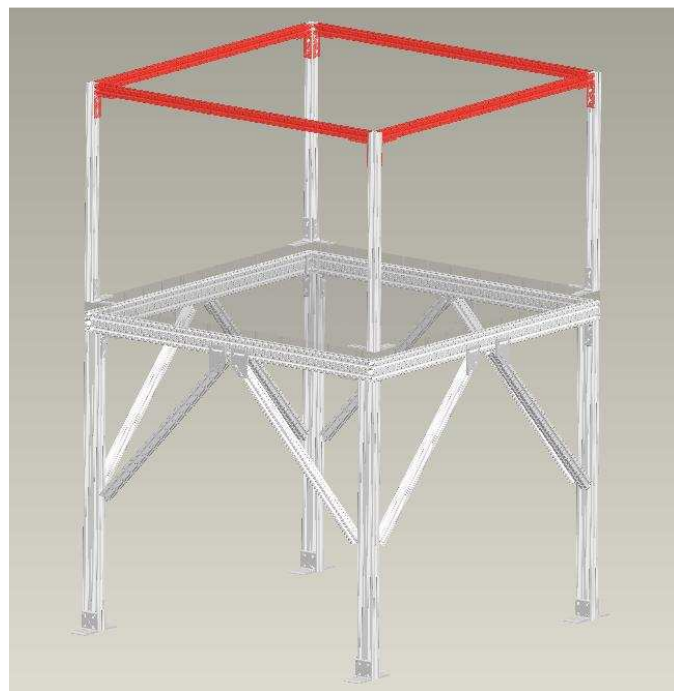
Figure 2.16 - Top Half of Frame Assembly with Horizontal Rods

The box frame allows for the four side walls to be bolted on to the frame in the same manner as the bottom acrylic sheet was bolted on. The side walls were made from 3'x2'x¼" thick polycarbonate sheets. The sheets were drilled in the same fashion as the one inch thick acrylic plate on the bottom. The sheets were also attached using the foam seal between the frame and plastic and combination of silicone and metal washers. Figure 2.17 shows the complete assembled container with side walls highlighted in pink.

Figure 2.17 - Complete Assembly of Container

2.7   High Speed Cameras

The motion of the obstacles was tracked by using a combination of two high speed digital cameras. Both cameras are products of Vision Research, Inc. The older camera is model Phantom v4.0 and is capable of recording 1,000 pictures per second at the maximum resolution of 512x512 pixels. Faster frame rates can be achieved using a lower resolution. The newer camera is model Phantom v7.1 and can achieve a much greater frame rate of 6,688 pictures per second at the maximum resolution of 800x600 pixels. Each camera connects to a laptop or PC through an Ethernet connection. The Phantom camera software allows the user to adjust camera settings such as resolution, frame rate and exposure time. Digital videos are recorded in the Vision Research proprietary "cine" format, but can be converted to more common video formats such as AVI and MOV. The same Tamron (IF) 28-75mm 1:2.8 MACRO   67 lens was used on both cameras. The zoom and focus of the picture were adjusted using the lens. Figure 2.18 is a photo of the Phantom v7.1 camera [5]. The Phantom v4.0 camera is similar in appearance.

2.8   *Phantom Camera Software*

The Phantom camera software from Vision Research, Inc. is used both for controlling the settings of the camera before recording as well as data analysis after the experiment has been recorded. Values such as resolution, exposure time and frame rate can be adjusted prior to recording. Image properties such as brightness, contrast and gamma can be adjusted before or after the video has been recorded. The software allows the user to track the motion of a point through each frame.   First, the user chooses a system of units and defines a reference length by clicking two endpoints of some object or marker with a known length. The user can choose an origin for the Cartesian coordinate system or leave the default value as the top left corner of the frame. The user then opens a file that tracks the data collected for each frame. The user simply clicks on the point he wishes to track in each frame and the results are recorded into a text file. The text file can later be exported into a database management system such as Microsoft Excel. Figure 2.19 shows an image of the graphic user interface (GUI) for the Phantom software.

Figure 2.19 - Phantom Camera Software GUI

35

Some sample video frames from an actual test are shown in Figure 2.20. In this test, the obstacles are clearly visible throughout the entire test and the motion can be tracked using the Phantom camera software.

0 ms	2.7 ms
12.7 ms	25.2 ms
60.2 ms	160.2 ms
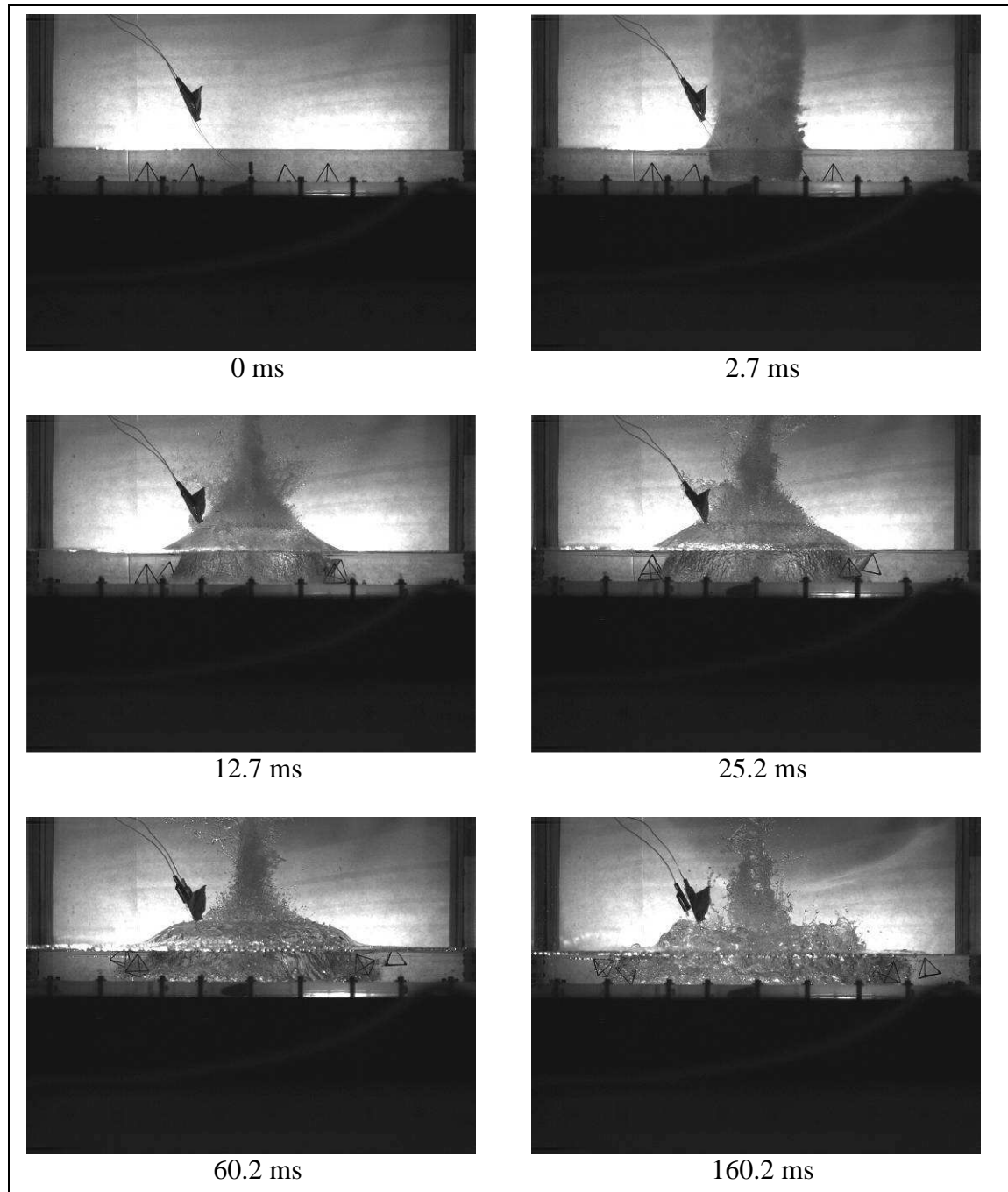
Figure 2.20 – Select Video Frames from Test 14

Chapter 3 – Experimental Setup

3.1   Overview

All of the tests using the clear-walled container were set up with two cameras filming the
motion of the obstacles. The blast chamber in which the container stands has a
rectangular porthole cut out of the side and an opening on the front end. One camera was
set up outside of the porthole to film the obstacle motion from the side. Figure 3.1 is the
front view and shows the relative location of the container and side view camera. Figure
3.2 is a photo that shows the same view, but only the container can be seen. The camera
is actually behind a wall that separates the blast chamber and the adjacent room so the
camera cannot be photographed together with the container. White poster board was
taped to the outside of the back window to provide a contrasting background for the black
obstacles.
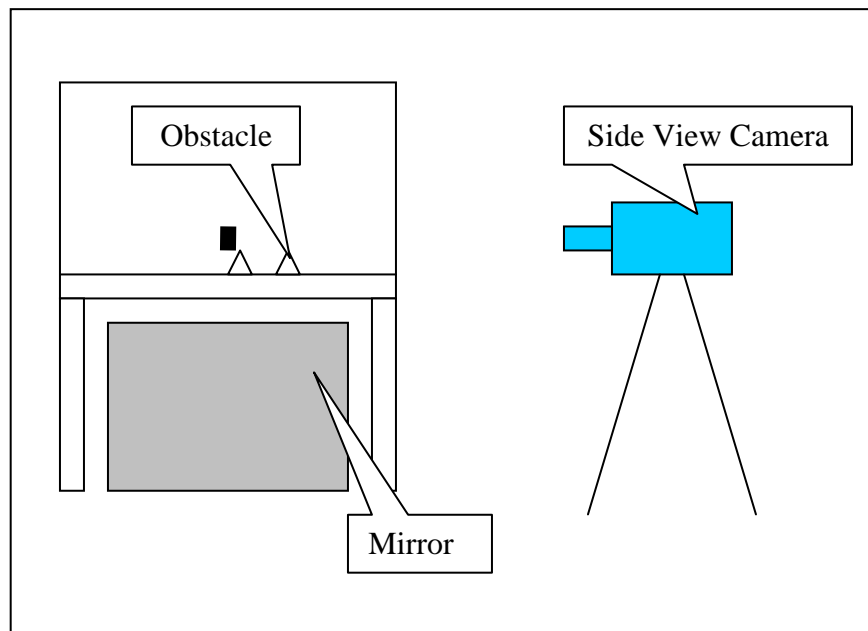
Figure 3.1 - Front View Drawing of the Experimental Setup
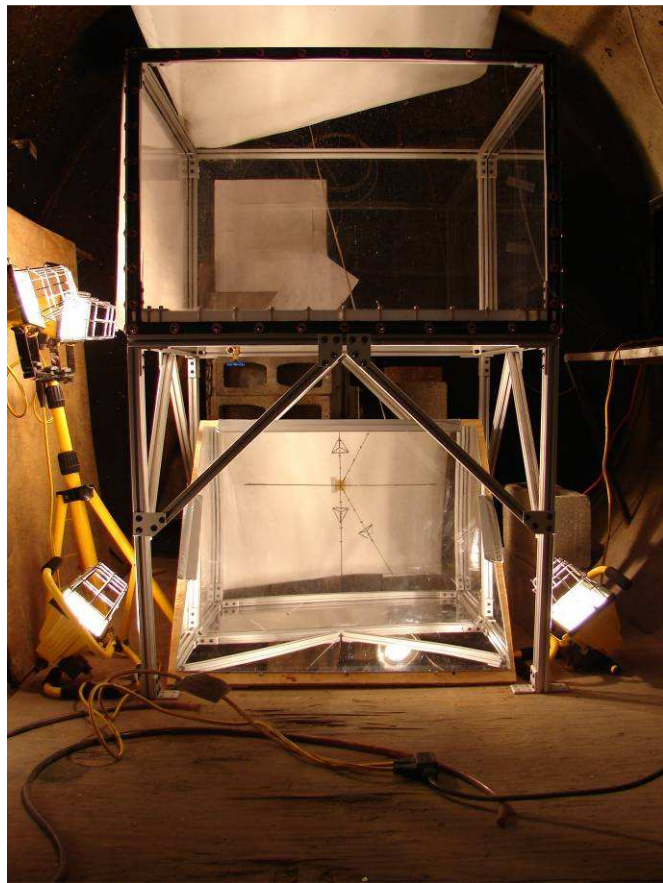
Figure 3.2 - Front View Photograph Without Side View Camera in Picture

The second camera was set up at the front entry of the blast chamber to film the bottom view. The bottom view was obtained by placing a mirror at a 45 degree angle underneath the container. The camera was then leveled and pointed at the mirror to provide a virtual image of the bottom of the container. A side view diagram of the setup is shown in Figure 3.3. A photo of the side view where only the container can be seen is shown in Figure 3.4. A white tarp was hung over the top of the container to provide a contrasting background for the black obstacles filmed by the bottom view camera.
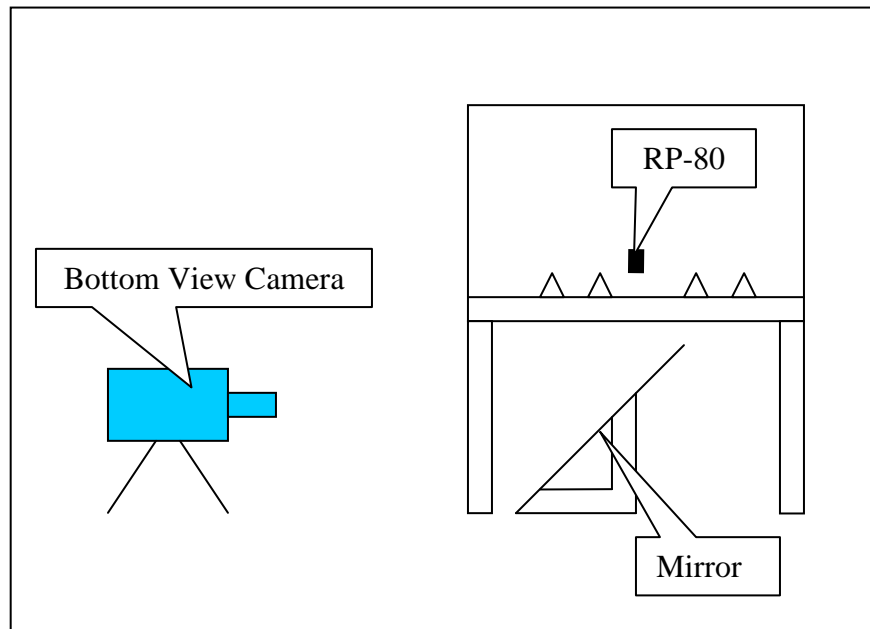
Figure 3.3 - Side View Drawing of the Experimental Setup
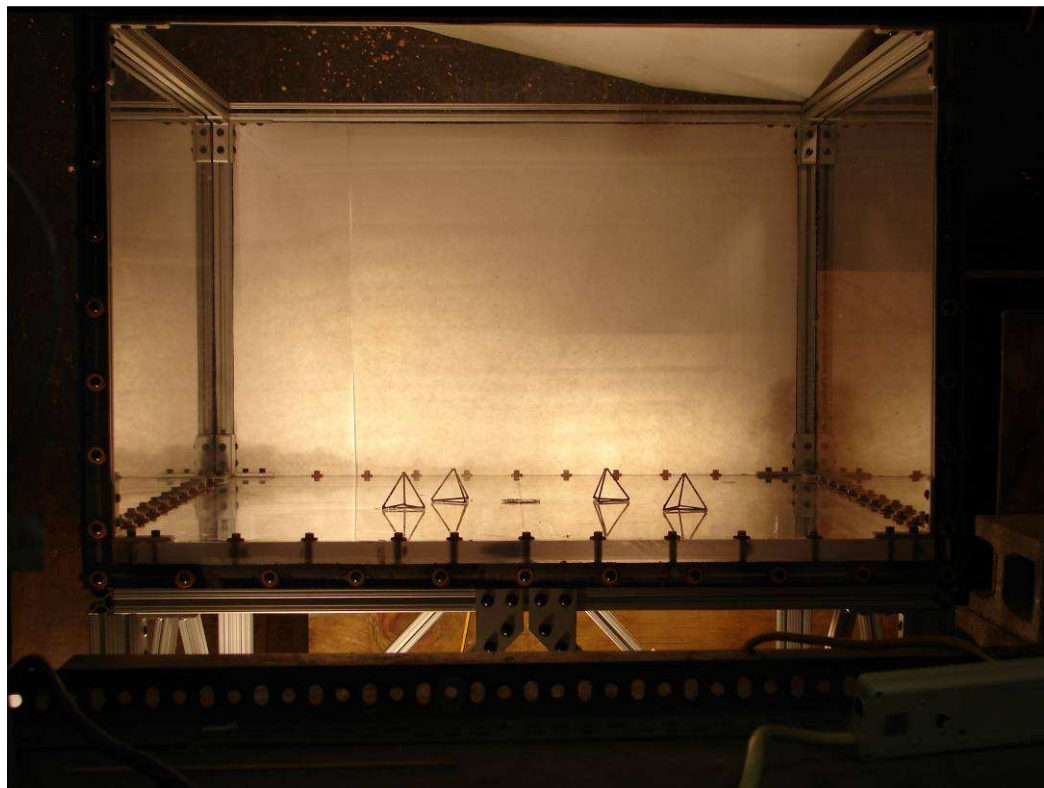
Figure 3.4 - Side View Photograph Without Front View Camera or Mirror in Picture

3.2   RP-80 and Obstacle Placement

The bottom of the container was marked for each series of experiments in order to establish the center of the plate and the location for placing the obstacles. First, two perpendicular line segments were drawn through the center of the bottom plate. A straight edge and dry-erase marker were used to draw a line segment that would connect the center bolts at opposite edges of the container. A Bevel Vernier Protractor was then used to draw two line segments that begin at the center of the plate and move out towards the side view camera at a 30 degree angle. The line segments were then marked some measured distance from the center to indicate the location for placement of the obstacles. Figure 3.5 shows the view of the bottom surface from above.
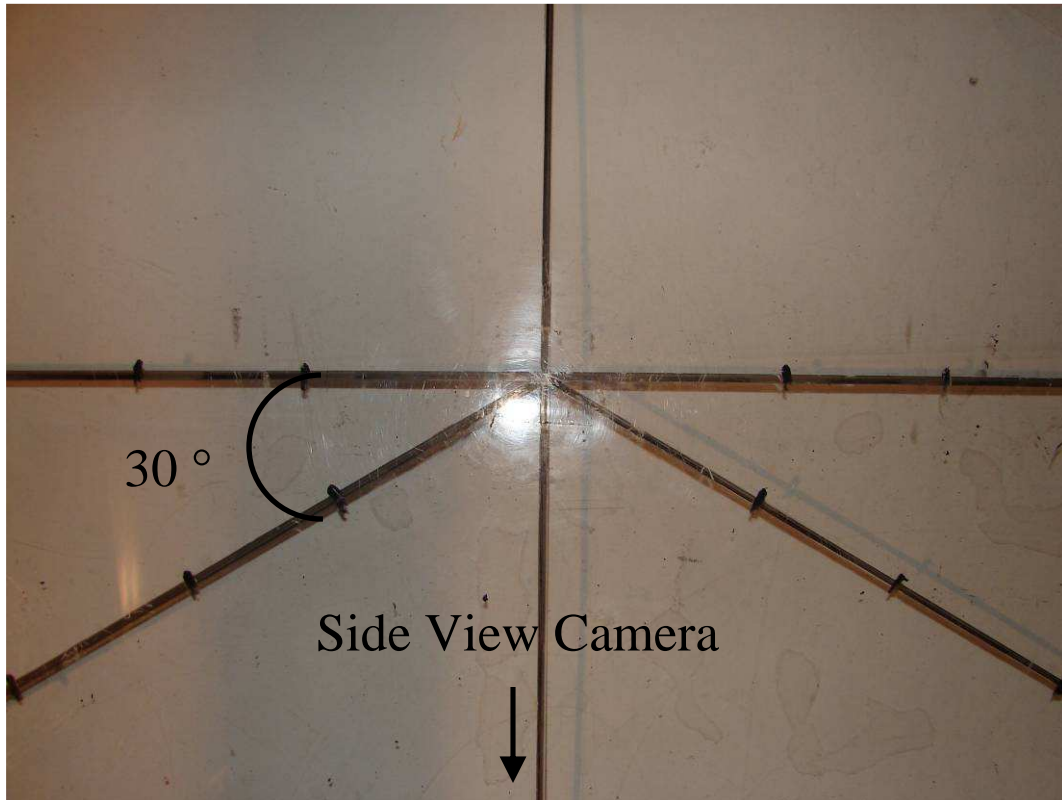
Figure 3.5 - Markings on the Bottom Surface Inside the Container

The typical test setup consisted of an RP-80 charge located at the center of the bottom surface. In order to protect the acrylic from damage due to the explosion, a small square sheet of material was taped to the bottom of the container. The material was marked with perpendicular lines to provide a cross-hair to line up with the perpendicular lines marking the center drawn on the bottom surface. A ¼" acrylic sheet was used in some of the earlier tests before switching to a 1/8" brass sheet. The acrylic sheet was replaced because it would easily crack and the brass could provide sufficient protection with a smaller thickness of the sheet.

The necessary distance from the bottom of the container to the plastic head of the RP-80 was calculated using the known dimensions of the RP-80, depth of water, and thickness of the protective material underneath the charge. The lead wires of the RP-80 were then bent to a ninety degree angle over a set of calipers, as shown in Figure 3.6, to provide the proper depth of charge.
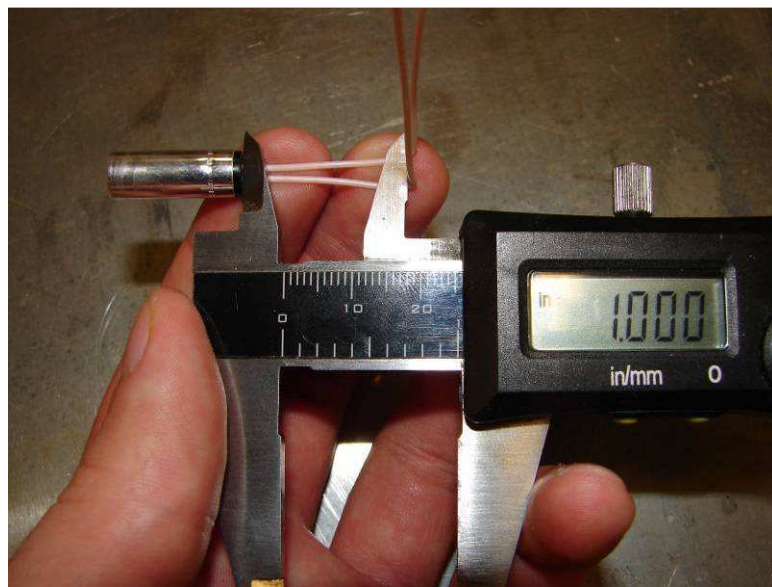
Figure 3.6 - Lead Wires of RP-80 Bent to a Right Angle Over a Set of Calipers

41

The lead wires were taped down to hold the charge in place. The placement of the charge was estimated visually by lining up the top of the charge with the set of cross-hairs etched on the protective sheet.

The obstacles were then placed around the charge at various stand-off distances. The obstacles were placed in one of two orientations. The Beta 0 orientation is when the triangle in contact with the ground points away from the charge. The Beta 180 orientation is when the triangle in contact with the ground points towards the charge. Figure 3.7, below, shows an overhead view of tetrahedrons in a Beta 0 or Beta 180 orientation relative to the RP-80 charge.

Beta 0   RP-80   Beta 180
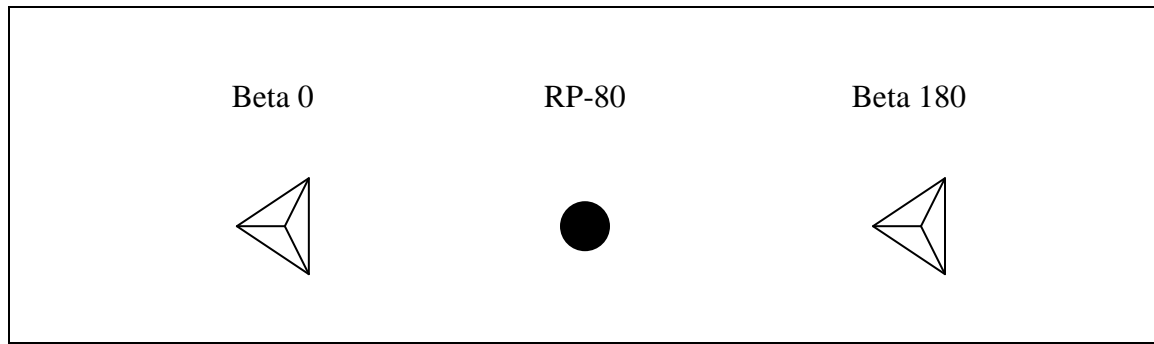
Figure 3.7 - Diagram of Obstacles in Beta 0 and Beta 180 Orientation

Each obstacle was placed along one of four marked lines that extend out in a radial direction (see Figure 3.5 on page 40) to allow at least 30 degrees of separation in the tangential direction. It was assumed that the 30 degree separation is enough to minimize any significant effects due to the interaction between obstacles. This assumption is examined in more detail in Section 4.10. Obstacles were placed using the marks on the bottom plate as a reference. The top vertex of the tetrahedron was lined up with the mark by visual inspection from directly above the obstacle.

3.3 Camera Settings and Adjustment

The placement of the side view camera was adjusted prior to filling the container with water. The camera was set on a tripod and leveled. The Phantom camera software displays a "live" image while setting up the camera and can be set to show a crosshair on the screen that was used to line up parts of the image. The height of the tripod was raised so that the center bolt can be seen on the front and rear edge of the bottom plate. The tripod was then shifted so that the two bolts were lined up with the vertical line of the cross hair. This ensured that the camera view was in line through the center of the container.

The camera was then lowered so that the horizontal line of the crosshair lines up with the top surface of the bottom sheet of acrylic. This camera setup was consistent through all experiments regardless of the depth of charge, height of water or other variables.

The side view camera was set to record 2,000 frames per second at a resolution of 800x600 pixels. The exposure time was set somewhere between 90 and 110 microseconds depending on the lighting conditions and depth of water for the particular experiment. The post trigger value was usually set to 4,400. Since the camera can record a total of 4,421 images at this particular frame rate and resolution, the post trigger setting tells the camera to take 4,400 pictures after the trigger signal which leaves room for 21 pictures before the trigger. The pictures taken before the trigger signal allow some room for error in case the camera malfunctions and does not trigger correctly (however, this did not occur during any of the tests in this study). The 4,400 pictures after the trigger is

more than adequate since most obstacle motion ceased before 1,000 frames had been recorded.

After setting up the side view camera, the container was then filled with water using a hose. The end of the hose was placed into the corner of the container to diffuse the flow of water and prevent the obstacles from moving. The height of water was measured using a ruler taped to the side wall of the container.

The bottom view camera was set on a tripod and leveled in the same fashion as the side view camera. The vertical line of the cross-hair was lined up with the line drawn on the bottom surface of the acrylic plate. The height of the tripod was adjusted so that the mirror would fit into the view. The proper height with the tripod coincidentally turned out to be the lowest possible height setting of the tripod. For consistency, the tripod was set to the lowest height for each experiment.

The bottom view camera was set to record 1,000 frames per second at a resolution of 512x512 pixels. These were the maximum frame rate and resolution attainable with the Phantom 4 bottom view camera. The exposure time was set to 600 microseconds and the post trigger value was set to 1000 since the camera can only record 1018 total pictures at these settings.

3.4   Analysis of Obstacles at an Angle

One of the challenges of analyzing the motion of the obstacles in the described setup is

that some of the obstacles move in such a way that a component of the displacement

vector is directed towards the camera. Obstacles that move along a line perpendicular to

the view of the side camera lens can be tracked by simply finding a length per pixel value

in that plane and tracking the displacement based on the scaling factor. Obstacles that

have some component of motion towards the camera will appear to travel a shorter radial

distance than they actually do. Some calculations based on geometry were used in order

to correct the data and determine the displacement of the obstacle in a radial direction.

The method for correcting the perceived displacement is described below [6]:

1) The origin of the Cartesian coordinate system was set so that the vertical axis

   passes through the center bolt and the horizontal axis lines up with the bottom

   surface of the container.

2) A scaling factor, S_w, was determined by using the known diameter of the RP-

   80 to find the inch/pixel value.

3) The apparent radial displacement as shown in Figure 3.8 is:

   $$d = S_w P_h,$$

   where P_h is the observed horizontal pixel displacement of the obstacle.

4) Using d and L, β and α can be calculated from

   $$\beta = \tan^{-1}(d/L) \text{ and } \alpha = 90^o\text{-}\beta,$$

   where L is the length measured from the center of the RP-80 to the front

   of the camera lens.

5) Using the fact that the sum of angles in a triangle is $180°$,

$$\gamma = 180° - \alpha - \theta$$

In our case, θ was taken to be $30°$. It is assumed that θ remains constant throughout the motion of the obstacle.

6) The radial displacement of the obstacle can be determined using the law of sines:

$$\frac{\sin(\alpha)}{d_h} = \frac{\sin(\gamma)}{d} \quad \Rightarrow \quad d_h = d\,\frac{\sin(\alpha)}{\sin(\gamma)}$$
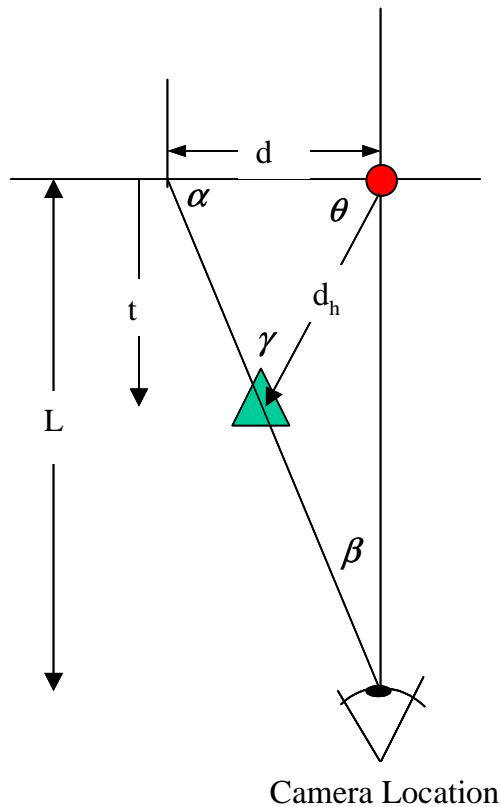
Figure 3.8 – Diagram of the Top View of Experimental Setup

The vertical position of the obstacle must also be compensated for:

1) Using the results from the calculation of radial displacement and the new variables introduced in Figure 3.9 gives

$$t = d_h \sin(\theta)$$

2) Then

$$s = L - t$$

3) Using similar triangles it is clear that

$$d_v = h*(s/L)$$

where h is the apparent height of the obstacle.
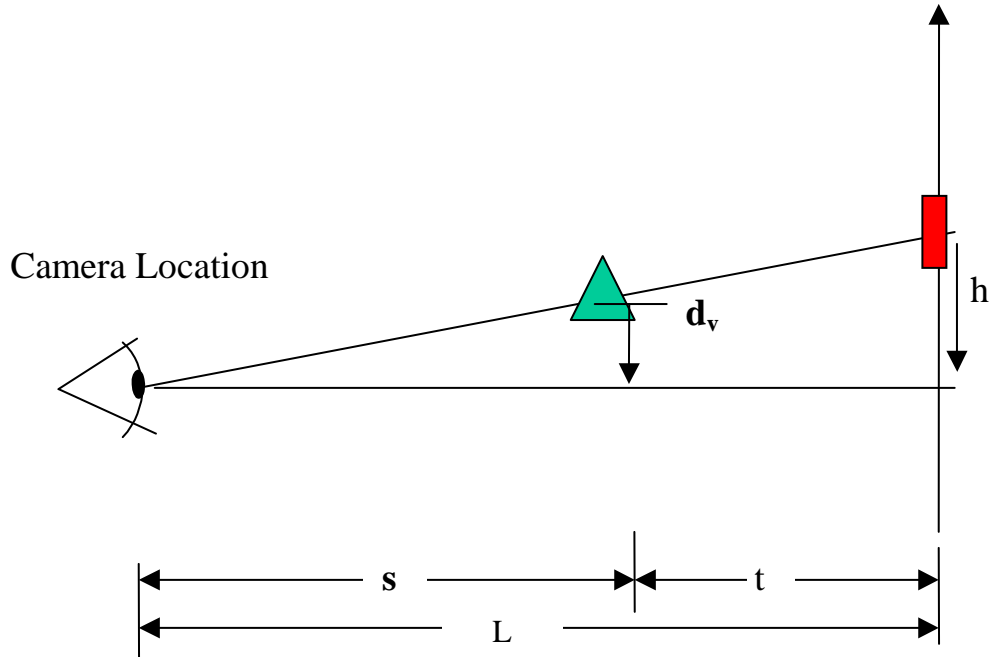
Figure 3.9 – Diagram of the Side View of the Experimental Setup

3.5   Test Conditions

The NSWC was interested in simulating obstacle motion under four different conditions.

Two of the conditions simulate an Mk-82 bomb at six feet and nine feet depth of water.

The other two conditions simulate an Mk-84 bomb at six and twelve feet depth of water.

The NSWC used computational means described in Section 1.5 to determine the

necessary scaling factor and depth of charge to simulate these conditions with an RP-80

EBW detonator. Table 3.1 summarizes the scaling factor and RP-80 depth necessary to

simulate the full scale conditions. The depth of the RP-80 is measured from the surface

of water to the center of the charge.

Bomb Size At Full Scale	Water Depth At Full Scale	Scale Factor	RP-80 Depth At Small Scale
Mk-82	6 feet	$\frac{1}{26}$	2.50 cm (0.98 in)
Mk-82	9 feet	$\frac{1}{28}$	2.25 cm (0.86 in)
Mk-84	6 feet	$\frac{1}{36}$	2.00 cm (0.79 in)
Mk-84	12 feet	$\frac{1}{42}$	2.00 cm (0.79 in)

Table 3.1 - Scaling Factors and RP-80 Charge Depths for Different Test Conditions

For each test condition the NSWC was interested in the motion of obstacles that had a

stand off distance of 7, 12, 18 or 24 feet at full scale lengths. The stand off distance was

measured in the radial direction from the center of the charge to the top vertex of the

tetrahedron-shaped obstacle. Each obstacle was placed in one of two possible

orientations, Beta 0 or Beta 180, as described in Section 3.2. If each test included one

obstacle then it would have required 32 tests to gather data for all the possible conditions.

However, the actual number of tests was much lower since multiple obstacles were used during each experiment.

A total of twenty five tests were conducted in this study. Only the first twenty tests will be discussed in this section because the last five tests were an attempt to explore the motion of obstacles other than tetrahedrons and will be discussed in Chapter 6. The first eight tests were exploratory tests used mostly to determine the necessary test setup and did not result in any valuable data. All eight of these tests, except for Test 5, simulated the Mk-82 bomb at a depth of six feet. Test 5 simulated the Mk-82 bomb at nine feet of water. The first test was conducted in a steel box with a camera filming from over the top of the water. No obstacle motion could be seen in this test and as a result the clear-walled container was built. Tests 2 through 5 used an improper arrangement of obstacles which resulted in the tetrahedrons colliding into each other and therefore no data could be collected. In Tests 6 through 8 there was only one camera being used and each of these tests had either poor lighting conditions so that no obstacles could be seen or an improper alignment of the camera which resulted in erroneous data.

Tests 9 through 20 yielded data that will be discussed in Chapter 4. Tests 9 through 13 were conducted to simulate the Mk-82 bomb in six feet of water. Tests 14 through 16 simulated the Mk-84 in six feet of water. Tests 17 and 18 simulated the Mk-84 bomb in twelve feet of water and Tests 19 and 20 simulated the Mk-82 bomb in nine feet of water. The exact details of each test are shown in Table 3.2. The bomb size, depth of water, and stand off distances shown in Table 3.2 are the values for full scale conditions. A table of

actual values measured at the small scale conditions for each of these tests can be found

in Appendix A, Table A.1. Note that in each test all of the obstacles were placed in the

same orientation.

Test Number	Condition (Bomb Size @ Depth of Water)	Scale Factor	Number of Obstacles	Stand off Distances (feet)	Orientation
9	Mk-82 @ 6 ft	$\frac{1}{26}$	2	7, 18	Beta 0
10	Mk-82 @ 6 ft	$\frac{1}{26}$	2	12, 24	Beta 0
11	Mk-82 @ 6 ft	$\frac{1}{26}$	2	7, 18	Beta 180
12	Mk-82 @ 6 ft	$\frac{1}{26}$	2	12, 24	Beta 180
13	Mk-82 @ 6 ft	$\frac{1}{26}$	4	7, 18, 7, 18	Beta 180
14	Mk-84 @ 6 ft	$\frac{1}{36}$	4	7, 12, 18, 24	Beta 0
15	Mk-84 @ 6 ft	$\frac{1}{36}$	4	7, 12, 18, 24	Beta 180
16	Mk-84 @ 6 ft	$\frac{1}{36}$	1	7	Beta 0
17	Mk-84 @ 12 ft	$\frac{1}{42}$	4	7, 12, 18, 24	Beta 0
18	Mk-84 @ 12 ft	$\frac{1}{42}$	4	7, 12, 18, 24	Beta 180
19	Mk-82 @ 9 ft	$\frac{1}{28}$	4	7, 12, 18, 24	Beta 0
20	Mk-82 @ 9 ft	$\frac{1}{28}$	4	7, 12, 18, 24	Beta 180

Table 3.2 - Summary of Each Test Using Tetrahedron Obstacles

Chapter 4 – Results

4.1   Introduction

The results of Tests 9 through 20 outlined in Table 3.2 will be discussed in the following sections. All of the test data has been scaled up to full scale conditions in order to make it easy to compare results between different tests. It was assumed that the obstacles move in a radial direction and this assumption will be investigated in this chapter. Other variables such as stand off distance, depth of water, obstacle orientation and bomb size will also be investigated in the following sections.

4.2   Verification of Data between Two Cameras

Since two cameras were used to film each of the tests, it is important to verify that the images from both cameras resulted in the same data. The use of two cameras provides the opportunity to check that the calculations made in Section 3.4 (Analysis of Obstacles at an Angle) correctly adjusted the data for obstacles that moved at an angle toward the camera. In Tests 9 through 12 only two obstacles were placed into the container so that they could be seen by both cameras. A review of the data from these tests found that the two cameras provided similar radial displacements over time. The data also indicates that the calculations in Section 3.4 are accurate, and therefore only the side camera was necessary to determine the trajectory of an obstacle. All of the remaining tests conducted after this point utilized both cameras, but the tests had up to four obstacles placed in the container. Only two of the obstacles could be seen by both cameras and the other two were only visible on the side view camera.

Figure 4.1 through Figure 4.4 are plots of the radial displacement versus time for the two obstacles in the container in Tests 9 through 12. Each obstacle in the four tests has two sets of data shown in the plot; one for each camera filming the test. Obstacle 2 on each of the plots was at a thirty degree angle towards the camera as shown in Figure 3.5 on page 40. It can be seen from these graphs that the data collected by the bottom view and side view cameras is similar. These graphs also show that the method for adjusting data due to the angled motion of the obstacle is valid and produces results that are similar to those obtained for obstacles perpendicular to the line of view of the camera. Tests 13 through 20 were completed using up to four obstacles in each test, but only two could be seen by both cameras in each of those tests. The radial displacement versus time plots for those tests yields similar results to those seen in Tests 9 through 12.

Radial Displacement vs Time
Mk-82 @ 6ft -- Beta 0
Test 9
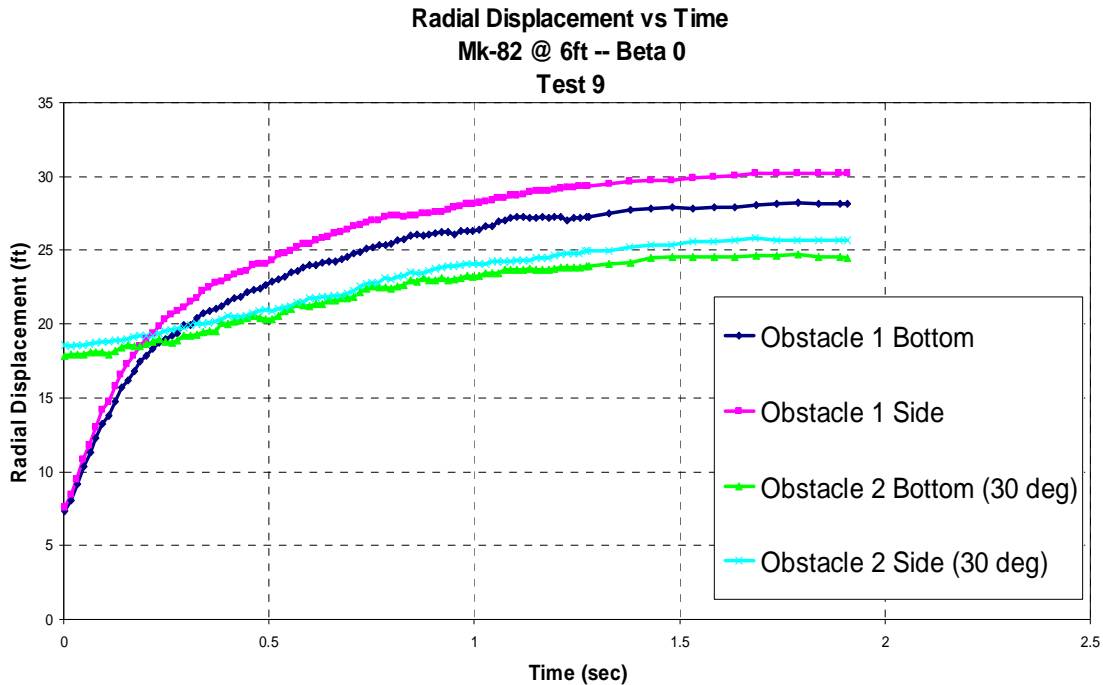
Figure 4.1 - Radial Displacement vs Time for Test 9
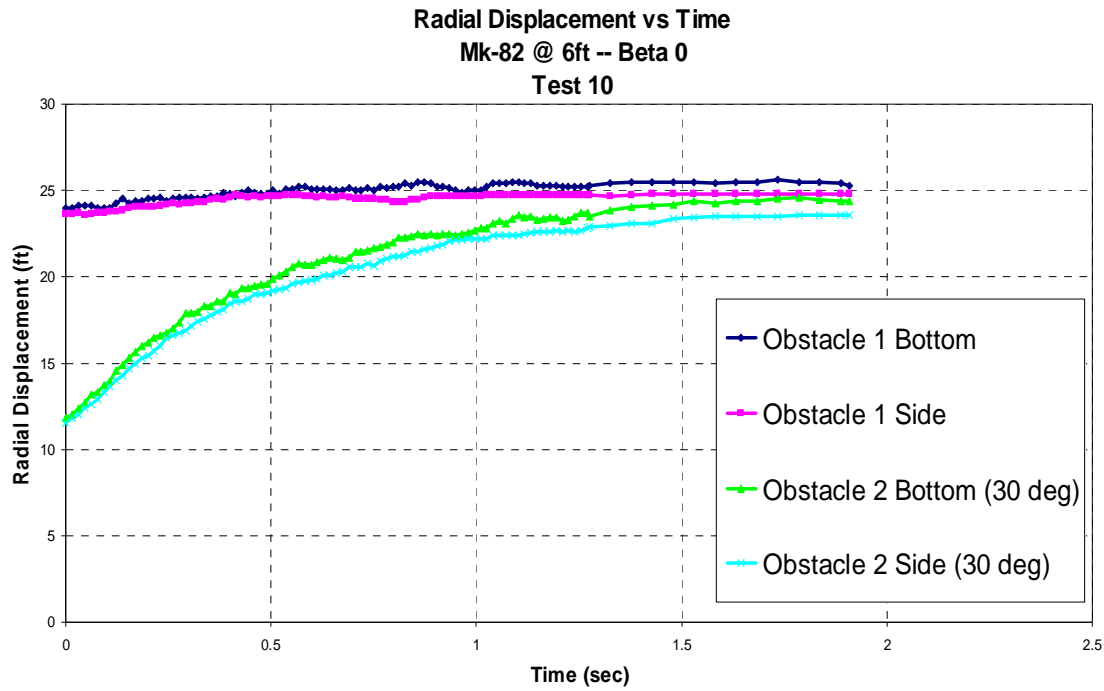
Figure 4.2 - Radial Displacement vs Time for Test 10
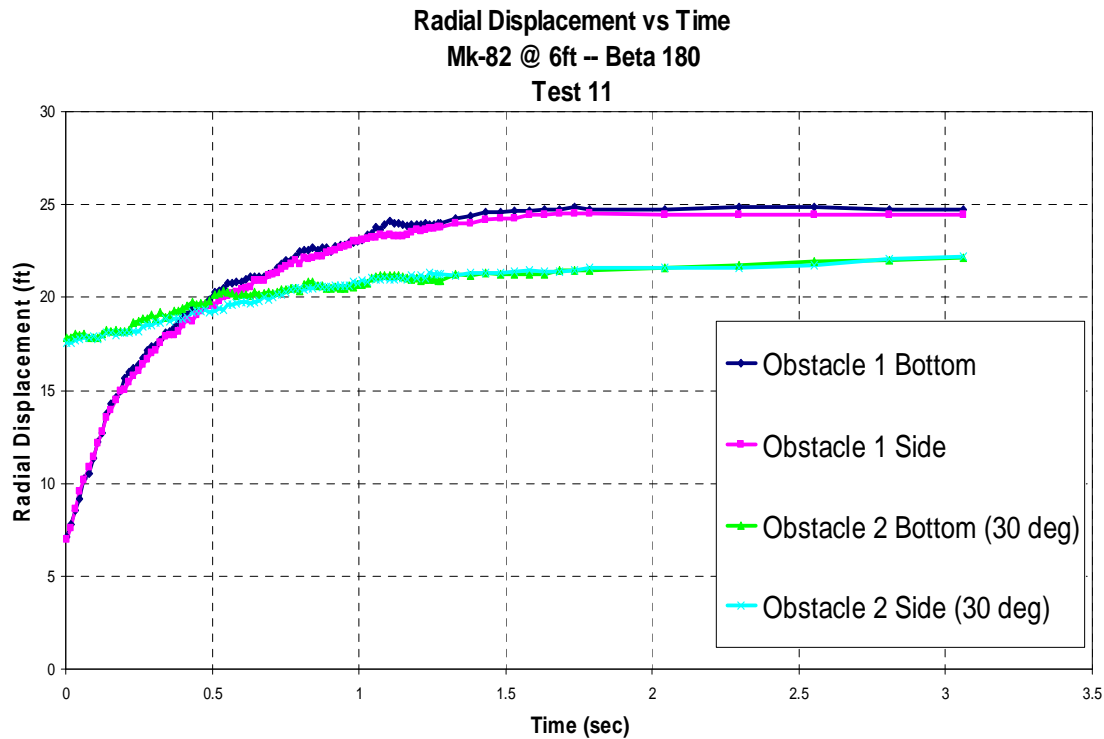
Figure 4.3 - Radial Displacement vs Time for Test 11
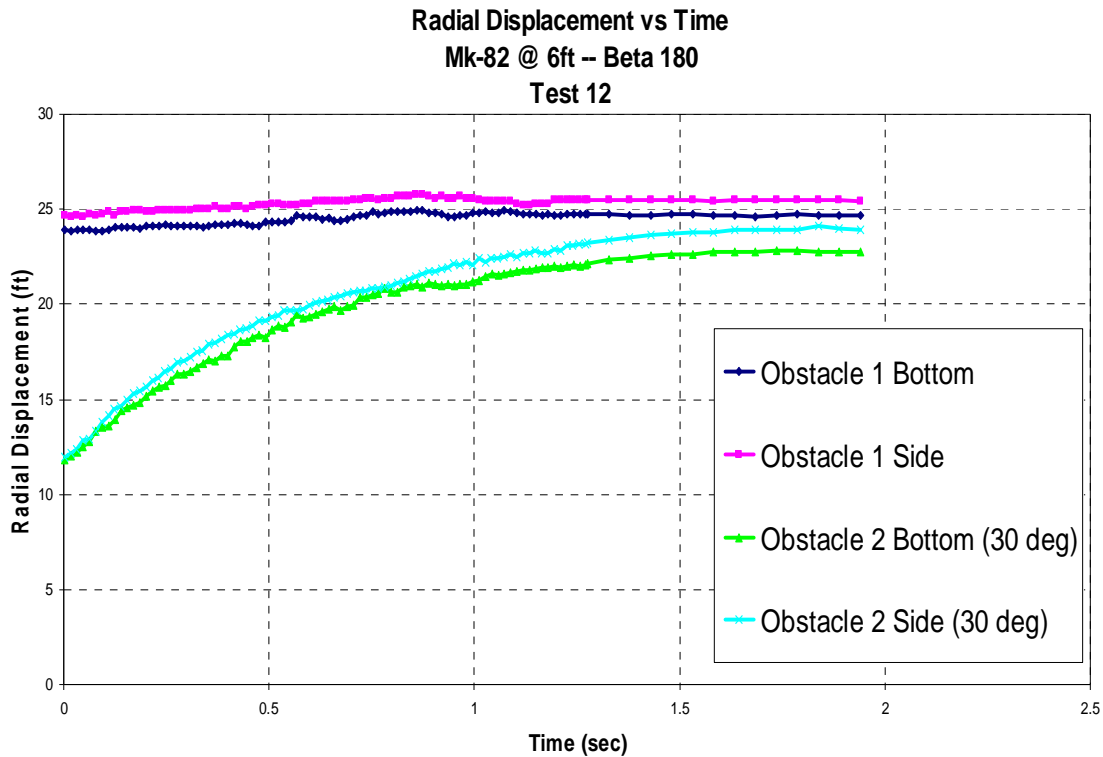
Figure 4.4 - Radial Displacement vs Time for Test 12

4.3   Verification of Radial Movement of Obstacles

When collecting data from the side view camera, it is assumed that the obstacles move in

a radial direction. This assumption can be checked using the bottom camera views.

Figure 4.5, next page, plots the angle to the obstacle measured from the y-axis. This

angle was calculated by taking the arctangent of the x and y coordinates obtained with the

bottom view camera. Tests 9 through 12 are a good representation of the typical angular

displacements for the tests conducted in this study. Obstacle 1 from Test 18 was plotted

as well because it had the greatest angular displacement of all the obstacles recorded with

the bottom view camera. It can be seen that most obstacles move only slightly in the

tangential direction and get displaced by only a few degrees. Even in the worst case, Obstacle 1 from Test 18 was only displaced by approximately six degrees.

Angle to Obstacle Measured from Y-Axis
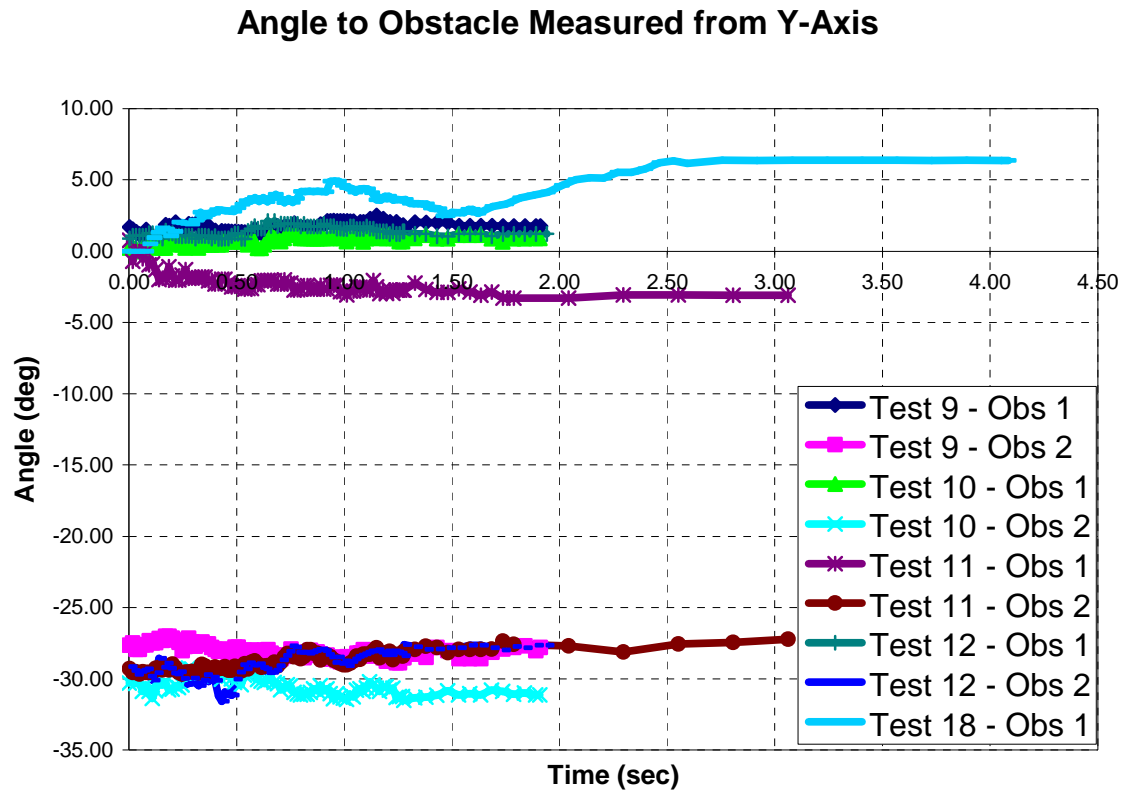
Figure 4.5 - Angle to Obstacle Measured from Y-Axis for Various Tests

4.4   Adjusting Height for Movement of the Floor

Upon review of the test videos, it was found that the entire testing container seemed to be oscillating vertically after the detonation. It is believed that this motion is caused by the movement of the plywood floor and not the bending of the acrylic plate on the bottom of the container. It can be seen in the side view videos that the entire edge of the plate moves together and there is not a greater displacement in the center as compared to the ends of the edge. This suggests that the motion is a not a bending of the bottom plate of the container. Since the floor of the testing chamber was made of plywood sheets

55

supported by beams it is likely that the detonation caused the plywood sheets to bend in an oscillatory motion and therefore caused the testing container to move in the vertical direction.

Figure 4.6, next page, is a plot of the vertical displacement of the container measured for Test 9. Unlike the other plots in this chapter, it shows the values of the actual data collected and it is not scaled up to full scale. All other tests produced similar results where the initial motion of the container is downward approximately one tenth of an inch and the rebound doubles in magnitude to about two tenths of an inch in the upward direction. The maximum measured vertical displacement was about one quarter of an inch in Test 15. The data for each test was adjusted according to the measured oscillation of the container. It was assumed that the container and everything inside of it moved as a whole and therefore the measured displacement of the container was subtracted from the measured height of the obstacles in order to obtain the height of the obstacles relative to the bottom surface. The oscillation had more effect on the smaller scale tests since the motion of the container gets multiplied by a larger scaling factor when scaling the results to full scale. However, these oscillations are still relatively small compared to the motion of the obstacles.

Vertical Oscillation of Container
Observed Motion from Test 9
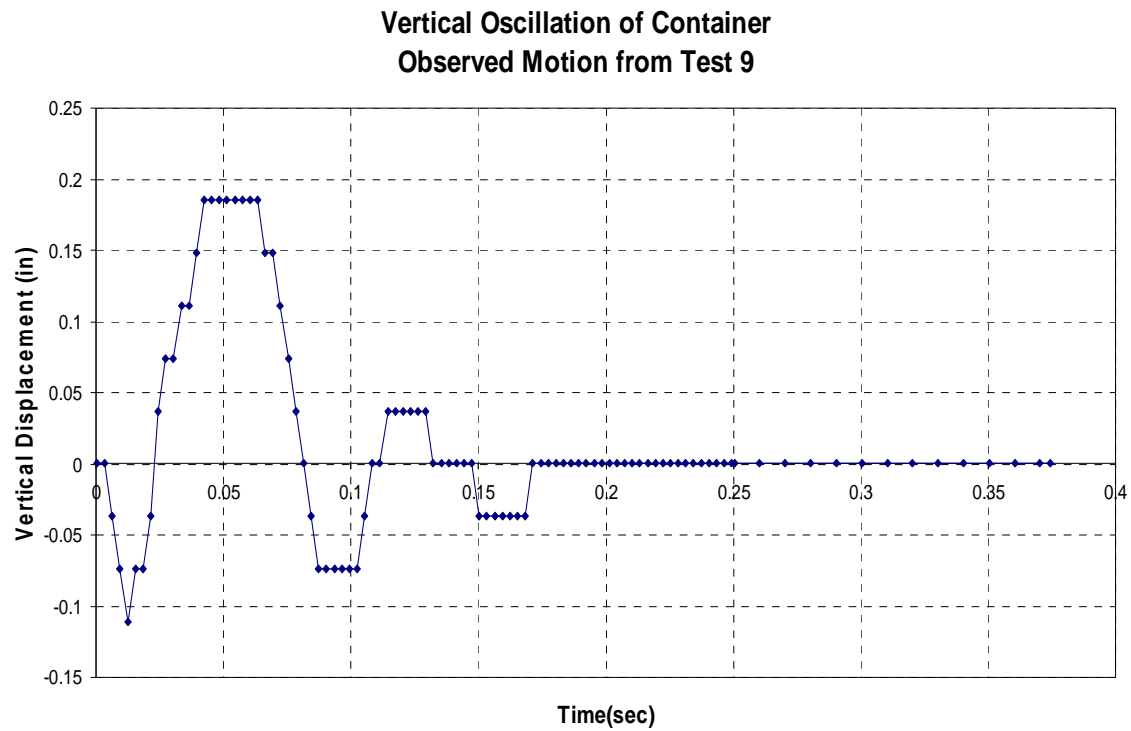
Figure 4.6 - Vertical Displacement of the Container Measured at the Bottom Surface

4.5   *Results for MK-82 at 6 Feet Depth of Water*

This section describes the results of the tests that model an MK-82 bomb in six feet depth of water. Figure 4.7 and Figure 4.8 on the next page show the trajectory plots of the obstacles at four different stand off distances. The conditions for the tests shown in Figure 4.7 and Figure 4.8 are the same, except that Figure 4.7 shows all trajectories for obstacles at a Beta 0 orientation and Figure 4.8 shows the trajectories for obstacles at a Beta 180 orientation. It can be seen that the obstacles that are initially closest to the charge travel the largest radial distance. The closer obstacles also tend to travel more in the vertical direction than the obstacles that are farther out.
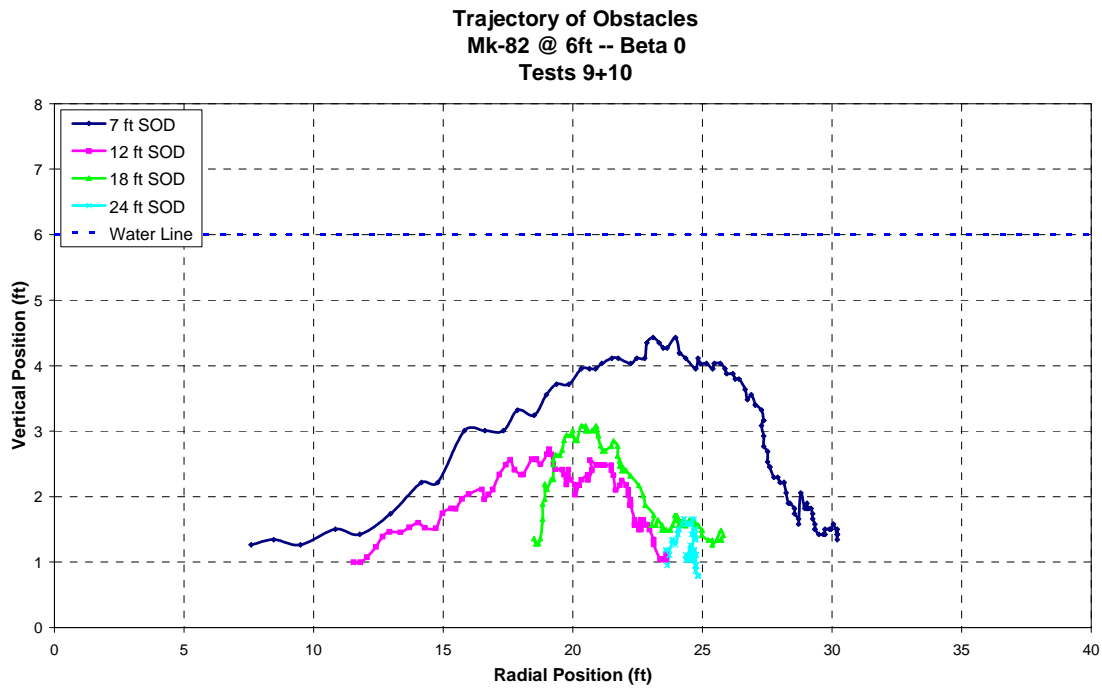
Figure 4.7 - Trajectory Plot for MK-82 at 6 Feet Depth of Water, Beta 0 Orientation
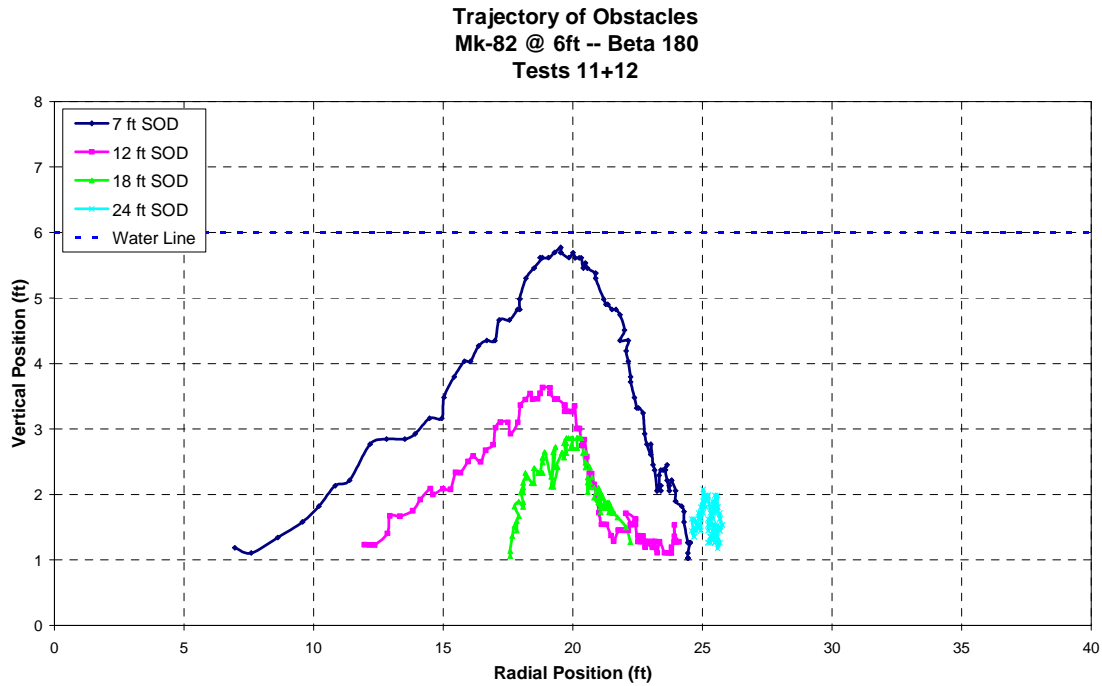
Figure 4.8 - Trajectory Plot for MK-82 at 6 Feet Depth of Water, Beta 180 Orientation

58

4.6   *Results for MK-82 at 9 Feet Depth of Water*

This section describes the results of the tests that model an MK-82 bomb in nine feet

depth of water. Figure 4.9 and Figure 4.10 show the trajectory plots of the obstacles at

four different stand off distances. The conditions for the two tests shown are the same,

except that Figure 4.9 shows all trajectories for obstacles at a Beta 0 orientation and

Figure 4.10 shows the trajectories for obstacles at a Beta 180 orientation. In Figure 4.10

there are some gaps in the data for the two obstacles at 7 and 12 feet stand off distance.

These gaps exist because the obstacles could not be seen for a brief moment due to the

distortion of the water. It may be difficult to see on the plot, but both obstacles ended up

approximately 25 feet out in radial distance. Once again, it can be seen that the obstacles

that are initially closest to the charge travel the largest radial and vertical distance.
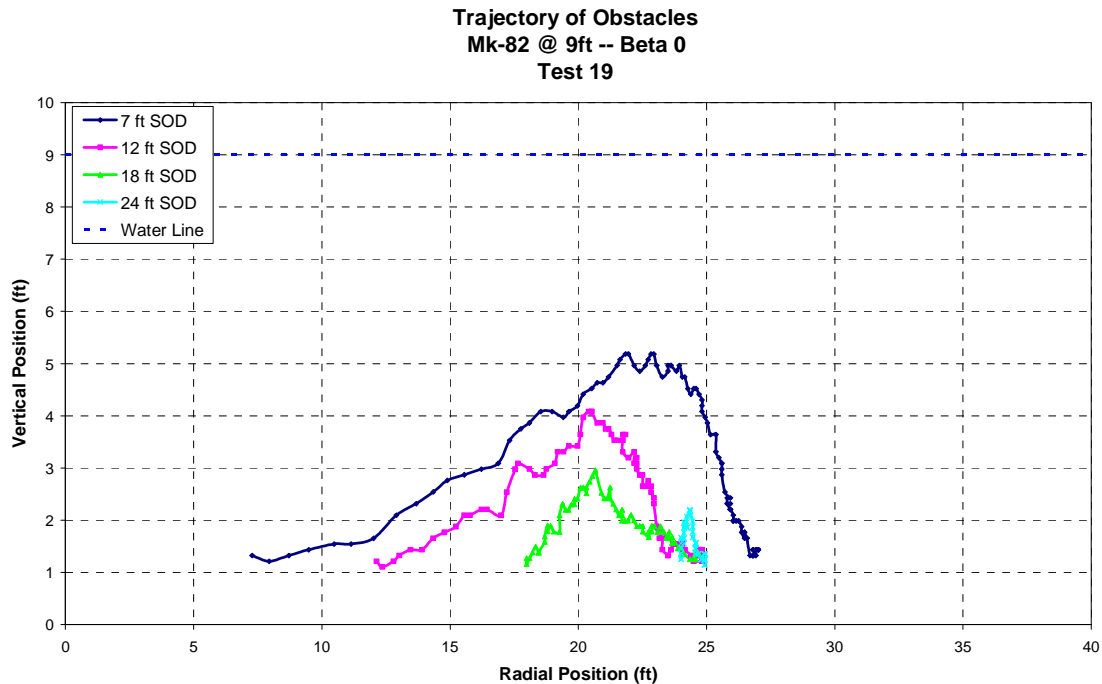
Figure 4.9 - Trajectory Plot for MK-82 at 9 Feet Depth of Water, Beta 0 Orientation

59
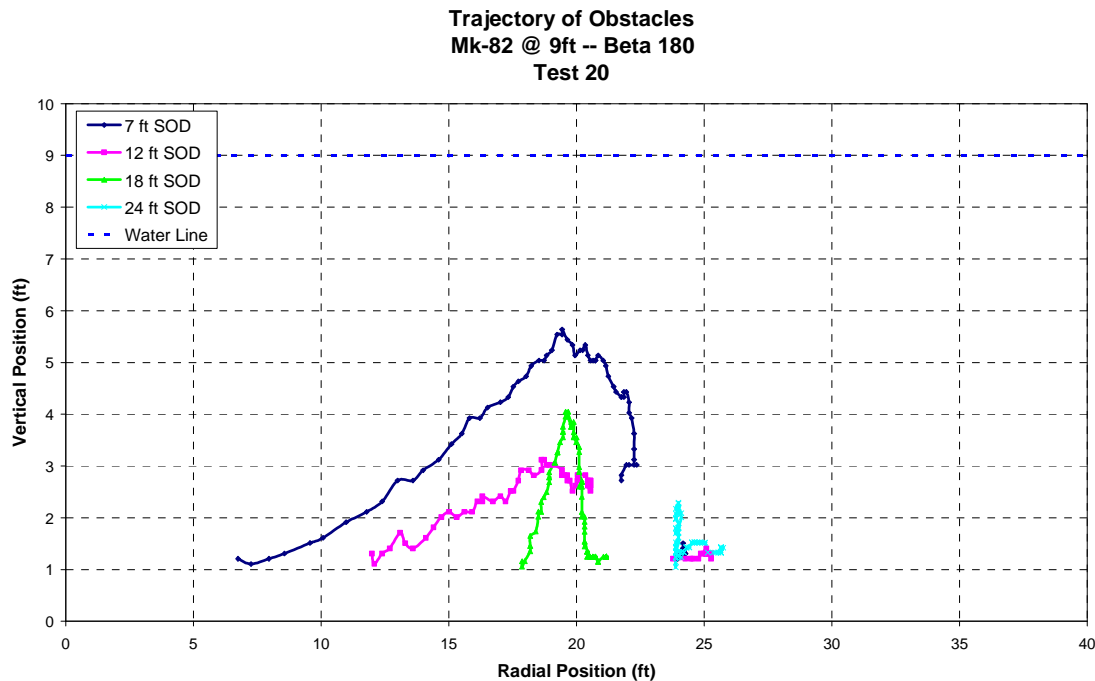
Figure 4.10 - Trajectory Plot for MK-82 at 9 Feet Depth of Water, Beta 180 Orientation

4.7   Results for MK-84 at 6 Feet Depth of Water

This section describes the results of the tests that model an MK-84 bomb in six feet depth

of water. The MK-84 bomb is the larger of the two bombs so it was expected that the

obstacles in these tests would have a greater distance of travel than those in the tests

modeling an MK-82 bomb. Note that the scale on the charts is different from those

shown in Sections 4.5 and 4.6. Figure 4.11 shows the trajectory plots for obstacles at a

Beta 0 orientation and Figure 4.12 shows the trajectory plots for obstacles at a Beta 180

orientation. One unique result that can be seen in Figure 4.12 is that the obstacle at seven

feet stand off distance was ejected from the water. In most cases, the obstacles that are

initially closest to the charge travel the largest radial and vertical distance.

60
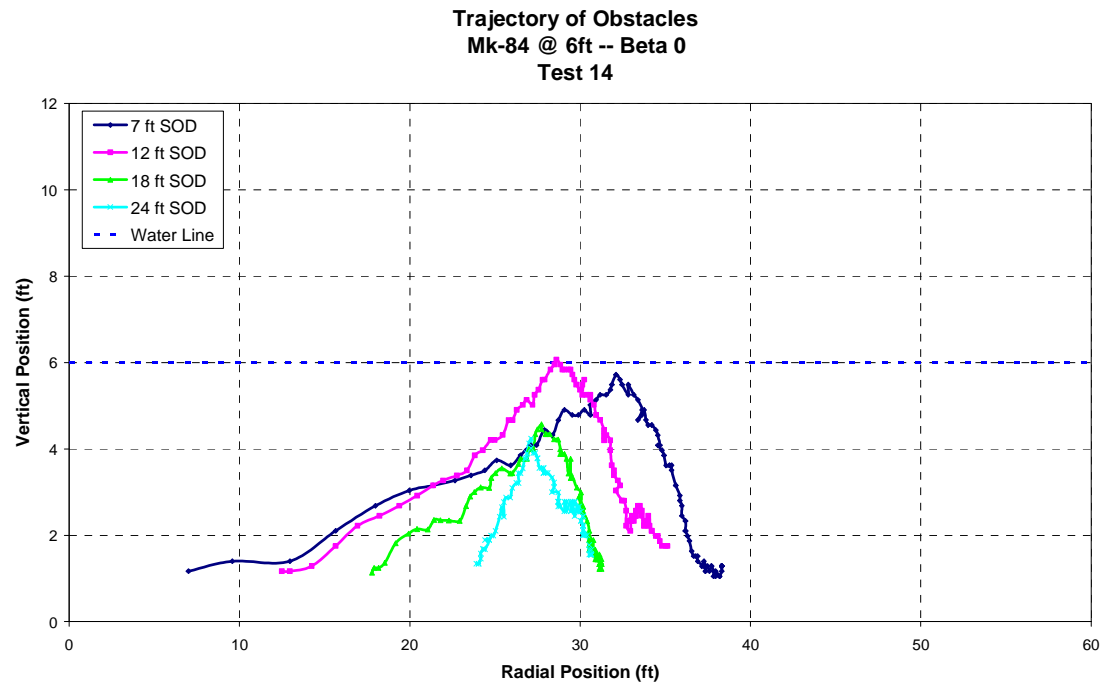
Figure 4.11 - Trajectory Plot for MK-84 at 6 Feet Depth of Water, Beta 0 Orientation
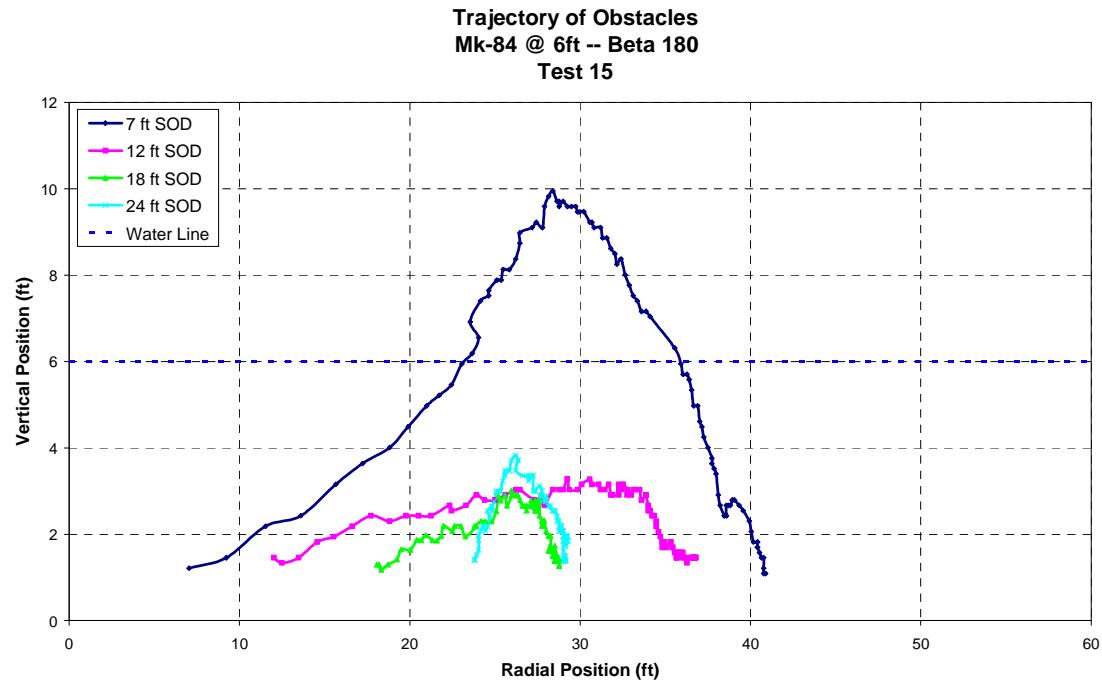
Figure 4.12 - Trajectory Plot for MK-84 at 6 Feet Depth of Water, Beta 180 Orientation

61

4.8   Results for MK-84 at 12 Feet Depth of Water

This section describes the results of the tests that model an MK-84 bomb in twelve feet

depth of water. Figure 4.13 shows the trajectory plots for obstacles at a Beta 0

orientation and Figure 4.14 shows the trajectory plots for obstacles at a Beta 180

orientation. As in all other test conditions, it can be seen that the obstacles that are

initially closest to the charge travel the largest radial and vertical distance.
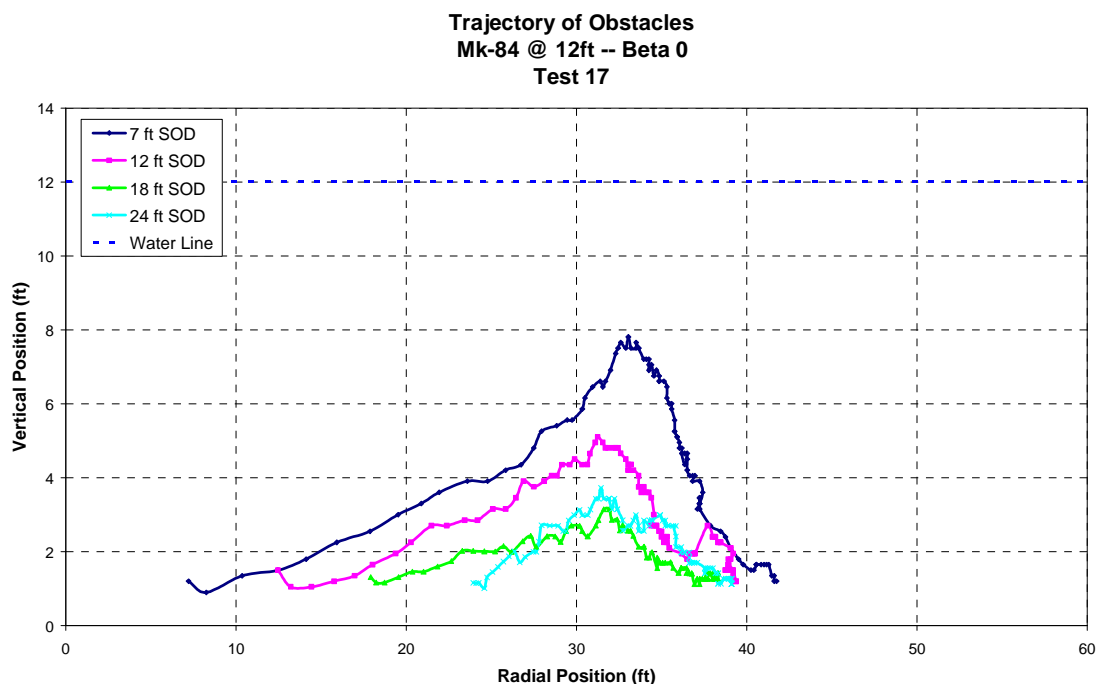
Figure 4.13 - Trajectory Plot for MK-84 at 12 Feet Depth of Water, Beta 0 Orientation

Trajectory of Obstacles
Mk-84 @ 12ft -- Beta 180
Test 18
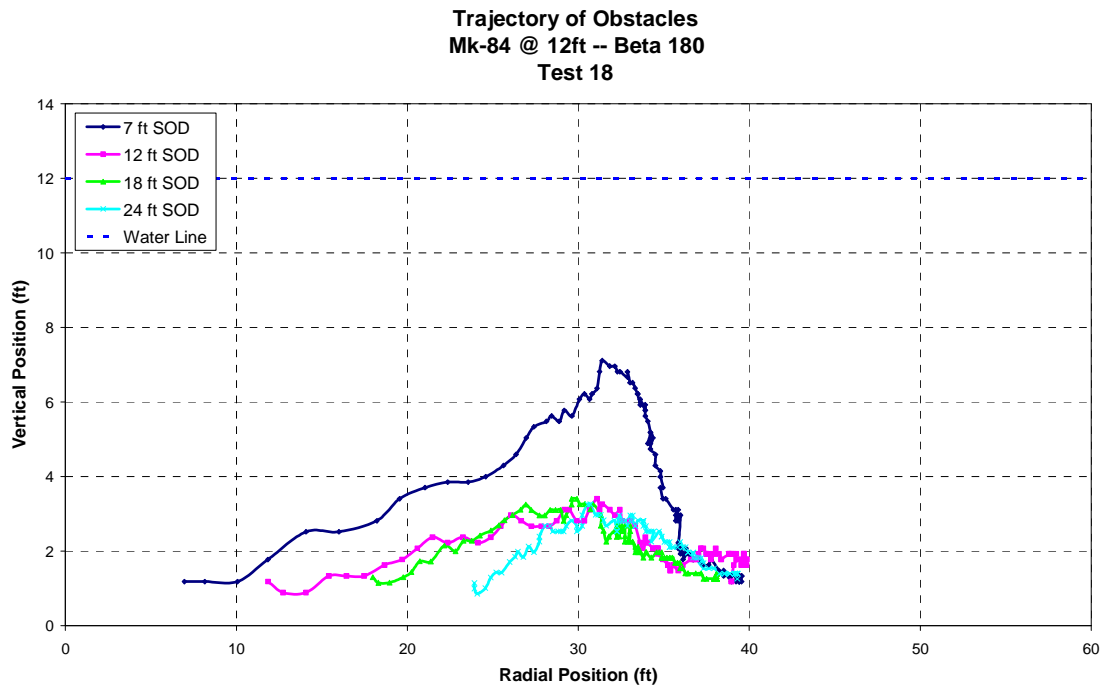
Figure 4.14 - Trajectory Plot for MK-84 at 12 Feet Depth of Water, Beta 180 Orientation

4.9   Repeatability of Tests

The MK-82 at 6 feet depth of water condition was chosen to examine the repeatability of tests in this study. Test 11 (the obstacles at 7 and 18 feet stand off distance shown in Figure 4.8) was repeated with four obstacles. Two obstacles with stand off distances of 7 and 18 feet were placed to the left of the charge. The setup was then mirrored so that two more obstacles at 7 and 18 feet stand off distance were also on the right side of the charge. The results of this test are shown in Figure 4.15, below. The obstacles that were farther out at 18 feet stand off distance had nearly identical trajectories. The obstacles at 7 feet stand off distance had the same final radial displacement, but the obstacle on the left side of the charge had a much greater vertical displacement and was even ejected from the water for a short period of time.

Trajectory of Obstacles
Mk-82 @ 6ft -- Beta 180
Test 13
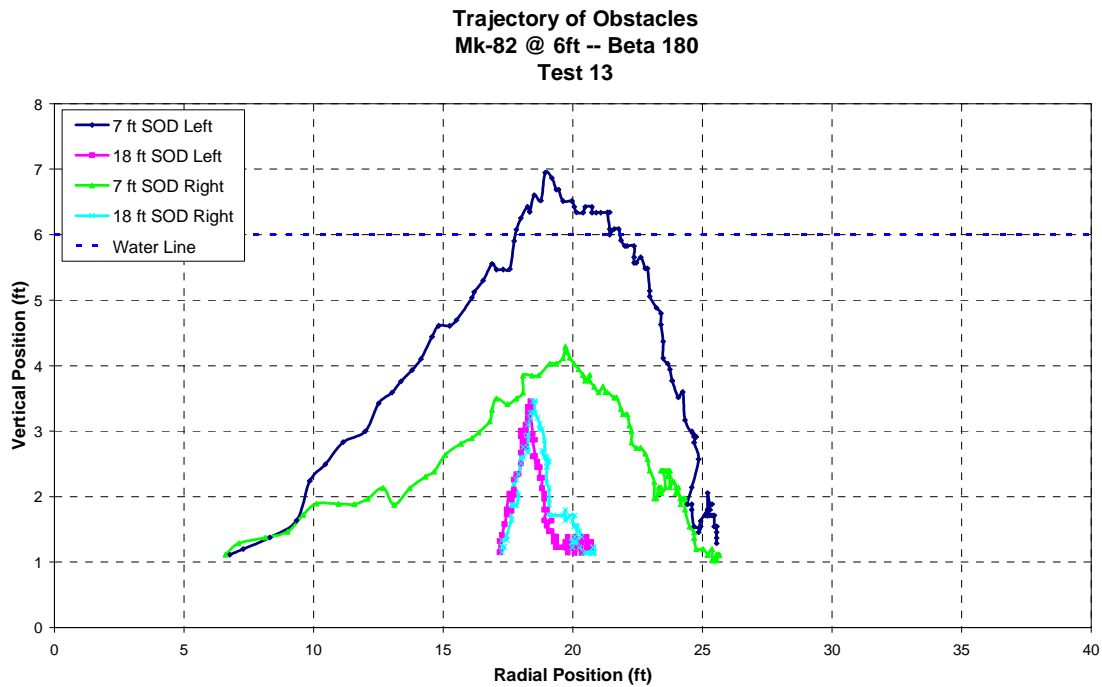
Figure 4.15 - Repeat of Test 11 with Four Total Obstacles

The next step, of course, is to compare the results of the repeat test (13) to the original

(11). Figure 4.16 shows the trajectory of the obstacle with 7 feet of stand off distance

from Test 11 and compares it to the trajectories of the two obstacles with the same stand

off distance in Test 13. The Left and Right labels in the legend are used to differentiate

between the two obstacles in Test 13. There is a fair amount of variance in the vertical

displacement of the obstacles (approximately 63% difference in maximum vertical

displacement). However, the final radial displacements are nearly the same.
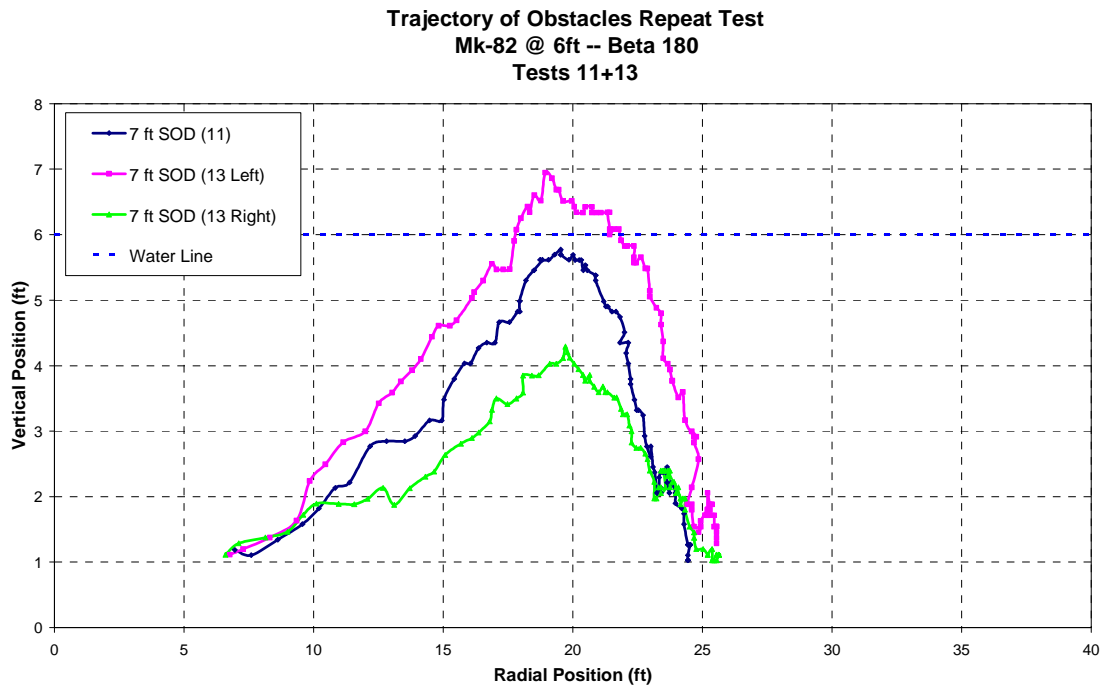
Figure 4.16 - Comparison of Repeat Test and Original Test with Obstacles at 7 feet SOD

Figure 4.17 shows the trajectory of the obstacle with 18 feet of stand off distance from Test 11 and compares it to the trajectories of the two obstacles with the same stand off distance in Test 13. Once again, it can be seen that the motion of the obstacles is nearly the same. The obstacle from Test 11 traveled slightly further in the radial direction and with a lower maximum vertical displacement than the obstacles from Test 13.

Taking the large data scatter often seen in explosive work into consideration, it can be said that these repeat tests show that the final radial displacement of obstacles are adequately repeatable and therefore scientifically significant. However, there is a large amount of variance in the maximum vertical displacement of obstacles. It would be beneficial to conduct more research to determine any possible causes of the large variance in maximum vertical displacements. It is important to keep in mind that the

65

motivation of this research is for the Navy to be able to move obstacles out of the projected path of a vehicle. The final radial displacement is the most appropriate measure of the effectiveness of using explosives to move obstacles. Therefore, it is more important to be able to achieve consistent radial displacements than it is to have consistent maximum vertical displacements.

Trajectory of Obstacles Repeat Test
Mk-82 @ 6ft -- Beta 180
Tests 11+13
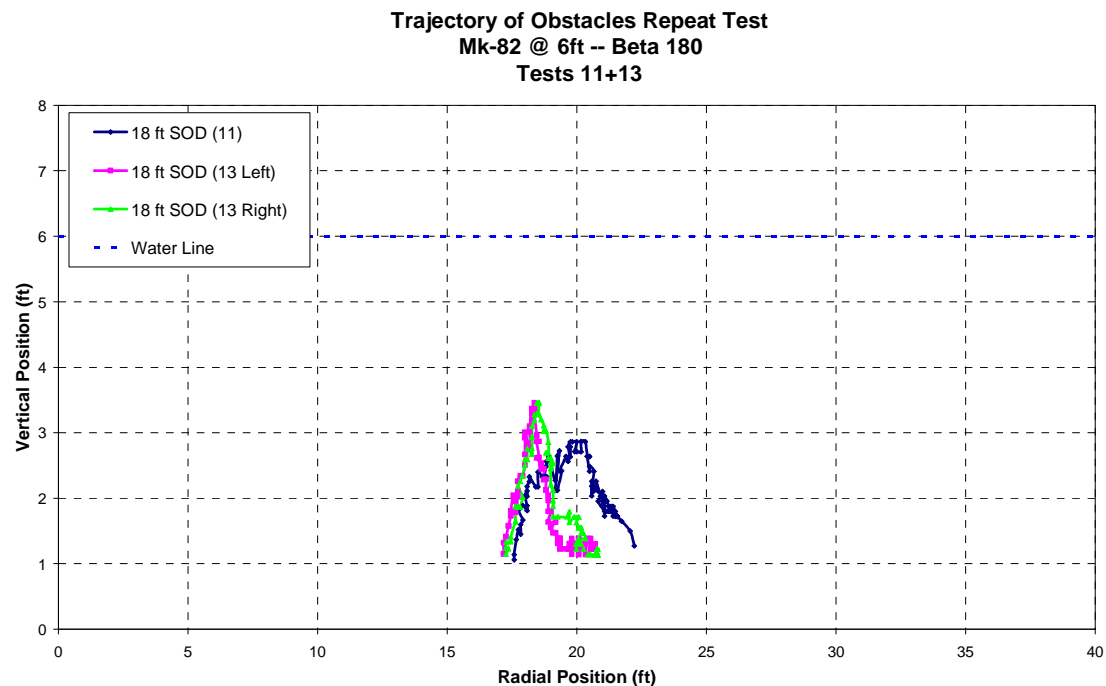
Figure 4.17 - Comparison of Repeat Test and Original Test with Obstacle at 18 ft SOD

4.10   Interference Between Obstacles

Since there were several obstacles in the container for every test, the interaction between obstacles should be considered when analyzing the data. It was assumed that the interaction between obstacles was minimal and would have no significant effect on the trajectories of each obstacle. In order to confirm this assumption, a test was performed

with a single obstacle at 7 feet stand off distance at the MK-84 at 6 feet depth of water test condition. Figure 4.18 compares the trajectory of the single isolated obstacle from Test 16 with the obstacle having the same stand off distance and orientation from Test 14 (See Figure 4.11). The two obstacles had similar trajectories, but the isolated obstacle had a slightly larger radial displacement (about 10% greater than the comparison obstacle) and traveled closer to the bottom surface. A difference of 10% is not considered to be a significant difference for explosive testing.   Therefore, it can be concluded that the interference between obstacles is likely very little or none at all.

Trajectory of Obstacles
Mk-84 @ 6ft -- Beta 0
Test 16
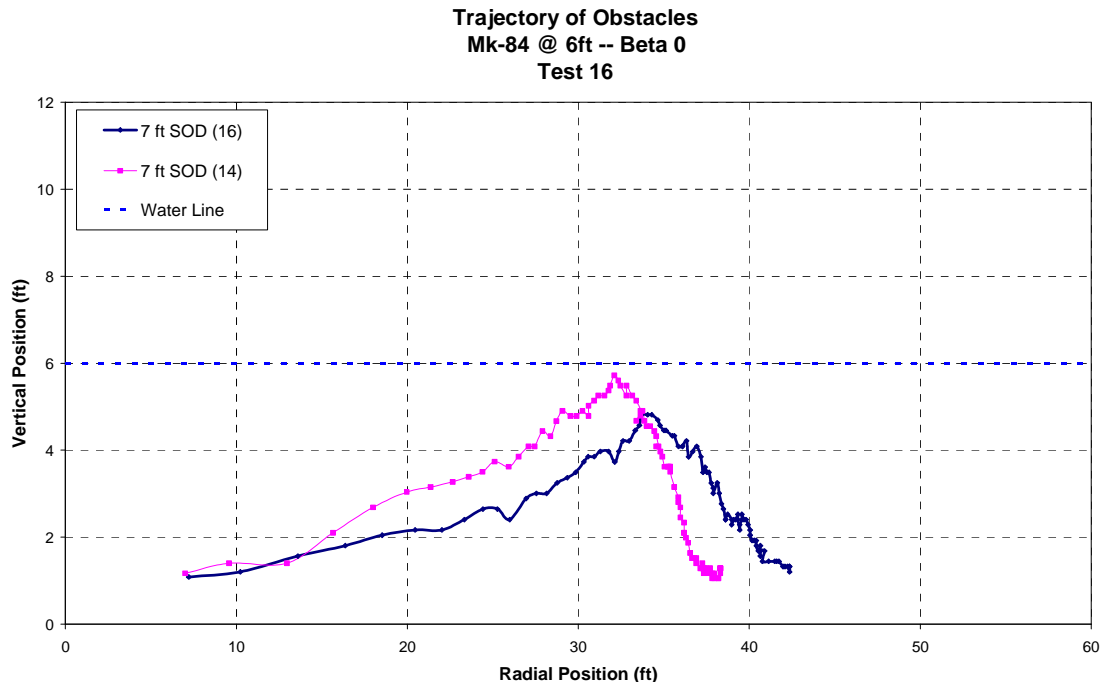
Figure 4.18 - Trajectory of Single Isolated Obstacle Compared to Obstacle from Test 14

4.11   Effect of Stand Off Distance on Obstacle Motion

As discussed in earlier sections, it is clear that the obstacles with shorter stand off distances have larger displacements than the obstacles with longer stand off distances. This can be clearly observed by examining the test results for each test condition in

Figure 4.7 through Figure 4.14. The obstacles with shorter stand off distances also usually travel higher than the other obstacles, but this is not always the case. However, the test data shows that when an obstacle with a longer stand off distance travels higher than the obstacles with a shorter stand off distance it is only higher by a small amount.

4.12   Effect of Orientation on Obstacle Motion

All of the obstacles were placed in one of two orientations (Beta 0 or Beta 180) during each test. A diagram of these orientations can be found in Figure 3.7 on page 42. Figure 4.19 through Figure 4.26 compare obstacles based on orientation with all other variables held constant.

Examination of the trajectories of obstacles for the MK-82 at 6 feet depth of water condition (Figure 4.19 and Figure 4.20) shows that the two obstacles with the greatest stand off distance (18 ft and 24 ft) had similar trajectories regardless of orientation. The two closest obstacles had slightly different trajectories for each orientation. Both the obstacles with Beta 180 orientation at 7 ft and 12 ft SOD seem to have a higher initial angle of ascent and end up traveling to a higher maximum vertical displacement. However, the difference in maximum vertical displacement is less than seen between obstacles compared in repeat tests. The obstacle at 7 feet stand off distance and Beta 180 orientation travels about 18% less in the radial direction than the same obstacle at Beta 0 orientation.

Trajectory of Obstacles - Orientation Comparison
Mk-82 @ 6ft - 7 and 18 SOD
Tests 9+11
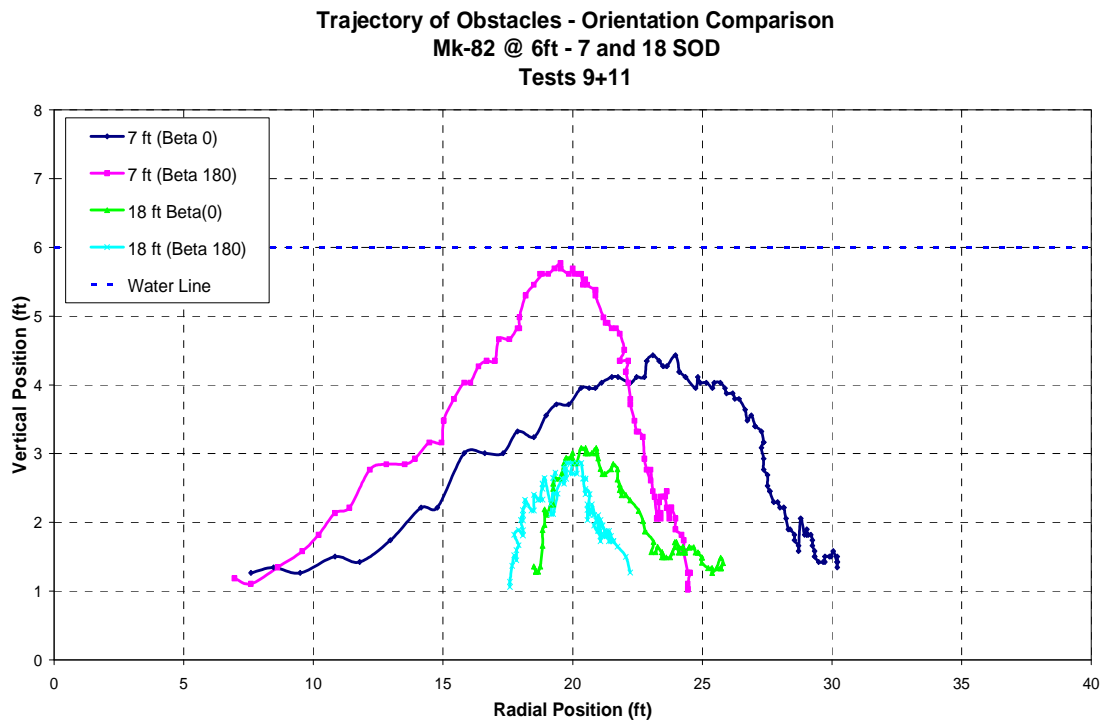
Figure 4.19 - MK-82 @ 6 Feet Orientation Comparison of Obstacles at 7 and 18 ft SOD

Trajectory of Obstacles - Orientation Comparison
Mk-82 @ 6ft - 12 and 24 SOD
Tests 10+12
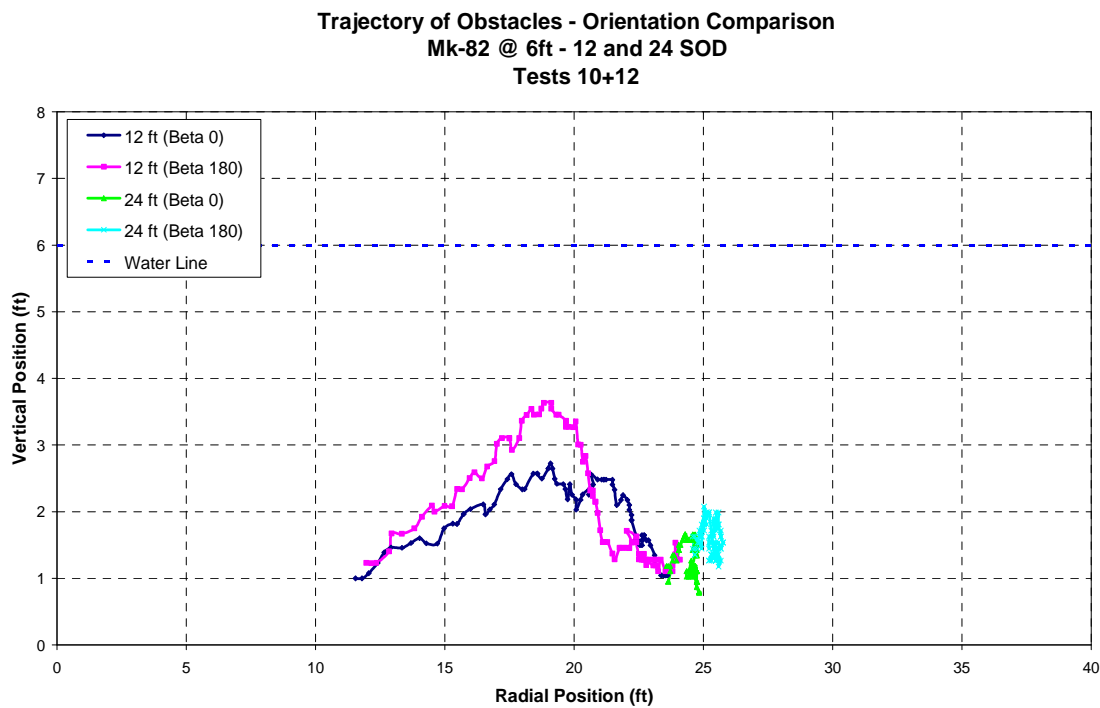
Figure 4.20 - MK-82 @ 6 Feet Orientation Comparison of Obstacles at 12 and 24 SOD

Figure 4.21 and Figure 4.22 compare the trajectories of obstacles for the MK-82 at 9 feet depth of water condition. In this case, the obstacles at 12 ft and 24 ft stand off distance have nearly identical trajectories when comparing the two orientations. However, at 7 ft and 18 ft stand off distance the obstacles with the Beta 180 orientation ascend with a steeper angle and travel to a higher vertical displacement than their Beta 0 counterparts. The final radial displacements of the Beta 180 obstacles at 7 and 18 ft stand off distance are about 10%-20% less than the Beta 0 counterparts. This is similar to the results discussed earlier for the MK-82 bomb at 6 feet depth of water.

Trajectory of Obstacles - Orientation Comparison
Mk-82 @ 9ft - 7 and 18 SOD
Tests 19+20
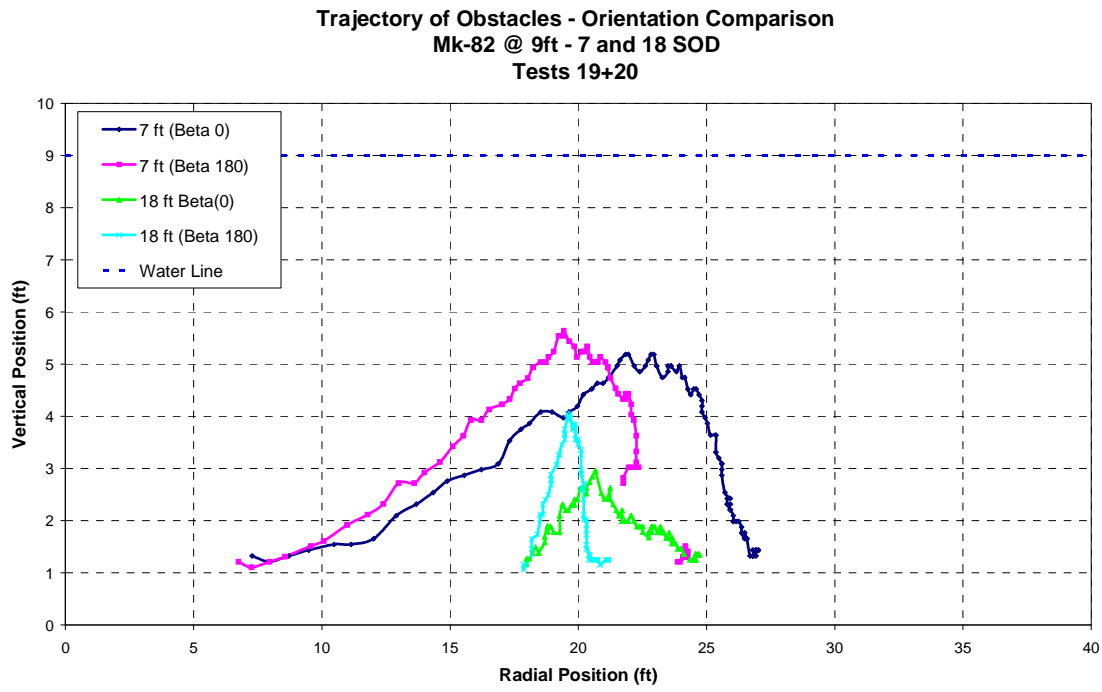
Figure 4.21 - MK-82 @ 9 Feet Orientation Comparison of Obstacles at 7 and 18 SOD

Trajectory of Obstacles - Orientation Comparison
Mk-82 @ 9ft - 12 and 24 SOD
Tests 19+20
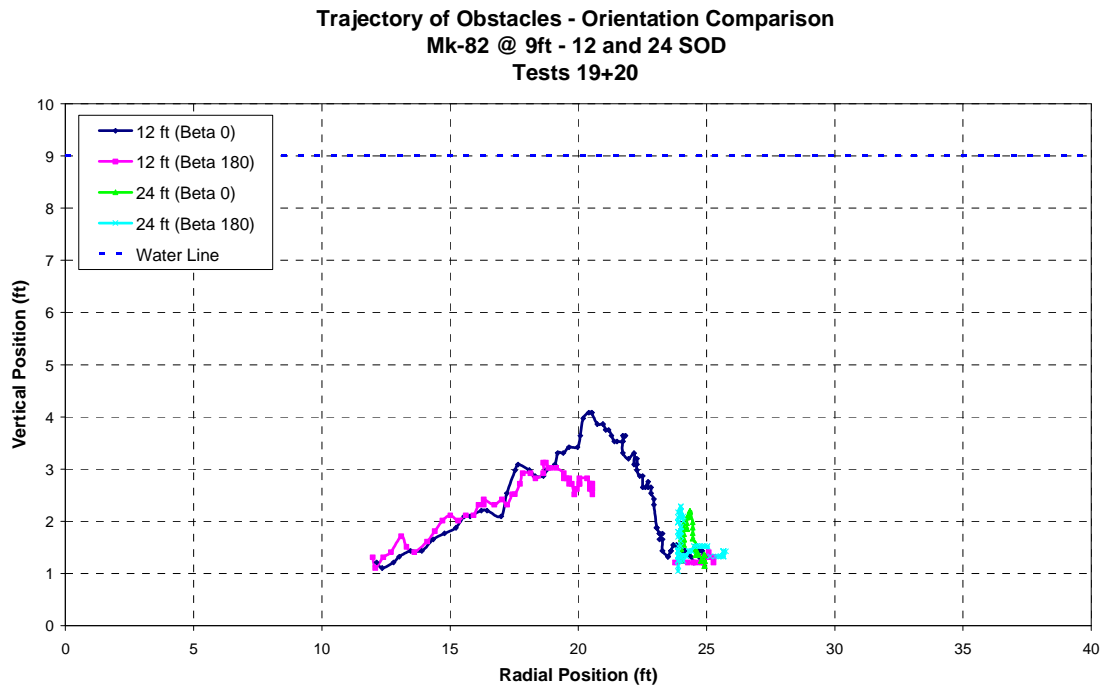
Figure 4.22 - MK-82 @ 9 Feet Orientation Comparison of Obstacles at 12 and 24 SOD

Figure 4.23 and Figure 4.24 compare the trajectories of obstacles for the MK-84 at 6 feet

depth of water condition. The obstacles farthest out with a 24 foot stand off distance

have nearly the same trajectory. As seen in the previous two cases, the obstacle at 7 feet

stand off distance ascends at a steeper angle and travels to a higher maximum elevation

than the obstacle with Beta 0 orientation. In this case the obstacle at 7 ft SOD and Beta

180 orientation also happens to be ejected from the water. Contrary to what would be

expected based on the results from the MK-82 simulations, the Beta 180 obstacles at 12 ft

and 18 ft SOD travel at a lower height and do not ascend as steeply as the Beta 0

obstacles.

Trajectory of Obstacles - Orientation Comparison
Mk-84 @ 6ft - 7 and 18 SOD
Tests 14+15
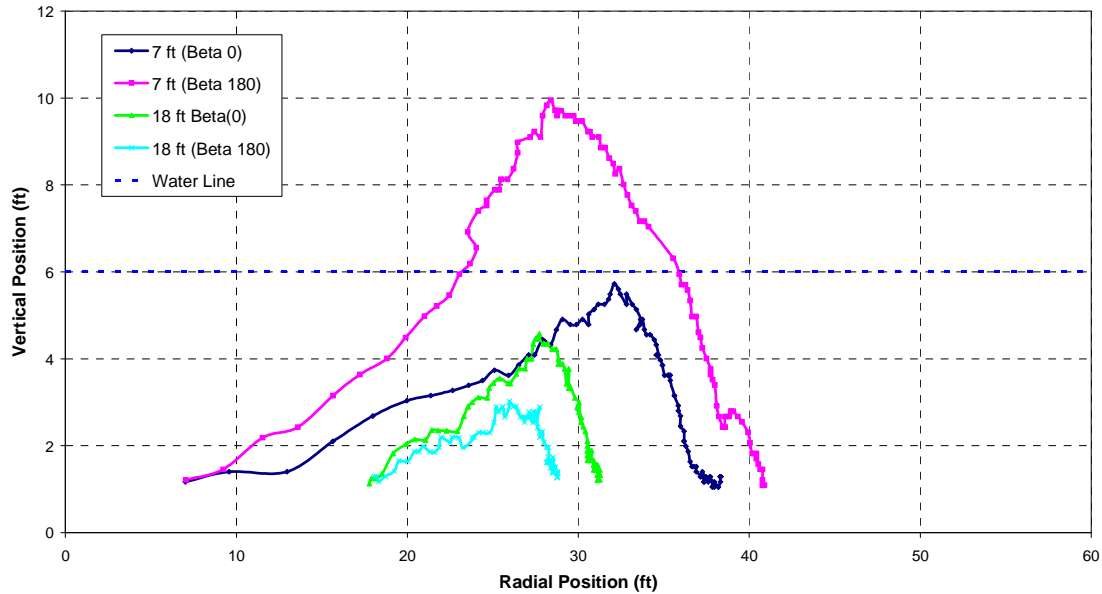
Figure 4.23 - MK-84 @ 6 Feet Orientation Comparison of Obstacles at 7 and 18 SOD

Trajectory of Obstacles - Orientation Comparison
Mk-84 @ 6ft - 12 and 24 SOD
Tests 14+15
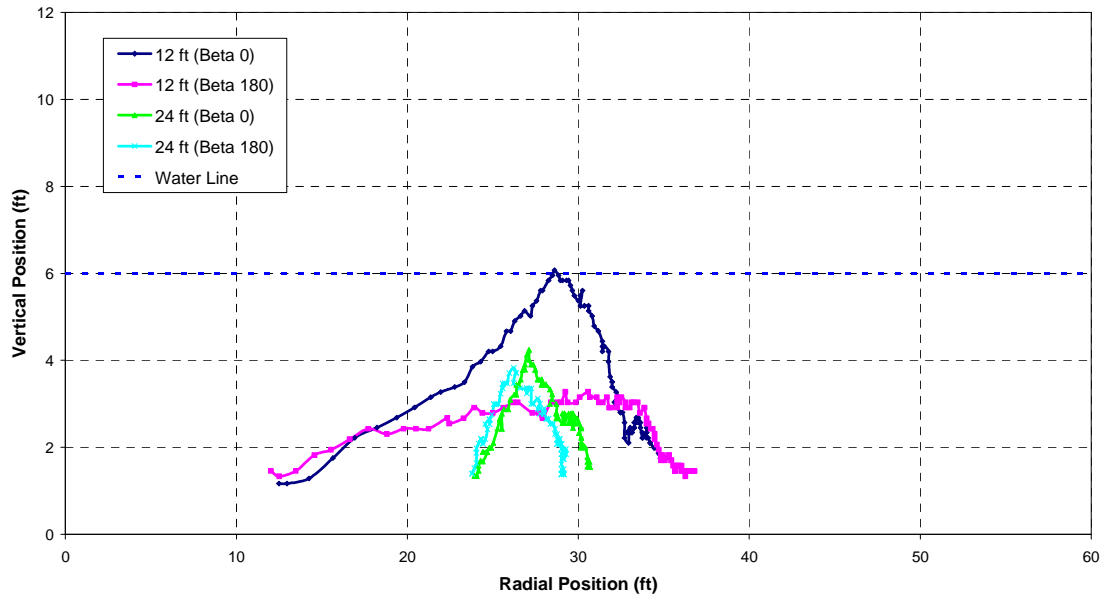
Figure 4.24 - MK-84 @ 6 Feet Orientation Comparison of Obstacles at 12 and 24 SOD

Figure 4.25 and Figure 4.26 compare the trajectories of obstacles for the MK-84 at 12 feet depth of water condition. The obstacles at 7 ft, 18 ft and 24 ft SOD have nearly identical trajectories. It could be said that the Beta 180 obstacle at 18 ft SOD has a slightly steeper angle of ascent than the Beta 0 obstacle, but there is not much difference. The obstacles with 12 ft stand off distance have nearly the same final radial position, but it appears that the obstacle with Beta 0 orientation had the steeper angle of ascent. It is also interesting to see that unlike any of the other tests, all of the obstacles for the MK-84 at 12 feet depth of water condition end up at approximately the same radial distance of forty feet.

Trajectory of Obstacles - Orientation Comparison
Mk-84 @ 12ft - 7 and 18 SOD
Tests 17+18
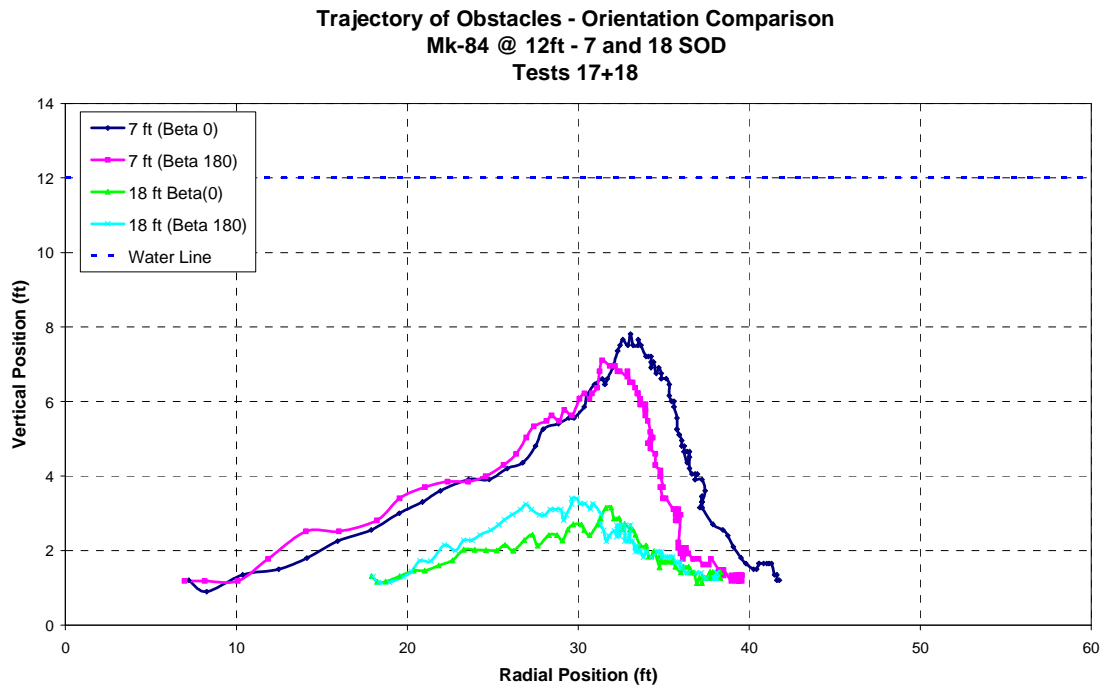
Figure 4.25 - MK-84 @ 12 Feet Orientation Comparison of Obstacles at 7 and 18 SOD
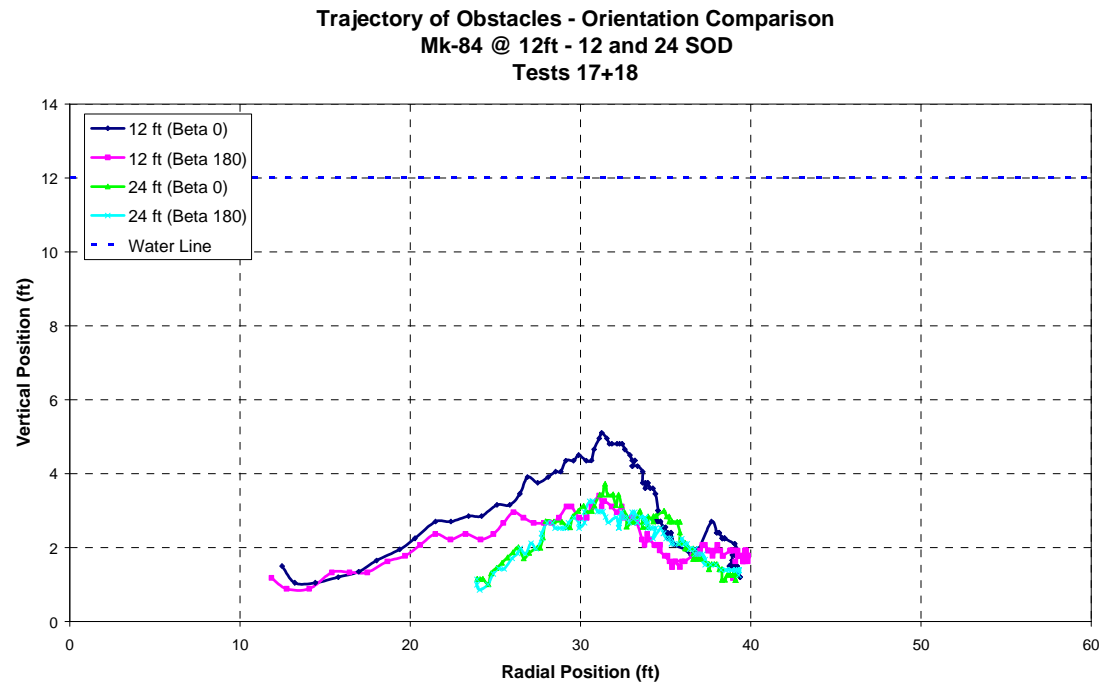
Figure 4.26 - MK-84 @ 12 Feet Orientation Comparison of Obstacles at 12 and 24 SOD

In general, it cannot be concluded that the orientation of an obstacle has a significant

effect on the resulting trajectory. Although some differences were noted upon

examination of the figures in this section, the differences were not large when compared

to the data in Figure 4.16 (page 65) where trajectories of repeated tests were compared.

The observed differences were also not consistent throughout all of the tests. At best, it

can be said that the differences in trajectory due to orientation were consistent for the

tests simulating MK-82 bombs. In all of these tests the obstacles with Beta 180

orientation either had the same trajectory or a trajectory with a steeper angle of ascent. In

order to gain a better understanding of how the obstacle orientation affects the results

more data would need to be collected and more tests would have to be repeated.

4.13 Effect of Depth of Water on Obstacle Motion

The MK-82 and MK-84 bombs were each simulated at two depths of water. The MK-82 was simulated for six feet and nine feet of water and the MK-84 was simulated for six feet and twelve feet of water. Figure 4.27 through Figure 4.34 compare the trajectories of the obstacles when all variables except for depth of water are held constant.

Figure 4.27, Figure 4.28, Figure 4.29 and Figure 4.30 compare the trajectories of obstacles in tests that simulated the MK-82 bomb. These trajectory plots show that the obstacles had similar trajectories regardless of the depth of water. If depth of water does play a role, then perhaps the difference between nine feet and six feet is not large enough to observe the difference in motion.
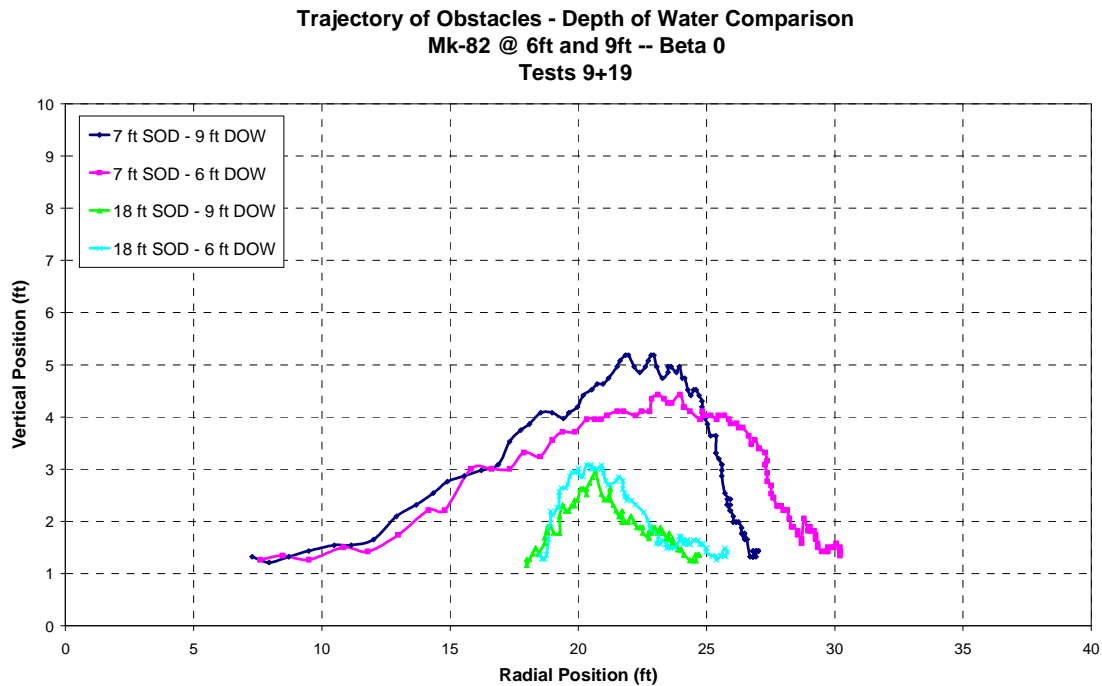
Figure 4.27 - MK-82 Depth of Water Comparison for Beta 0 Obstacles at 7 and 18 SOD

75

Trajectory of Obstacles - Depth of Water Comparison
Mk-82 @ 6ft and 9ft -- Beta 0
Tests 10+19
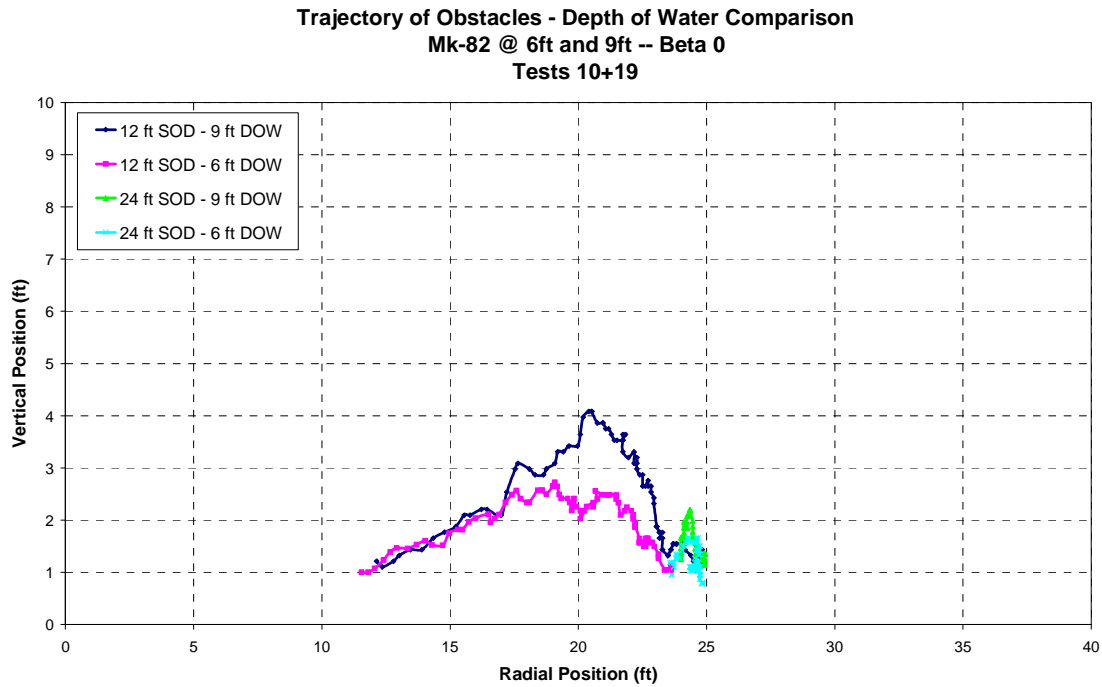
Figure 4.28 - MK-82 Depth of Water Comparison for Beta 0 Obstacles at 12 and 24 SOD

Trajectory of Obstacles - Depth of Water Comparison
Mk-82 @ 6ft and 9ft -- Beta 180
Tests 11+20
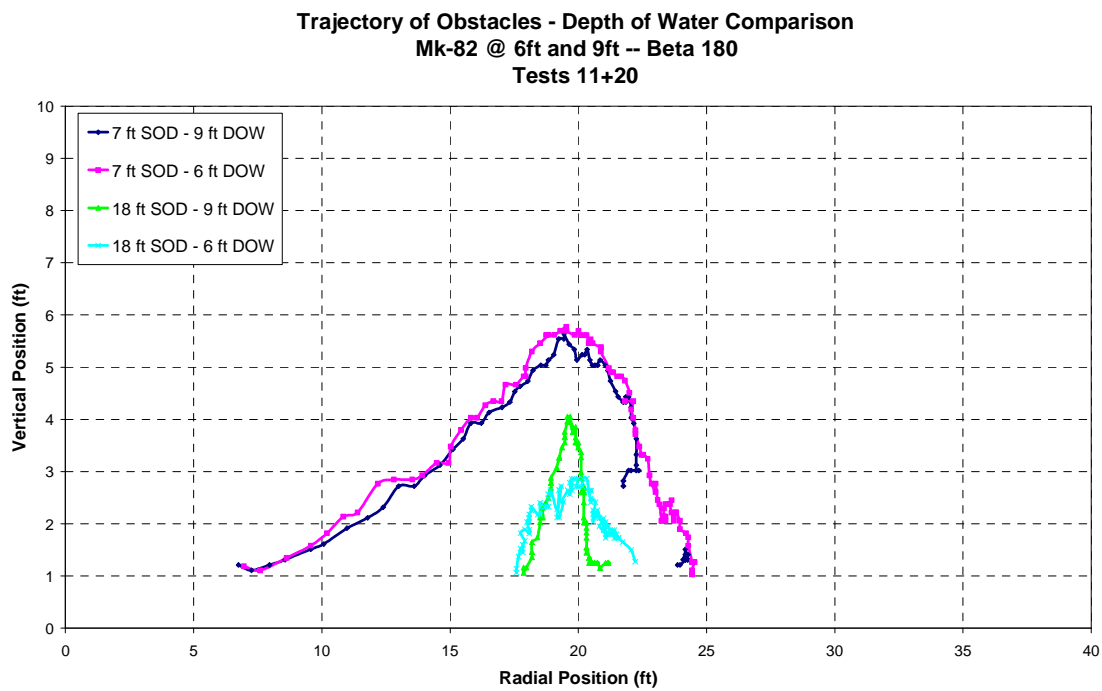
Figure 4.29 - MK-82 Depth of Water Comparison for Beta 180 Obstacles at 7 and 18 SOD

76
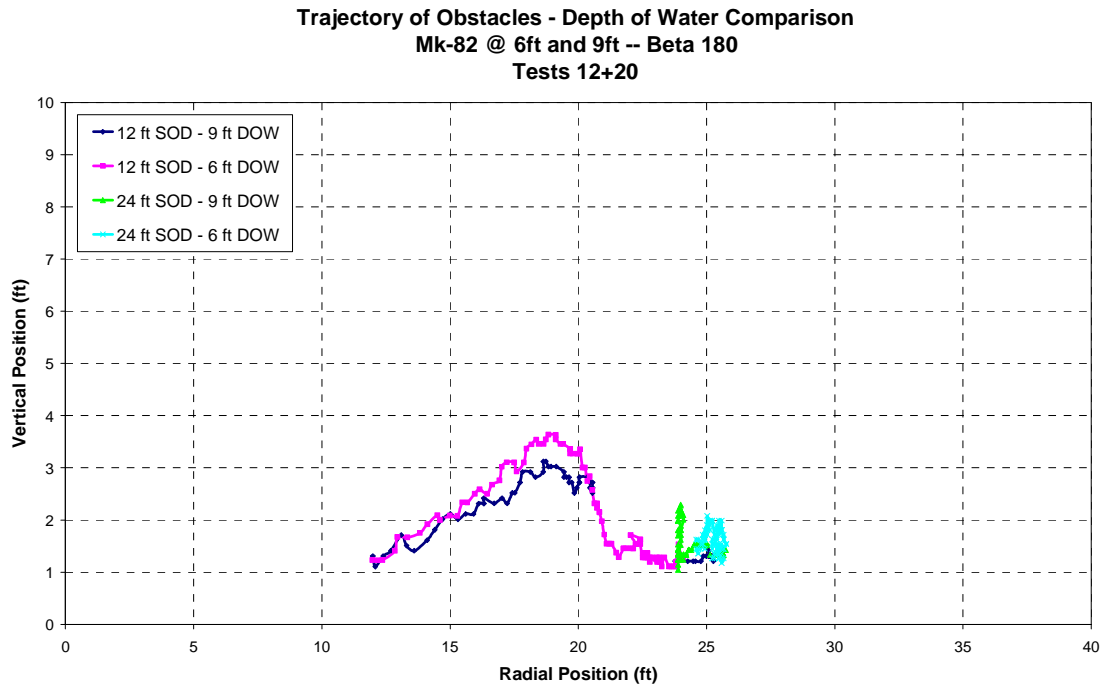
Figure 4.30 - MK-82 Depth of Water Comparison for Beta 180 Obstacles at 12 and 24 SOD

Figure 4.31, Figure 4.32, Figure 4.33 and Figure 4.34 compare the trajectories of

obstacles in tests that simulated the MK-84 bomb. The obstacles with seven feet and

twelve feet stand off distance have similar trajectories in both depths of water. Although

the trajectories for the close-in obstacles are similar, there does seem to be slightly more

variation between the trajectories of the close-in obstacles in the MK-84 tests than there

is in the MK-82 tests. Also, the obstacles at 18 feet and 24 feet stand off distance seem to

be affected significantly by the depth of water of the test. In each of the four figures

below, it can be seen that the farther-out obstacles with the 12 feet depth of water

condition have approximately twice as much radial displacement as the obstacles with the

six feet depth of water condition.

The difference in radial displacement between obstacles at 18 and 24 feet stand off distance can also be observed in Figure 4.35 on page 82. The blue triangles and plus signs are data for the MK-84 at twelve feet depth of water and the blue squares and x's are data for the MK-84 at six feet depth of water. It can be clearly seen on this plot that the obstacles with 18 and 24 feet stand off distance from the twelve feet depth of water tests had a greater displacement than the corresponding obstacles in the six feet depth of water tests.

Trajectory of Obstacles - Depth of Water Comparison
Mk-84 @ 6ft and 12ft -- Beta 0
Tests 14+17
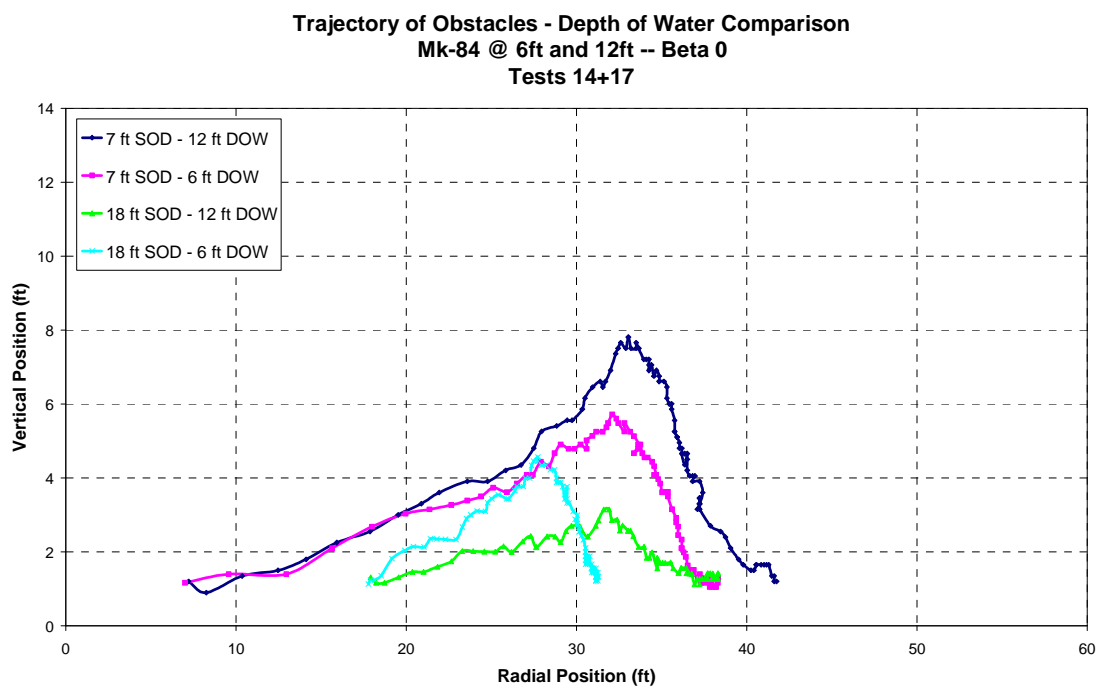
Figure 4.31 - MK-84 Depth of Water Comparison for Beta 0 Obstacles at 7 and 18 SOD

Trajectory of Obstacles - Depth of Water Comparison
Mk-84 @ 6ft and 12ft -- Beta 0
Tests 14+17
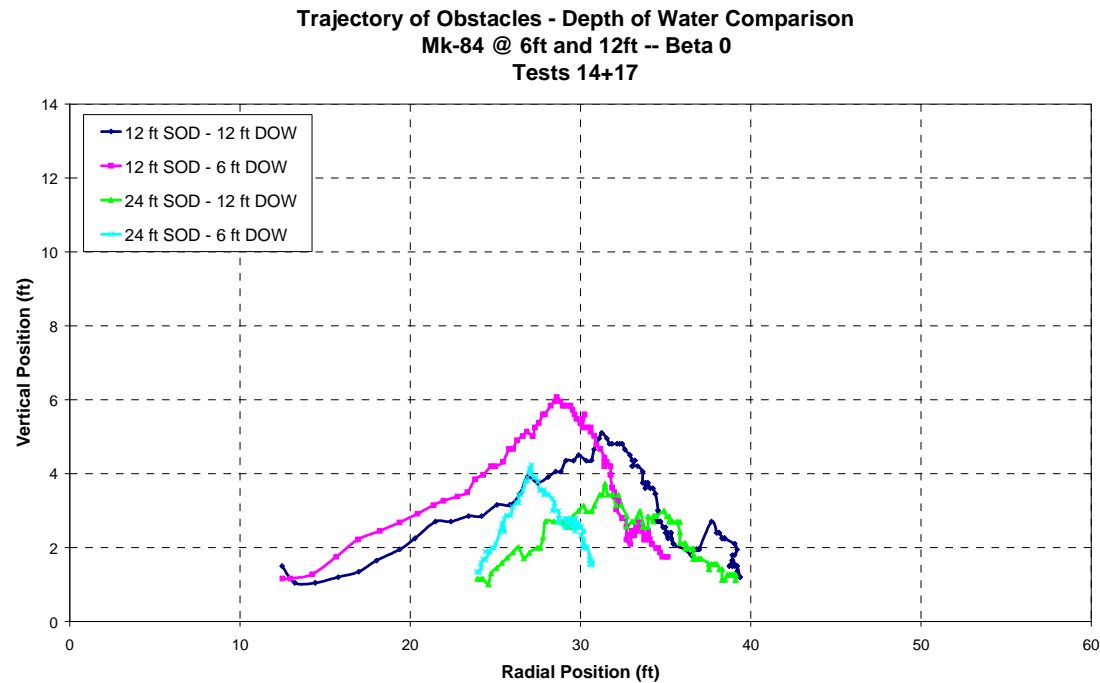
Figure 4.32 - MK-84 Depth of Water Comparison for Beta 0 Obstacles at 12 and 24 SOD

Trajectory of Obstacles - Depth of Water Comparison
Mk-84 @ 6ft and 12ft -- Beta 180
Tests 15+18
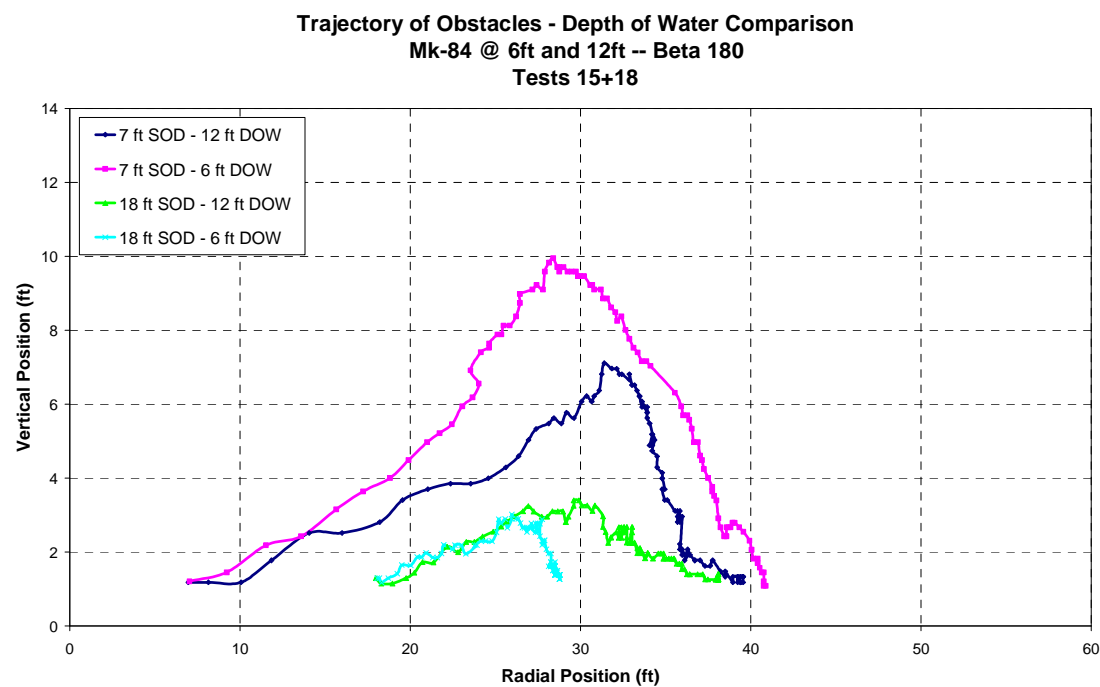
Figure 4.33 - MK-84 Depth of Water Comparison for Beta 180 Obstacles at 7 and 18 SOD

Trajectory of Obstacles - Depth of Water Comparison
Mk-84 @ 6ft and 12ft -- Beta 180
Tests 15+18
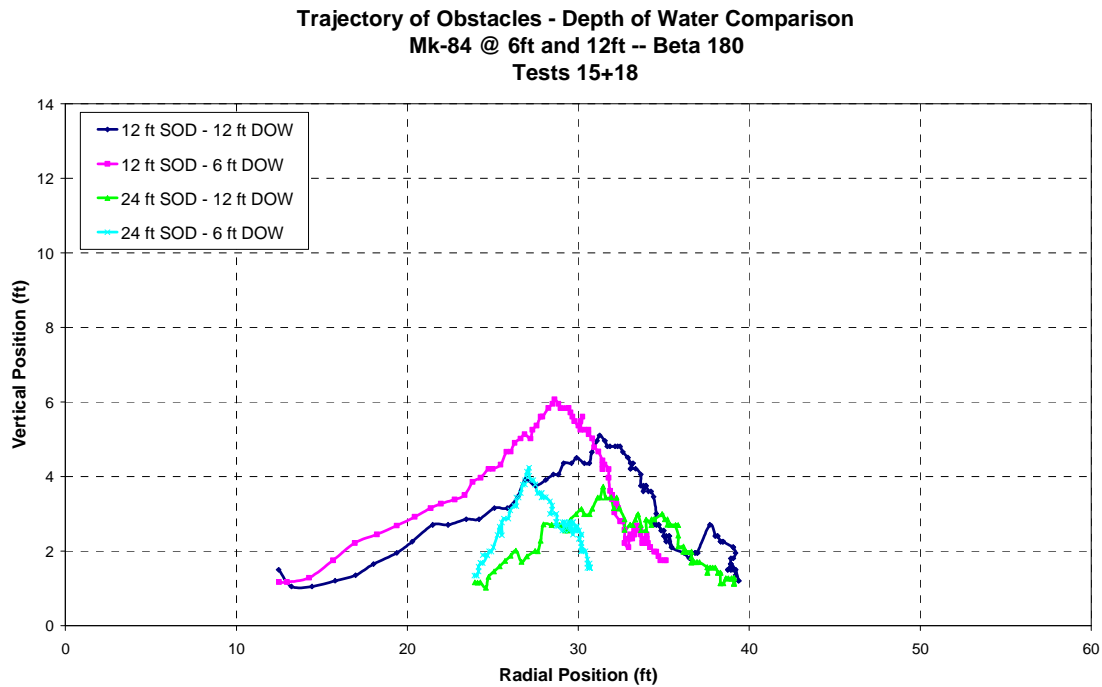
Figure 4.34 - MK-84 Depth of Water Comparison for Beta 180 Obstacles at 12 and 24 SOD

An investigation of how the depth of water affects the trajectories of the obstacles shows that there was no significant difference in the trajectories due to depth of water for the MK-82 bomb simulations. However, the MK-84 bomb simulations showed that the obstacles with a greater initial stand off distance (18 ft and 24 ft) tend to travel more in the radial direction when the water depth is greater. It is possible that there would be a difference in trajectories due to water depth with the MK-82 bomb, but the tests conducted in this study simulated the MK-82 at only nine feet depth of water while the MK-84 was simulated in twelve feet depth of water. This disparity in test conditions could be the reason that no significant difference in trajectories was observed for the MK-82 tests.

4.14   Effect of Bomb Size on Obstacle Motion

The tests conducted in this study simulated two different explosive charges: the MK-82 and MK-84 general purpose bombs. More information on these bombs can be found in Section 1.2. One would expect that the larger MK-84 bomb would cause the obstacles to have a greater displacement than the smaller MK-82 bomb.

Figure 4.35 shows the final displacement of obstacles as a function of initial stand off distance. The red markers are data for obstacles from MK-82 tests and the blue markers are data for MK-84 tests. It is clear that the MK-84 simulated bomb displaced obstacles further than the MK-82 bomb. As expected, the bomb with more explosive material causes obstacles to move further away from the point of detonation.
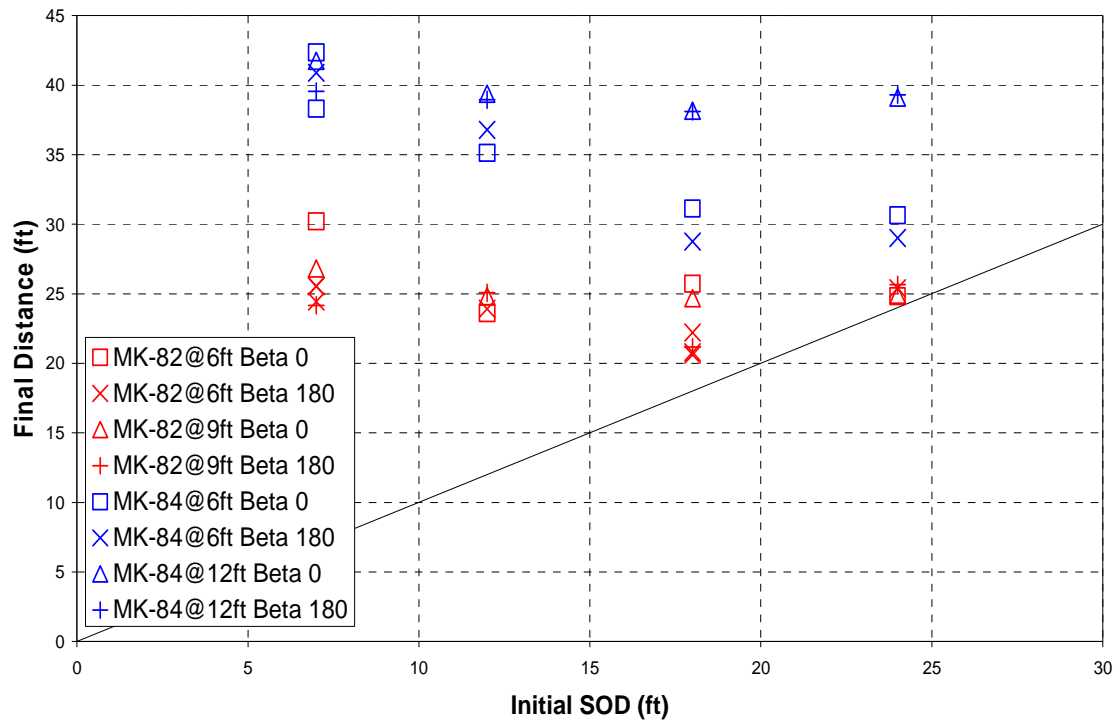
Figure 4.35 - Plot of Final Distance vs Initial Stand Off Distance for All Tests

Chapter 5 – Comparison of Data to Other Studies

5.1   Introduction

In order to test the validity of the Low Pressure scaling theory proposed by McDonald [3] the results of this study must be compared to results of other studies where tests with the same conditions were conducted at a different scale. Two such sources of data are available at this time: the tests conducted by SRI International at the $1/12^{th}$ scale [13] and full scale tests organized by the Panama City Division of the Naval Surface Warfare Center. By scaling all of the results to full scale and comparing data from the different studies, the validity of the Low Pressure scaling theory can be examined. In theory, one would expect to have the same results regardless of the scale factor when comparing data.

5.2   Comparison to SRI Study

SRI International reported the results of a study on underwater obstacle motion in March 2006 [13]. The SRI study conducted tests using both Hopkinson and Low Pressure scaling methods, but the majority of their work was done using the Hopkinson method. Their study also involved both tetrahedron and hedgehog shaped obstacles whereas the tests described in Chapter 4 only used tetrahedron obstacles. Only the tests with Low Pressure scaling that involved tetrahedron shaped obstacles will be compared in this section.

A limited number of trajectory plots are available for the SRI tests. The test results described in Chapter 4 will be compared to the available trajectory plots from SRI that have matching test conditions. Data from both studies have been scaled up to full scale

measurements so that they can be easily compared. Figure 5.1 through Figure 5.16 compare trajectories of obstacles in SRI tests and the tests in this study (Chapter 4). The tests reported in Chapter 4 are labeled with the "UMD" prefix in the legend of each graph. There are four plots for each simulation of a specific bomb size, water depth and obstacle orientation. The first plot shows the trajectories of all obstacles from SRI and UMD tests that have the bomb size, water depth and obstacle orientation in common. The next three plots break down the first plot and show the data for an obstacle at a given stand off distance so that the results are easier to follow.

Figure 5.1 through Figure 5.4 compare results for an MK-82 bomb at six feet depth of water with all obstacles having the Beta 0 orientation. In this case, none of the obstacles were ejected from the water. It appears that the obstacles in the SRI and UMD tests had similar trajectories, except for some commonly occurring differences. One obvious discrepancy is that the obstacle at 18 feet SOD from the SRI test ended up closer to the location of the charge than it started. SRI reported that some obstacles would move back towards the location of the charge when the water began to flow back and fill the void created by the venting of explosive gases. The backwards motion of tetrahedron obstacles was not observed in UMD tests.
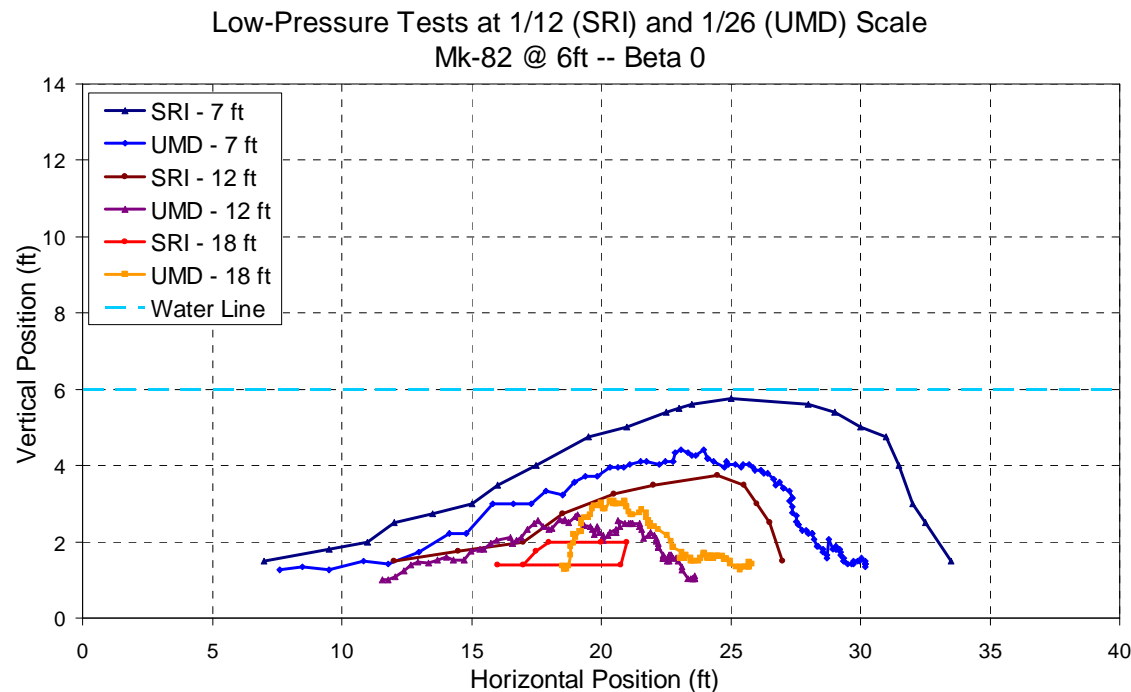
Figure 5.1 - Comparison of SRI/UMD Data for MK-82@6ft and Beta 0 Orientation
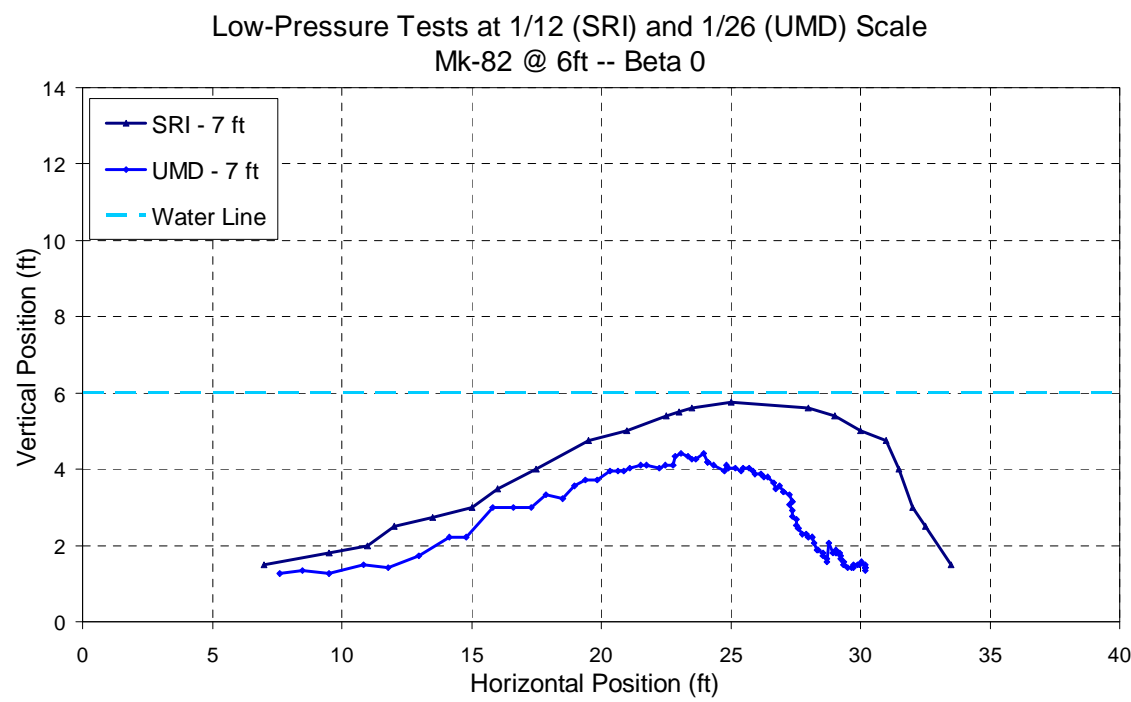
Figure 5.2 - Comparison of SRI/UMD Data for MK-82@6ft, 7ft SOD and Beta 0 Orientation
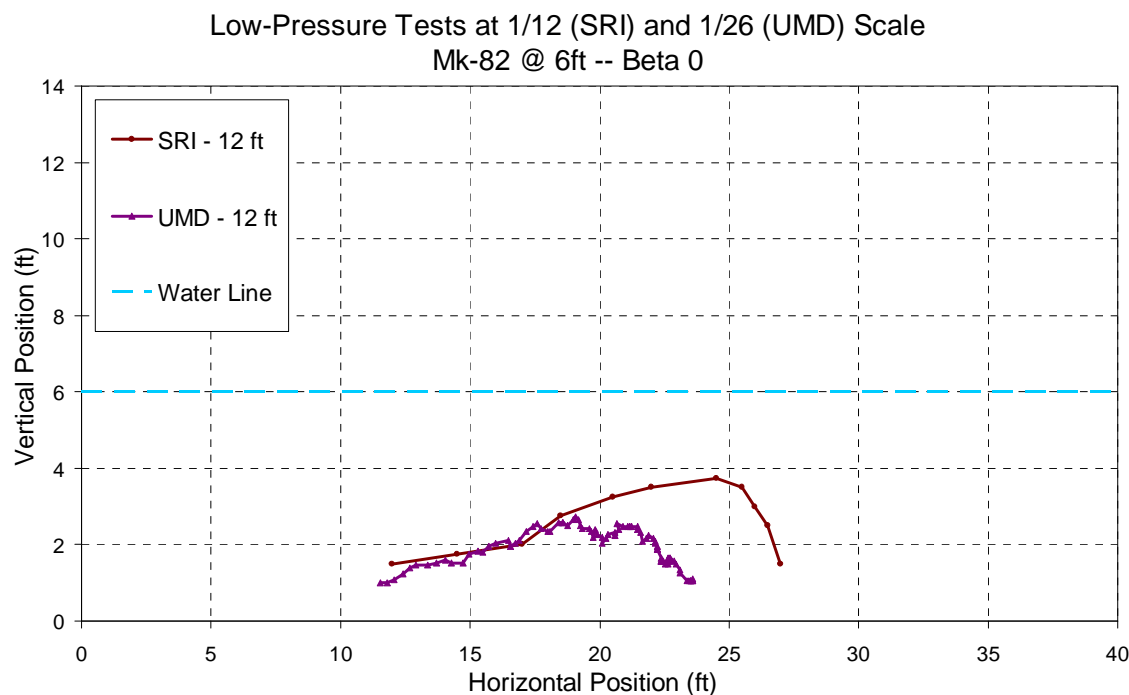
Figure 5.3 - Comparison of SRI/UMD Data for MK-82@6ft, 12ft SOD and Beta 0 Orientation
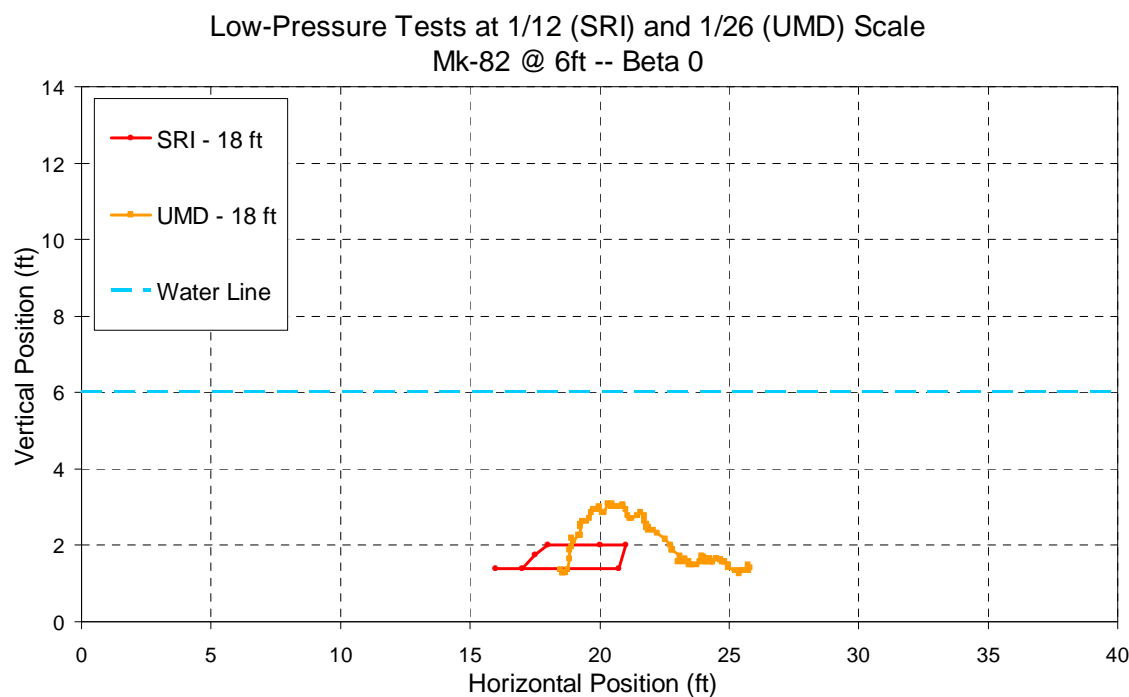
Figure 5.4 - Comparison of SRI/UMD Data for MK-82@6ft, 18ft SOD and Beta 0 Orientation

Figure 5.5 through Figure 5.8 compare results for an MK-82 bomb at six feet depth of water with all obstacles having the Beta 180 orientation. There are multiple sets of data available for two of the stand off distances from the UMD tests. The extra sets of data come from Test 14 which was a repeat test. The notation "R1" and "R2" used in the legends denotes data that came from this repeat test. This repeat test had a total of four obstacles; two at 7 feet stand off distance and two at 18 feet stand off distance. More information on this repeat test can be found in Chapter 4.

Unlike the Mk-82@6ft Beta 0 case, the MK-82@6ft Beta 180 condition did not result in similar trajectories for all obstacles. Multiple obstacles were ejected from the water for this set of conditions. The trajectory of the obstacles is similar for obstacles that did not get ejected. When comparing obstacles that were ejected, the trajectories are drastically different. It is no surprise that the ejected obstacles had the shortest stand off distance since it was found that obstacles with shorter stand off distances have greater radial displacements and maximum vertical displacements. As with the previous case, the obstacle from the SRI tests with 18 feet stand off distance was significantly affected by the backflow of water and ended up close to the original stand off distance. If the last portion of backwards travel by this obstacle is ignored then the trajectory is similar to the trajectories of the UMD obstacles.
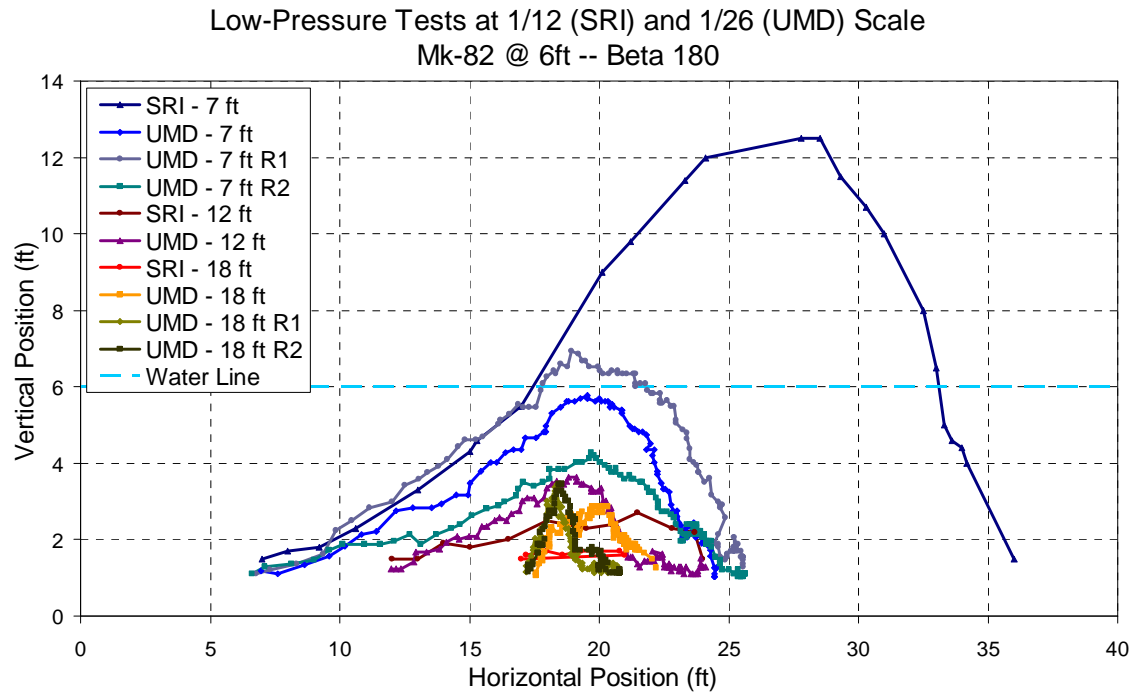
Figure 5.5 - Comparison of SRI/UMD Data for MK-82@6ft and Beta 180 Orientation
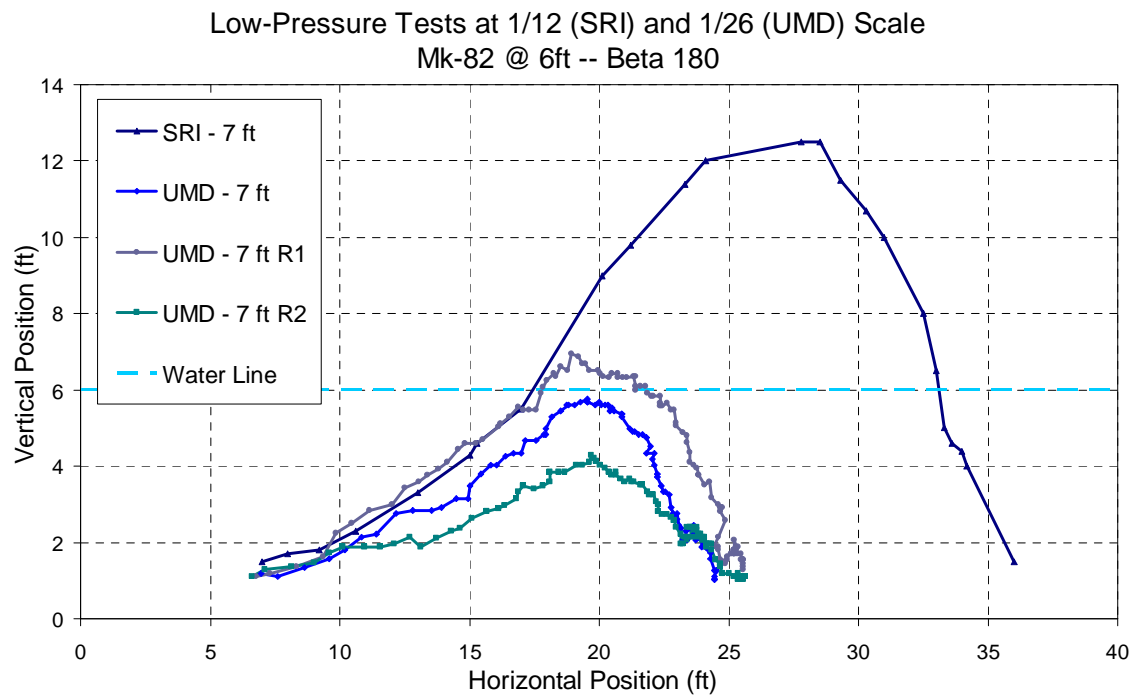
Figure 5.6 - Comparison of SRI/UMD Data for MK-82@6ft, 7ft SOD and Beta 180 Orientation
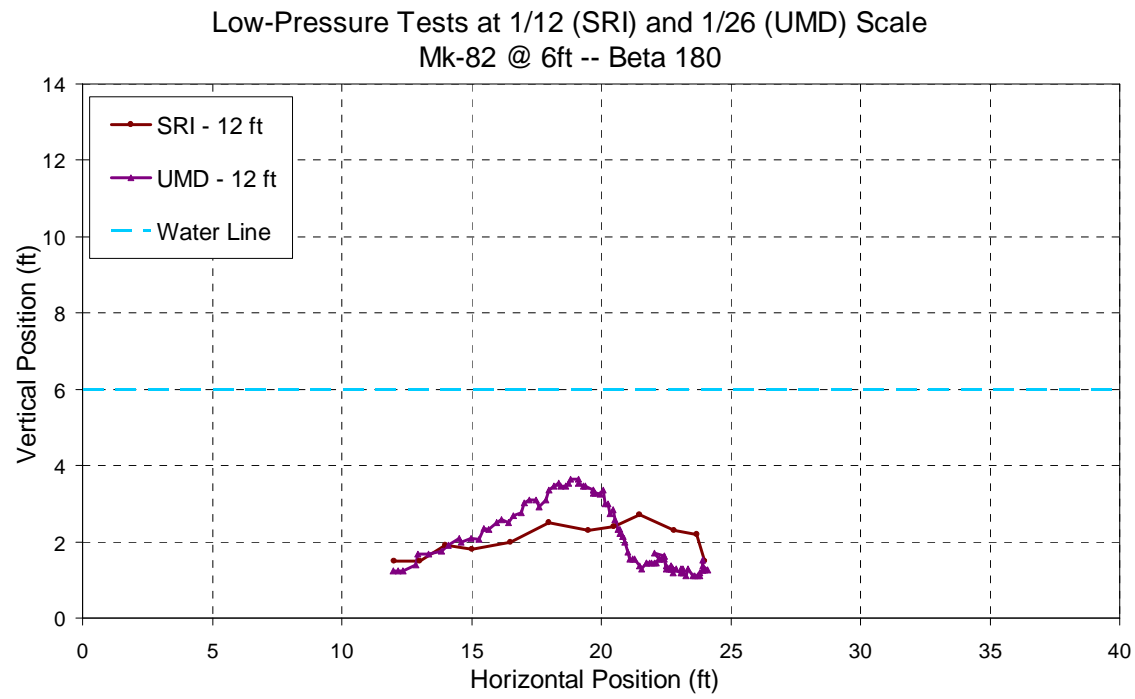
Figure 5.7 - Comparison of SRI/UMD Data for MK-82@6ft, 12ft SOD and Beta 180 Orientation
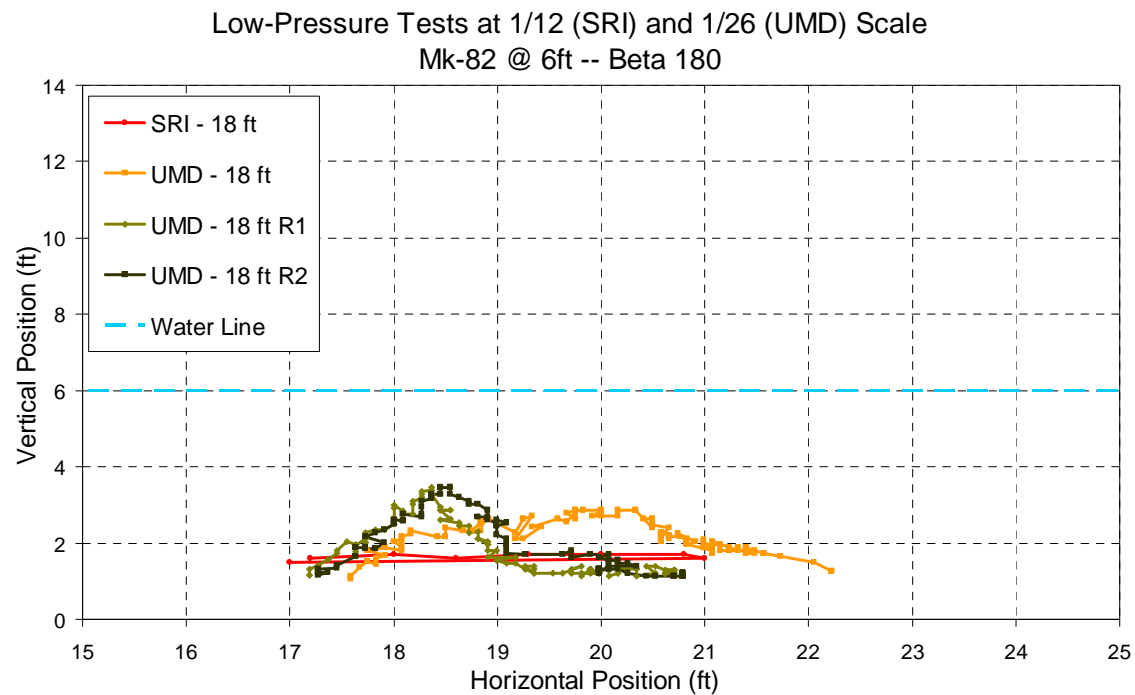
Figure 5.8 - Comparison of SRI/UMD Data for MK-82@6ft, 18ft SOD and Beta 180 Orientation

Figure 5.9 through Figure 5.12 compare results for an MK-84 bomb at six feet depth of water with all obstacles having the Beta 0 orientation. This test condition has one extra set of data for the UMD test at seven feet stand off distance. This is extra set of data is denoted with the suffix "R" and came from Test 16, which was a repeat test conducted to determine the effects of interaction between obstacles. More information on this test can be found in Chapter 4. As seen in the previous case, some obstacles were ejected from the water. The SRI obstacle at seven feet stand off distance had a much greater displacement than the UMD obstacles. The SRI obstacle at 12 feet stand off distance was also ejected, but was only out of the water for a brief period of time. Its trajectory was similar to the UMD obstacle. The SRI obstacle at 18 feet stand off distance had some backward travel as seen in previous cases, but it did not travel back as far as the other SRI obstacles in the MK-82 bomb simulations. Other than the travel due to backflow of water, the trajectory of the SRI and UMD obstacles with 18 feet SOD was similar.
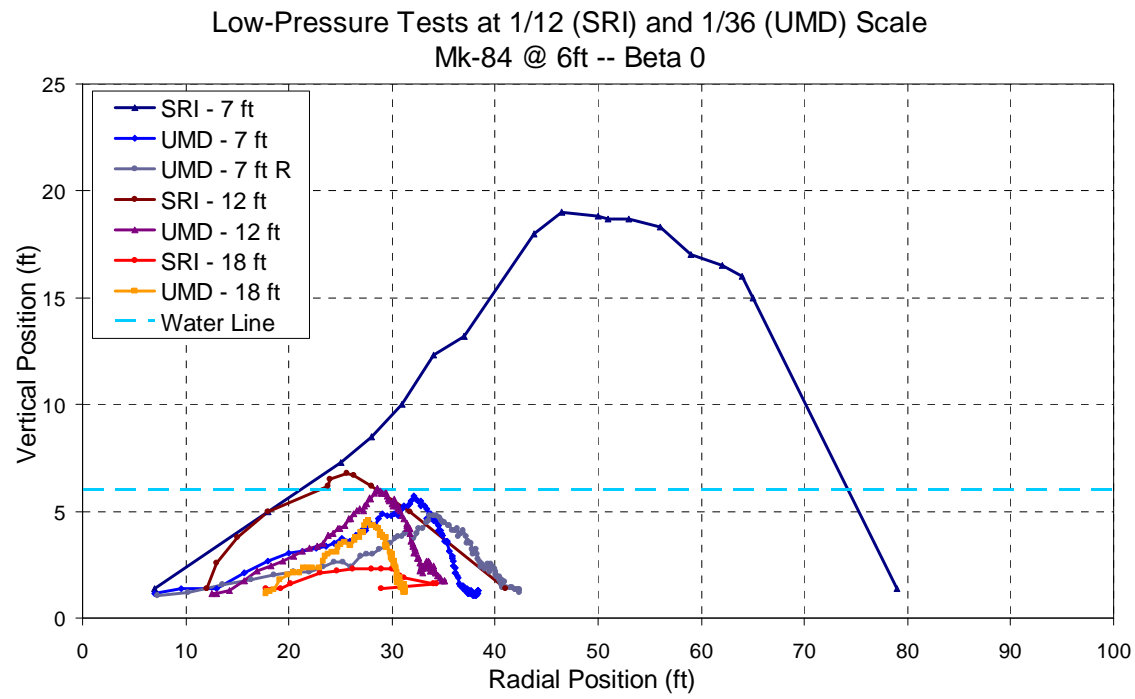
Figure 5.9 - Comparison of SRI/UMD Data for MK-84@6ft and Beta 0 Orientation
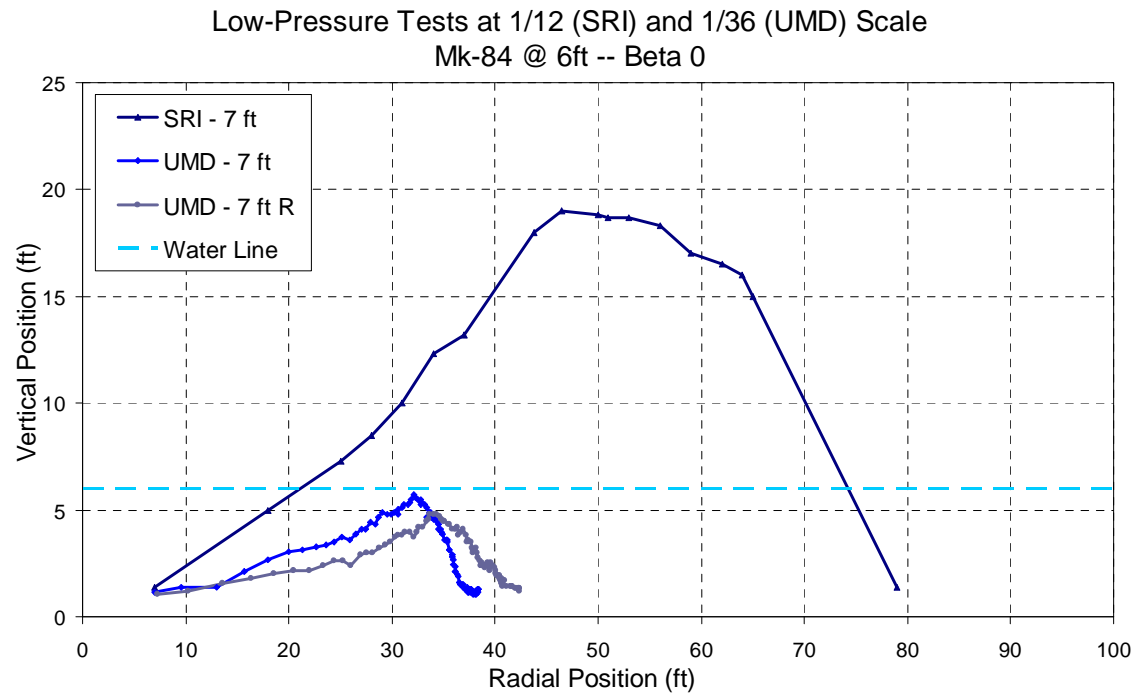
Figure 5.10 - Comparison of SRI/UMD Data for MK-84@6ft, 7ft SOD and Beta 0 Orientation
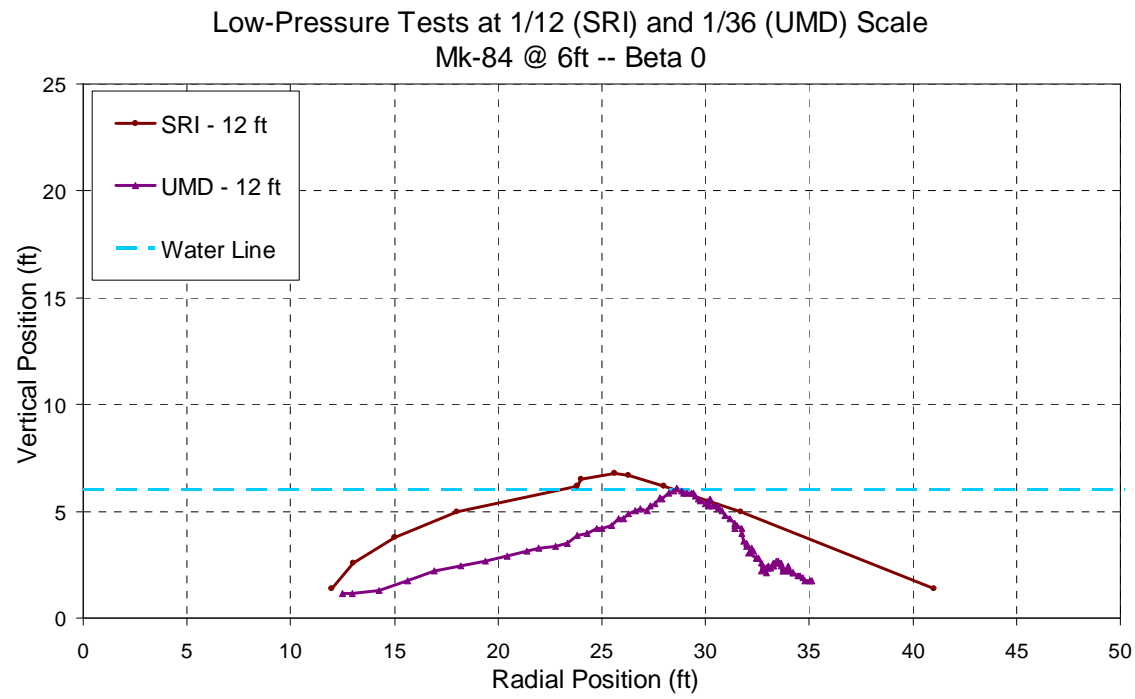
Figure 5.11 - Comparison of SRI/UMD Data for MK-84@6ft, 12ft SOD and Beta 0 Orientation
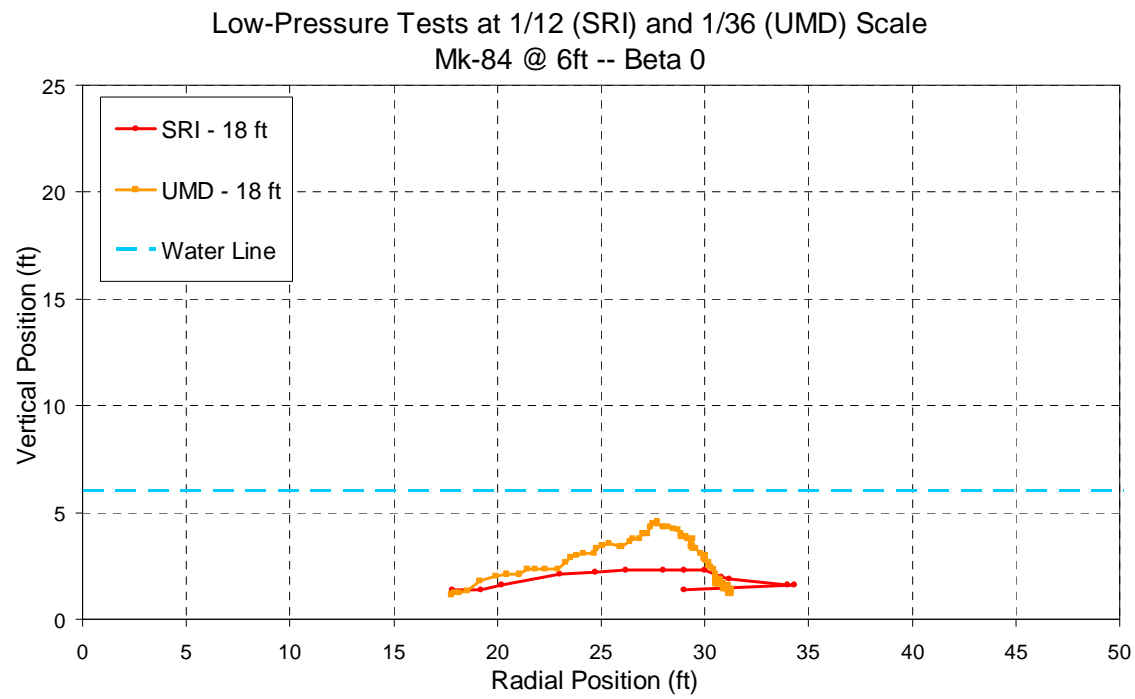
Figure 5.12 - Comparison of SRI/UMD Data for MK-84@6ft, 18ft SOD and Beta 0 Orientation

Figure 5.13 through Figure 5.16 compare results for an MK-84 bomb at six feet depth of water with all obstacles having the Beta 180 orientation. In this case, both the SRI and UMD obstacles at seven feet stand off distance were ejected from the water. Despite both being ejected, they did not have similar trajectories. The SRI obstacle was displaced more than twice the distance of the UMD obstacle. However, the obstacles with 12 feet and 18 feet stand off distance had similar trajectories. And as with all other cases, the SRI obstacle at 18 feet stand off distance had some backwards motion due to the water flowing back towards the point of detonation.
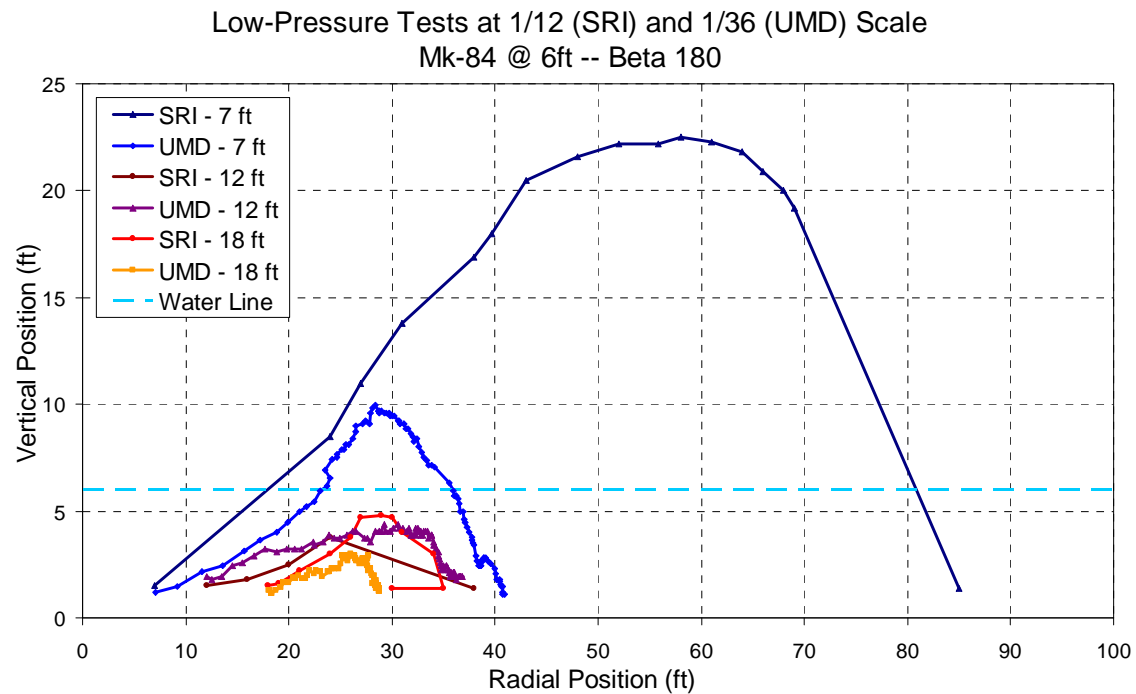
Figure 5.13 - Comparison of SRI/UMD Data for MK-84@6ft and Beta 180 Orientation
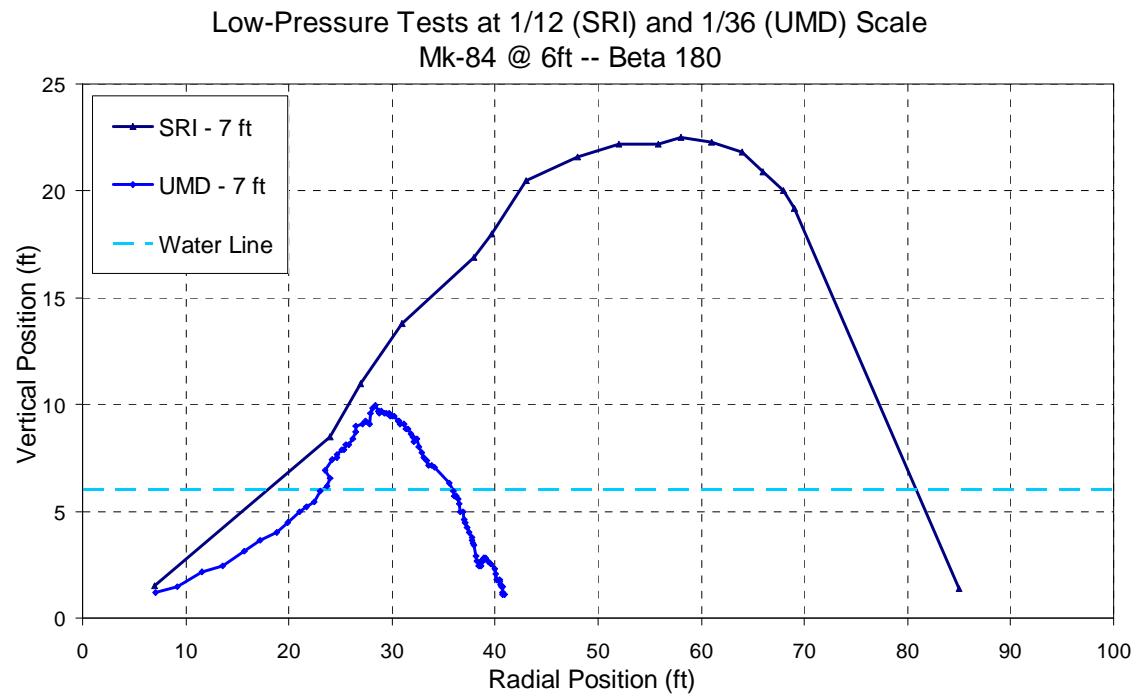
Figure 5.14 - Comparison of SRI/UMD Data for MK-84@6ft, 7ft SOD and Beta 180 Orientation
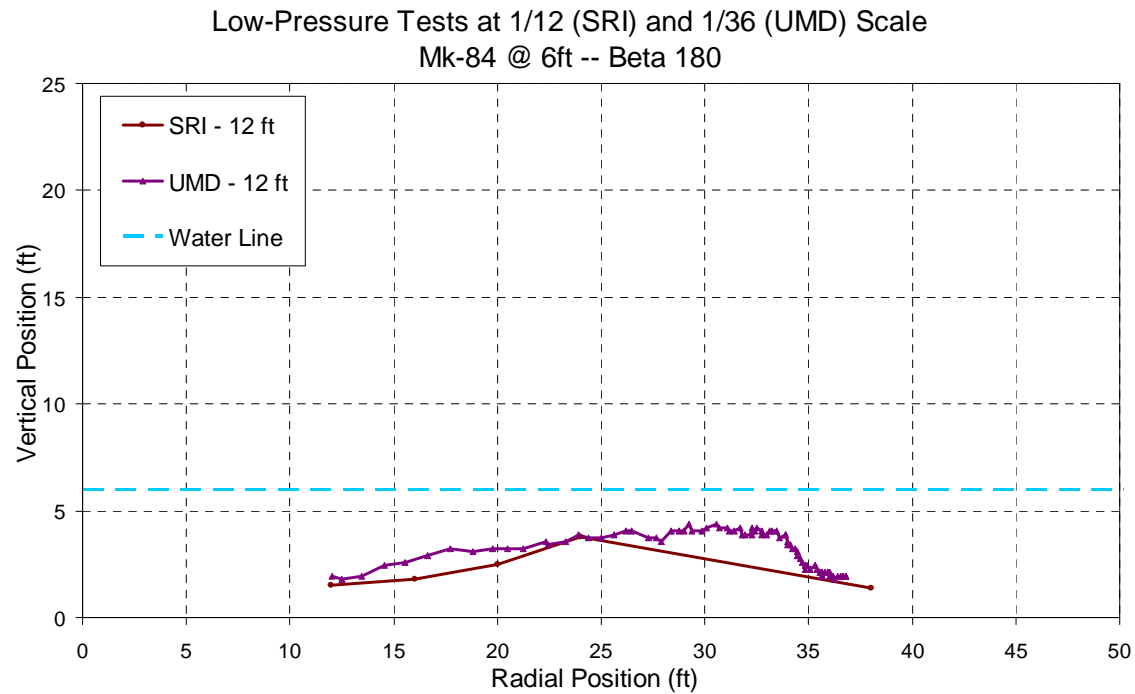
Figure 5.15 - Comparison of SRI/UMD Data for MK-84@6ft, 12ft SOD, Beta 180 Orientation
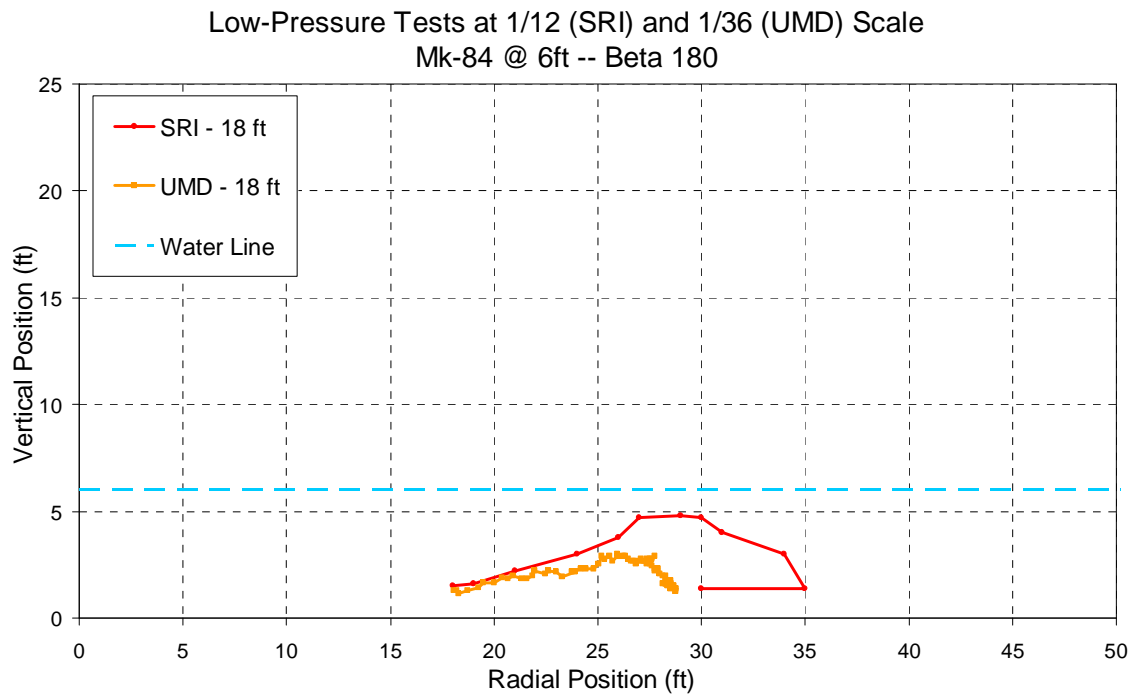
Figure 5.16 - Comparison of SRI/UMD Data for MK-84@6ft, 18ft SOD, Beta 180 Orientation

The comparison of obstacle trajectories between SRI and UMD tests shows that the data agree well for cases when the obstacles are not ejected from the water. Most of the obstacles that were ejected had the shortest stand off distance of seven feet, but the case with the MK-82 bomb at six feet depth of water and Beta 0 orientation did not result in the SRI obstacle at seven feet SOD being ejected from the water, and the SRI and UMD results matched well for this case. The author presumes that the Low Pressure scaling theory cannot apply to ejected obstacles because the atmospheric pressure has not been scaled. The atmospheric pressure should be proportional to the scaling factor and is therefore much greater than it should be for small scales. The high pressure (and therefore high density of air) could be restricting the motion of obstacles. When converting the small scale results to full scale, the full scale atmospheric pressure for UMD tests is much greater than for SRI tests and this could explain the greater distance

95

of travel for SRI obstacles that were ejected from the water. It was also observed for

every case of SRI tests that the obstacles at 18 feet stand off distance were affected by the

backflow of water.

It is helpful to compare the UMD results to the SRI results by plotting the final radial

position versus the initial stand off distance. Figure 5.17 and Figure 5.18 compare the

SRI data to UMD data for the MK-82 at 6 feet depth of water and MK-84 at 6 feet depth

of water, respectively. The plots only show data for obstacles that were not ejected from

the water. When obstacles are not ejected, the data is similar.

McDonald [3] makes a comparison of SRI and full scale radial displacements of

obstacles for the MK-82 at 6 ft depth of water condition. SRI values for obstacles at 7 ft

stand off distance were greater than the full scale results. Obstacles with 7 ft stand off

distance in SRI tests had approximately 25-33 ft of radial displacement and full scale

obstacles had approximately 18-25 ft of radial displacement. For obstacles with 12 and

18 feet stand off distance the SRI and full scale results matched well. However, there is

no indication of which SRI or full scale obstacles were ejected from the water. From the

trajectories shown in this section, it can be assumed that many of the SRI obstacles at 7

feet stand off distance were ejected. If full scale obstacles at 7 ft stand off distance were

not ejected, then this might explain why SRI results were higher for 7 feet stand off

distance.
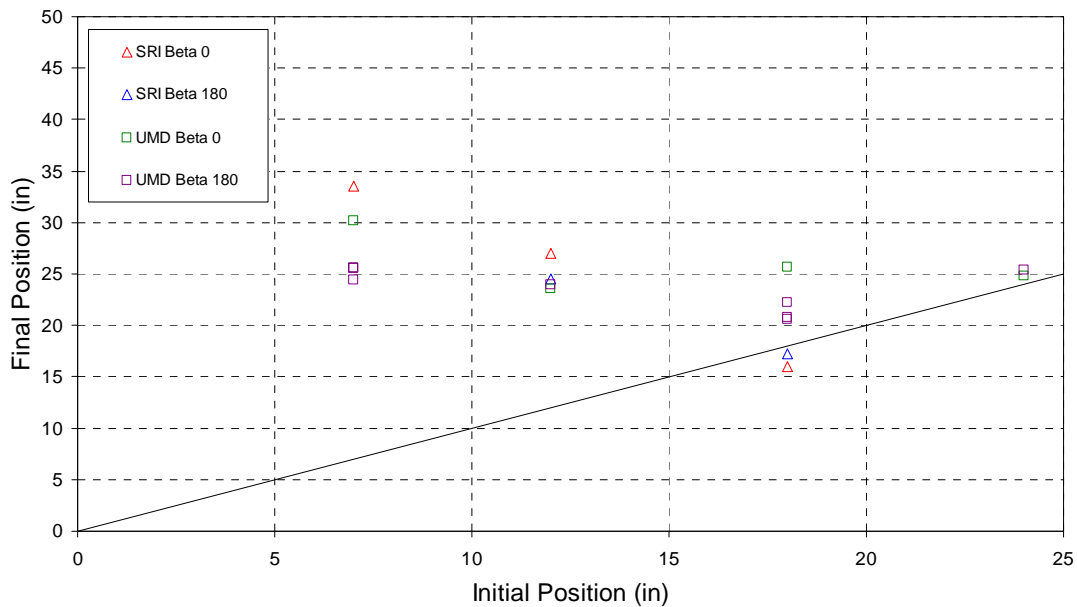
Figure 5.17 – Comparison of Data for SRI and UMD Tests at the MK-82 @ 6ft Condition
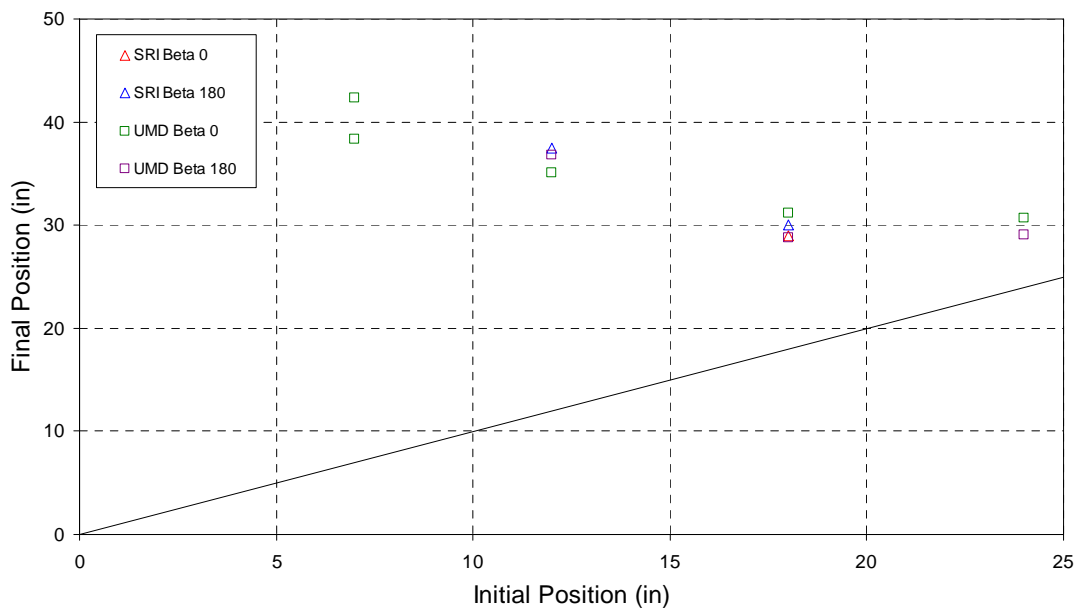
Figure 5.18 – Comparison of Data for SRI and UMD Tests at the MK-84 @ 6ft Condition

5.3   Comparison to Full Scale Data

Limited data was available for tests that used full scale bombs and obstacles. The full

scale tests were part of a study by the Naval Surface Warfare Center, Indian Head

division [14]. Only data for tests conducted with an MK-82 bomb at 6 feet depth of

water were available. The full scale data are also limited in the fact that they only include

initial and final radial position of the obstacles. It is not known if the full scale obstacles

were ejected from the water or not.

Figure 5.19 shows the final displacement as a function of initial displacement for full

scale and UMD obstacles. The full scale tests did not place any obstacles at 24 feet stand

off distance so there is no comparison available for that data. It is clear the final

displacements compare very well given the nature of data scatter in explosive testing.

Figure 5.19 - Comparison of Full Scale and UMD Data

Chapter 6 – Additional Testing with Other Obstacles

6.1   Introduction

Several additional tests were conducted in order to gain insight into other variables that might affect the motion of an obstacle due to an underwater explosion. The factors that were briefly studied in the additional tests are the amount of surface area on an obstacle and the weight of an obstacle. All of these additional tests were conducted under the conditions simulating an MK-82 bomb in six feet of water ($1/26^{th}$ scale). The first of these tests was an attempt to understand and record the flow of the water following the detonation of the charge using neutrally buoyant spheres. Several other tests were conducted to measure the effects of adding solid walls to the tetrahedron obstacles. Finally, concrete blocks were used in place of the obstacles to determine how a relatively heavy object would react to an underwater explosion. Table 6.1 lists all of the additional tests conducted using the previously described obstacles. Table A.2, in Appendix A, lists the actual measurements for depth of water and stand off distance used in testing.

Test Number	Condition	Scale Factor	Type of Obstacle	Stand off Distances (Feet)	Orientation
21	Mk-82 @ 6 ft	$\frac{1}{26}$	Neutrally Buoyant Spheres	7, 12, 18, 24	N/A
22	Mk-82 @ 6 ft	$\frac{1}{26}$	Walled Tetrahedrons	7, 12, 18, 24	Beta 0
23	Mk-82 @ 6 ft	$\frac{1}{26}$	Walled Tetrahedrons	7, 12, 18, 24	Beta 0
24	Mk-82 @ 6 ft	$\frac{1}{26}$	Walled Tetrahedrons	7, 12, 18, 24	Beta 180
25	Mk-82 @ 6 ft	$\frac{1}{26}$	Concrete Blocks	7, 12, 18, 24	N/A

Table 6.1 - List of Tests Conducted Using Other Obstacles

6.2   Construction of Additional Obstacles

The neutrally buoyant spheres were made by injecting water into table tennis balls. A small pinhole was punched into each table tennis ball and a syringe was used to inject water through the hole into the ball. The hole was then sealed with epoxy and the ball was painted black to provide contrast against the white background of the testing container. The nominal diameter of a table tennis ball is 1.5 inches but was measured to be 1.49 inches (37.85 mm). Using a density of 1.00 g/cm^3 for water, the target weight of a table tennis ball was calculated to be 28.39 grams. The actual weight of the water-filled table tennis balls was measured to be 29.24 grams on average. According to this calculation, the balls were a little bit heavier than their equivalent volume of water. However, the added volume of the spray paint and epoxy was not taken into account during this calculation which explains the weight of the balls being slightly heavier than expected.

The walled tetrahedrons were made from the tetrahedrons used in Tests 9-13 (1/26th scale tests). Triangular pieces of transparency film were cut out and affixed with epoxy onto the faces of each tetrahedron obstacle. Small gaps were left open at the corner of each triangular face to allow water to fill into the tetrahedron obstacles when they were placed under water.

The concrete blocks were made by pouring gypsum cement into a cube-shaped mold that was two inches long on each side. The dry weight for the concrete blocks was

approximately 185 grams. This models a 52 inch, 7168 pound, cube of concrete in the full scale conditions. Figure 6.1 shows the additional obstacles described in this section.

Figure 6.1 - Neutrally Buoyant Sphere, Walled Tetrahedron, Concrete Block

6.3   Neutrally Buoyant Spheres

One test was conducted using neutrally buoyant spheres placed on the bottom surface of the container. The obstacle location was measured by tracking the geometric center. Much of the motion of the obstacles was blocked from view by the expanding gas bubble. However, whatever data was captured is presented in Figure 6.2 and Figure 6.3. Another issue with this test is that some of the obstacles moved out of place during the interval between setup and detonation. The two closest obstacles at 7 and 12 feet stand off distance did not move much and were in the proper position. The two obstacles that were supposed to be at 18 and 24 feet stand off distance moved significantly and were measured to be at 15.65 and 22.34 feet stand off distance respectively, based on the pre-detonation frames of the high speed video.

Figure 6.2 shows the trajectory of the neutrally buoyant spheres at 7 and 18 feet stand off

distance and compares it to the trajectory of tetrahedrons at the Beta 0 and Beta 180

orientations under the same test conditions. The trajectory of the tetrahedron obstacles

was obtained from Tests 9 and 11. It can be seen that the sphere closest to the charge did

not move much in the radial direction and traveled in a vertical motion out of the water.

The sphere at 18 feet stand off distance did not move much, but compared more closely

to the tetrahedron motion than the sphere at 7 feet stand off distance. The trajectory of

the sphere at 18 feet stand off distance is not a continuous curve because the sphere was

not visible for some portion of the video. The initial motion of the sphere was an up and

down motion, and then the sphere was lost from view. When the sphere appeared in view

again it was floating at a higher vertical position than previously recorded in earlier

frames.

Trajectory of Neutrally Buoyant Spheres and Obstacles
Mk-82 @ 6ft - 7 and 18 SOD
Tests 9+11+21
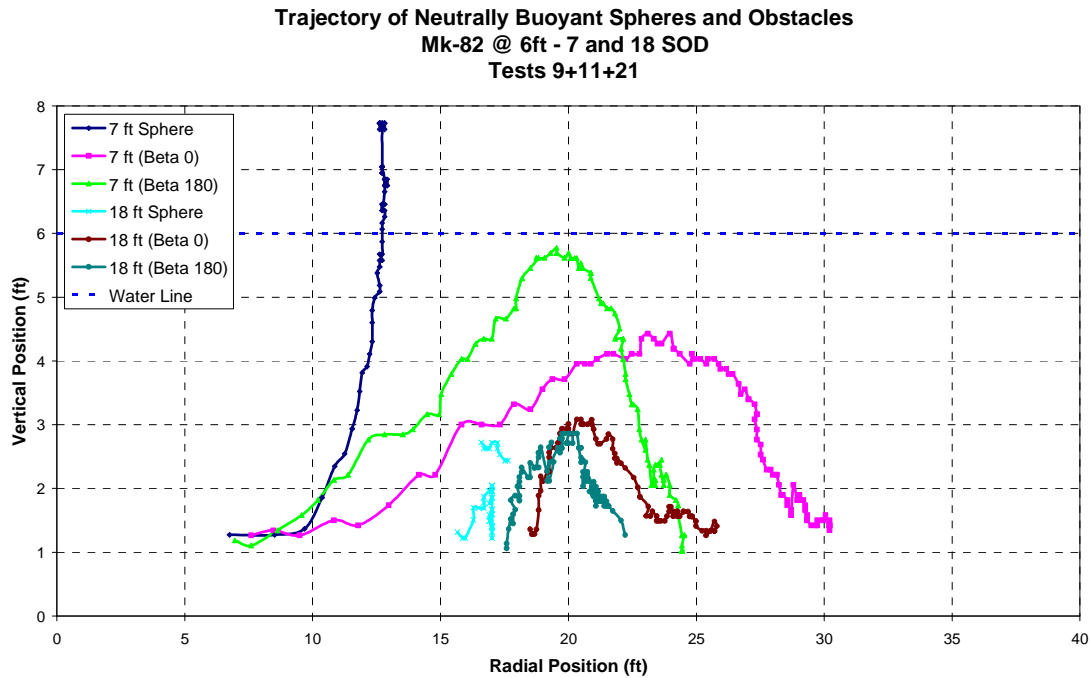
Figure 6.2 – Comparison of Trajectory of Neutrally Buoyant Spheres and Tetrahedrons

Figure 6.3 shows the trajectory of the neutrally buoyant spheres at 12 and 24 feet stand

off distance and compares it to the trajectory of tetrahedrons at the Beta 0 and Beta 180

orientations under the same test conditions. The trajectory of the tetrahedron obstacles

was obtained from Tests 10 and 12. The sphere at 12 feet stand off distance was lost

from the view of the camera after a relatively short amount of time, but the trajectory that

was recorded compares well with the trajectory of the tetrahedron obstacles under the

same conditions. The sphere at 24 feet stand off distance did not show much movement,

but unlike the tetrahedron obstacles it floated back towards the charge. The plot shows

that the sphere initially moved out in the radial direction and up towards the surface, and

then proceeded to float back towards the charge.

Trajectory of Neutrally Buoyant Spheres and Obstacles
Mk-82 @ 6ft - 12 and 24 SOD
Tests 10+12+21
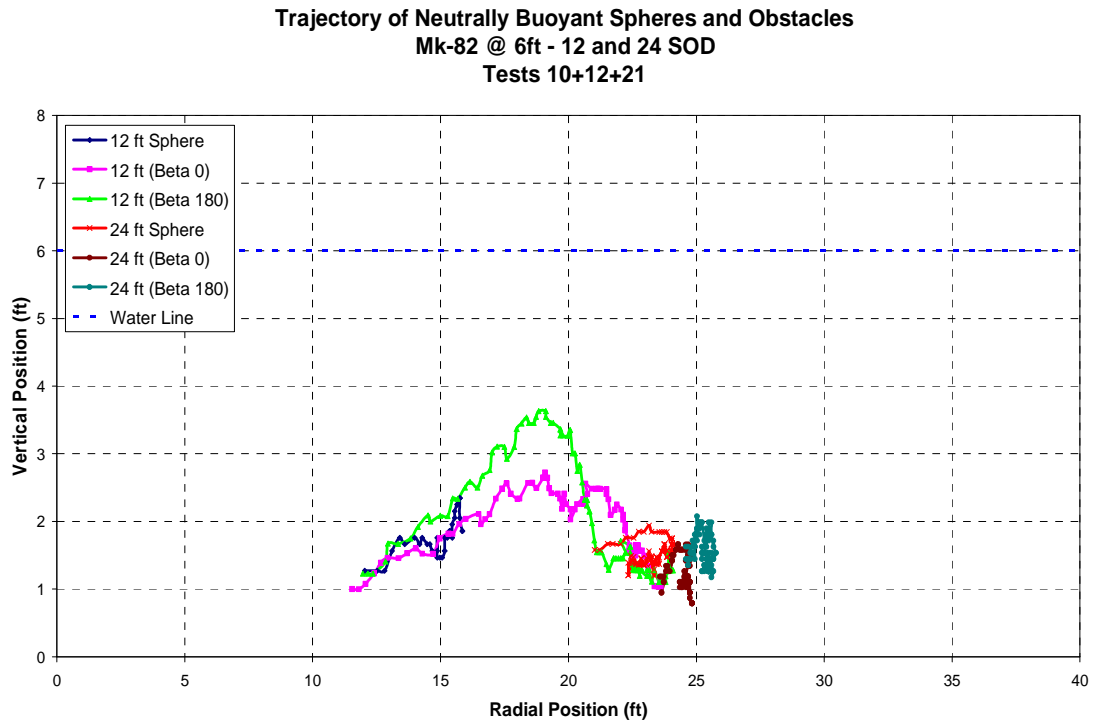
Figure 6.3 - Comparison of Trajectory of Neutrally Buoyant Spheres and Tetrahedrons

6.4   *Walled Tetrahedrons*

Several tests were conducted using the walled tetrahedrons. Tests 22 through 24 simulated the MK-82 bomb at 6 feet depth of water. Tests 22 and 23 had an identical setup with the obstacles at the Beta 0 orientation. Test 24 had the same conditions as Tests 22 and 23 except that the obstacles were placed at a Beta 180 orientation.

Figure 6.4 and Figure 6.5 show the trajectory plot for obstacles in Tests 22 and 23. Since these tests had identical conditions one would expect to see the same results. Indeed, the trajectories of the obstacles are similar in both tests except for the obstacles at 12 feet stand off distance shown in Figure 6.5. In both tests, the obstacles were lost from view for a brief period of time. In Test 22, the obstacle was moving out in the radial direction before being lost from view and then continued to move out in the radial direction when it was spotted again. However, in Test 23, the obstacle at 12 feet stand off distance began to move back towards the charge after being lost from view. This obstacle ended up approximately 16.5 feet away from the location of the charge while the obstacle in Test 22 ended up nearly 26 feet away from the charge.

Since it is difficult to see the trajectory of the obstacles at 18 feet stand off distance in Figure 6.4 those trajectories are shown in more detail in Figure 6.6. Both obstacles have similar trajectories and both were affected by the backflow of water. The obstacle in Test 22 moved out to a maximum radial displacement of 22 feet and then came back to a final position of approximately 19.5 feet. The obstacle in Test 23 moved out to a maximum radial displacement of 21 feet and came back to a final position of about 19.25 feet.
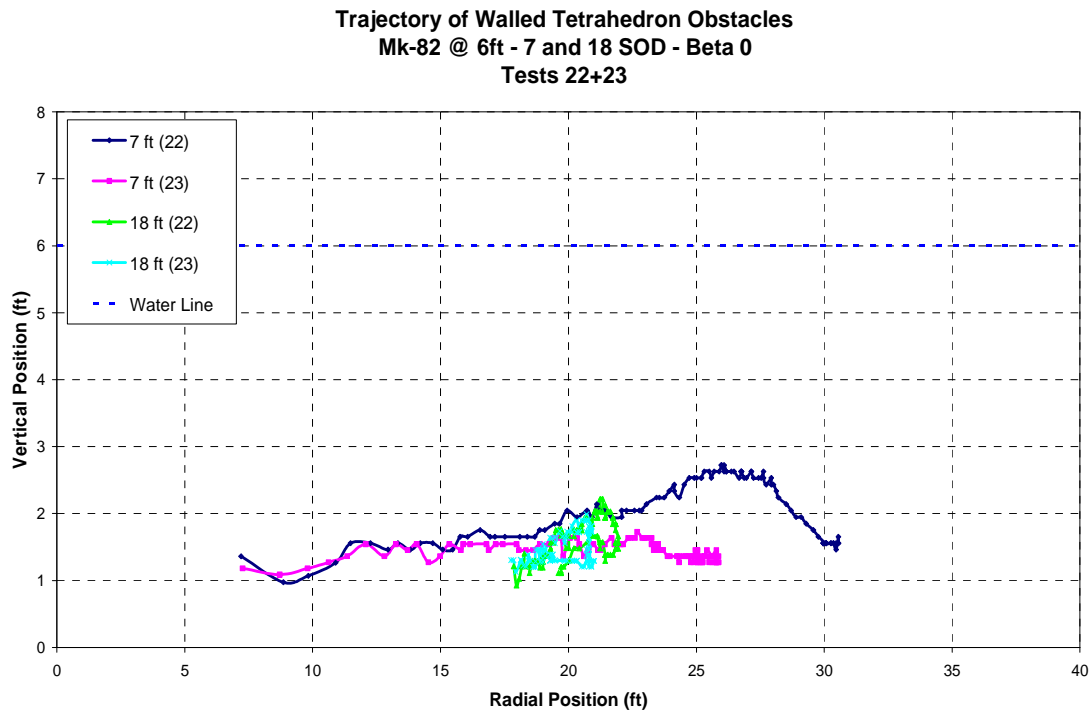
Figure 6.4 - Trajectories of Walled Tetrahedrons in Test 22 and 23 (Identical Conditions)
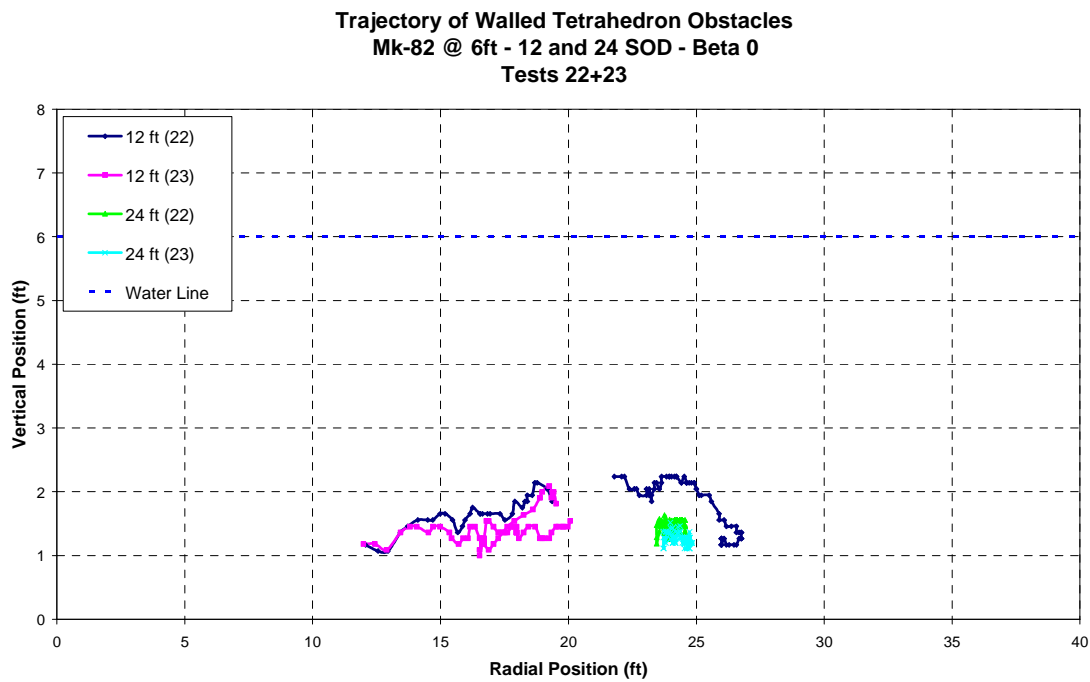
Figure 6.5 - Trajectories of Walled Tetrahedrons in Test 22 and 23 (Identical Conditions)

106
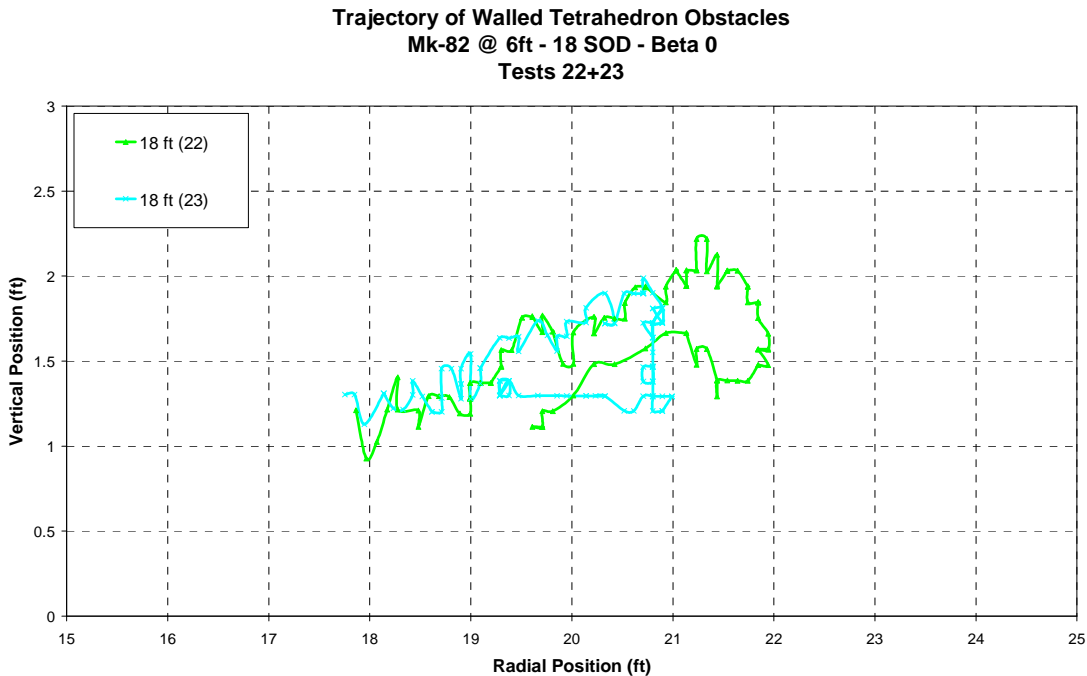
Figure 6.6 – Detailed View of Trajectory of Obstacles at 18 feet SOD in Tests 22 and 23

Since the trajectories of the obstacles in Tests 22 and 23 are similar only the data from

Test 22 will be used to plot the comparison of obstacles at Beta 0 and Beta 180

orientations, except for the data of obstacles at 12 feet stand off distance, which will be

discussed later. Figure 6.7 and Figure 6.8 compare the motion of walled-tetrahedrons at

the two different orientations. The two obstacles that are at 18 and 24 feet stand off

distance have similar trajectories for both orientations. However, the two closer in

obstacles at 7 and 12 feet stand off distances have vastly different trajectories. The

obstacle at 7 feet stand off distance with Beta 180 orientation travels nearly vertically and

then comes back down to end up at 12 feet from the charge. The motion of this obstacle

is similar to the motion of the neutrally buoyant sphere at this stand off distance and the

trajectory of the sphere is shown on the plot for comparison. The obstacle with 12 feet

stand off distance and Beta 180 orientation also does not get displaced in the radial

direction as much as the obstacle with Beta 0 orientation from Test 22. However, the

motion of the obstacles with different orientations at 12 feet stand off distance are similar if comparing between Tests 23 and 24. It can be seen in Figure 6.8 that the obstacle with 12 feet SOD and Beta 180 orientation has a similar trajectory to the obstacle with Beta 0 orientation from Test 23.

Trajectory of Walled Tetrahedron Obstacles and Neutrally Buoyant Spheres
Mk-82 @ 6ft - 7 and 18 SOD - Beta 0 and Beta 180
Tests 21+22+24
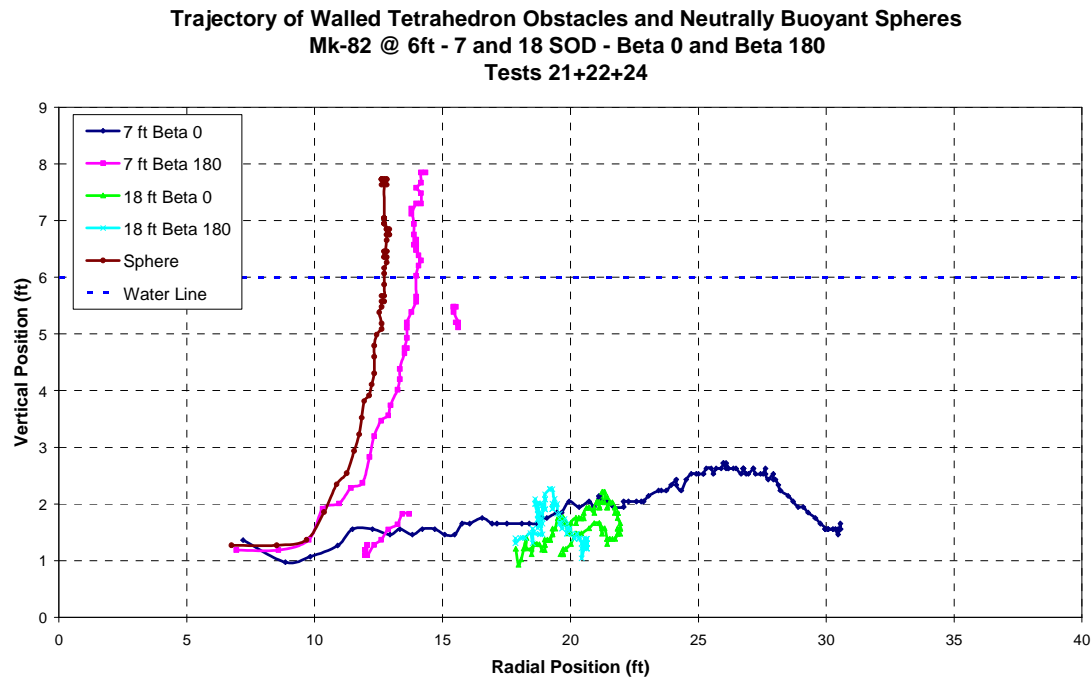
Figure 6.7 – Comparison of Walled Tetrahedron Motion Based on Obstacle Orientation

Trajectory of Walled Tetrahedron Obstacles
Mk-82 @ 6ft - 12 and 24 SOD - Beta 0 and Beta 180
Tests 22+24
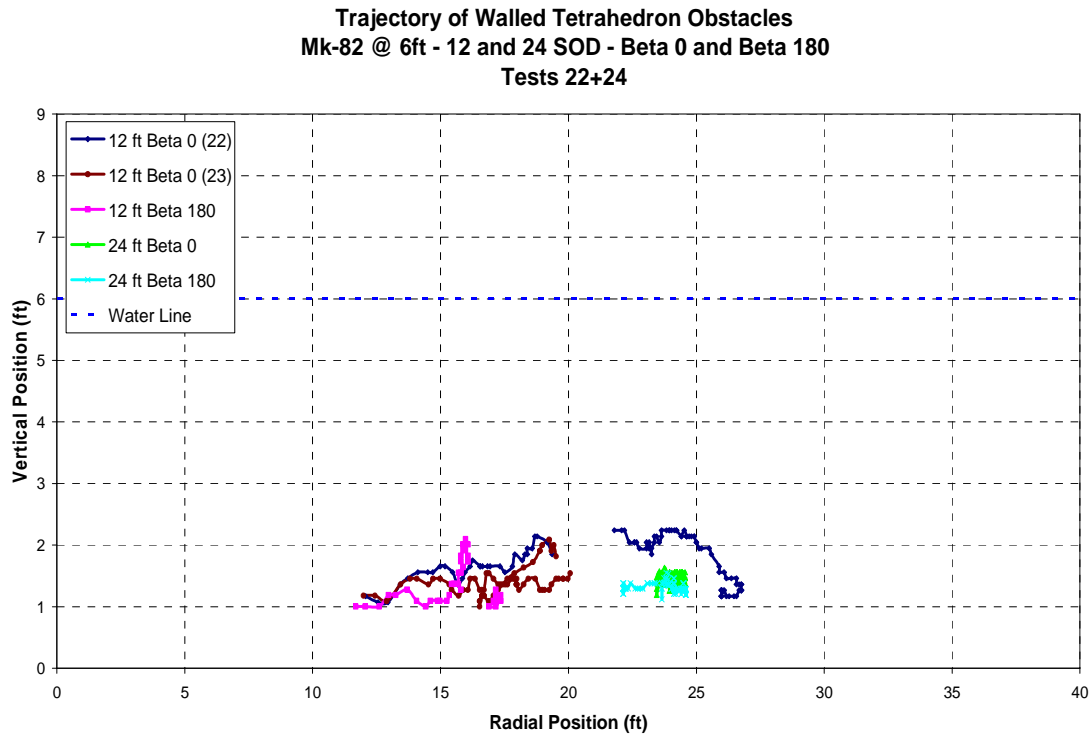
Figure 6.8 - Comparison of Walled Tetrahedron Motion Based on Obstacle Orientation

Figure 6.9 and Figure 6.10 compare the trajectory of walled tetrahedrons at the Beta 0

orientation to the non-walled tetrahedrons from Tests 9 and 10. The legends for these

plots shows a 'W' for walled tetrahedrons and a 'NW" for non-walled tetrahedrons.

There does not seem to be any conclusive pattern regarding the motion of walled

tetrahedrons when compared to non-walled tetrahedrons for the Beta 0 orientation. The

obstacles with 7 and 24 feet stand off distance have similar trajectories regardless of the

presence of walls. The two obstacles at 18 feet stand off distance have similar motion but

the walled tetrahedron had some backwards motion whereas the non-walled tetrahedron

did not. In the case of the obstacles at 12 feet stand off distance, one walled tetrahedron

had backwards motion towards the charge while the other walled tetrahedron did not.

The non-walled tetrahedron for this stand off distance had a trajectory that did not quite

fit with either of the walled tetrahedrons. It is interesting to note that in all of the tests

conducted using non-walled tetrahedrons there was no backward motion of obstacles in the radial direction. However, backward motion occurred on several occasions with the walled tetrahedron obstacles.

Trajectory of Walled and Non-Walled Tetrahedron Obstacles
Mk-82 @ 6ft - 7 and 18 SOD - Beta 0
Tests 9+22
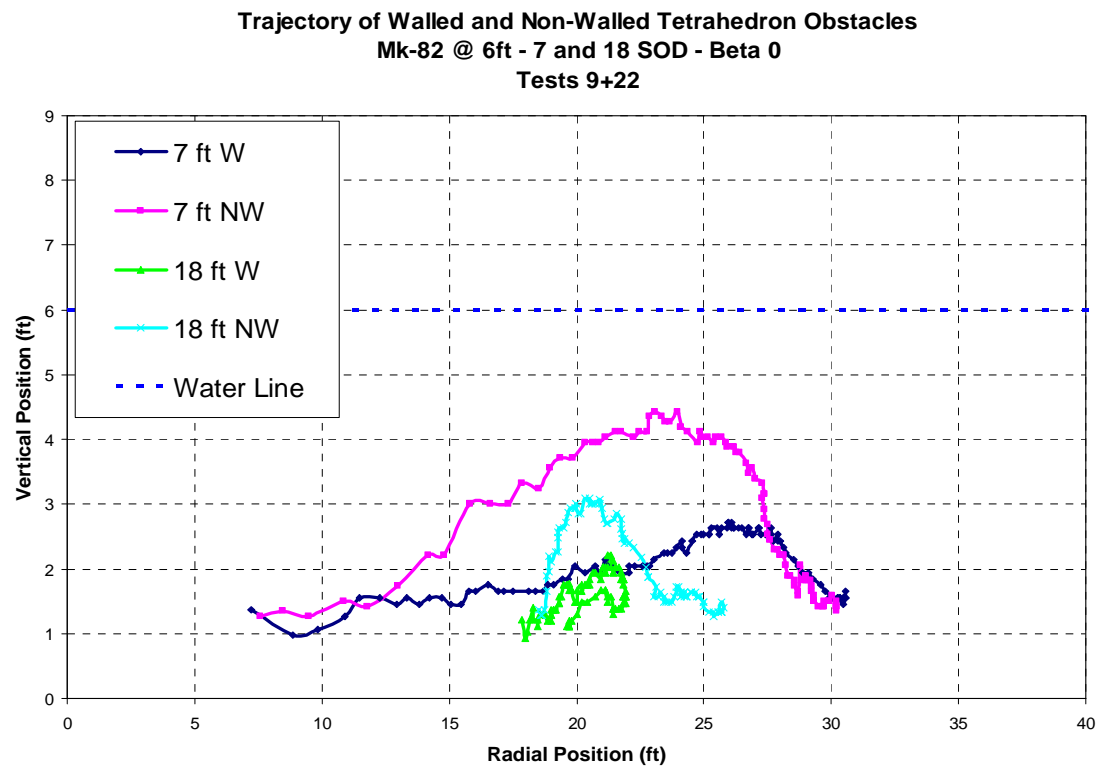
Figure 6.9 - Comparison of Walled and Non-Walled Tetrahedrons for Beta 0 Orientation

Trajectory of Walled and Non-Walled Tetrahedron Obstacles
Mk-82 @ 6ft - 12 and 24 SOD - Beta 0
Tests 10+22+23
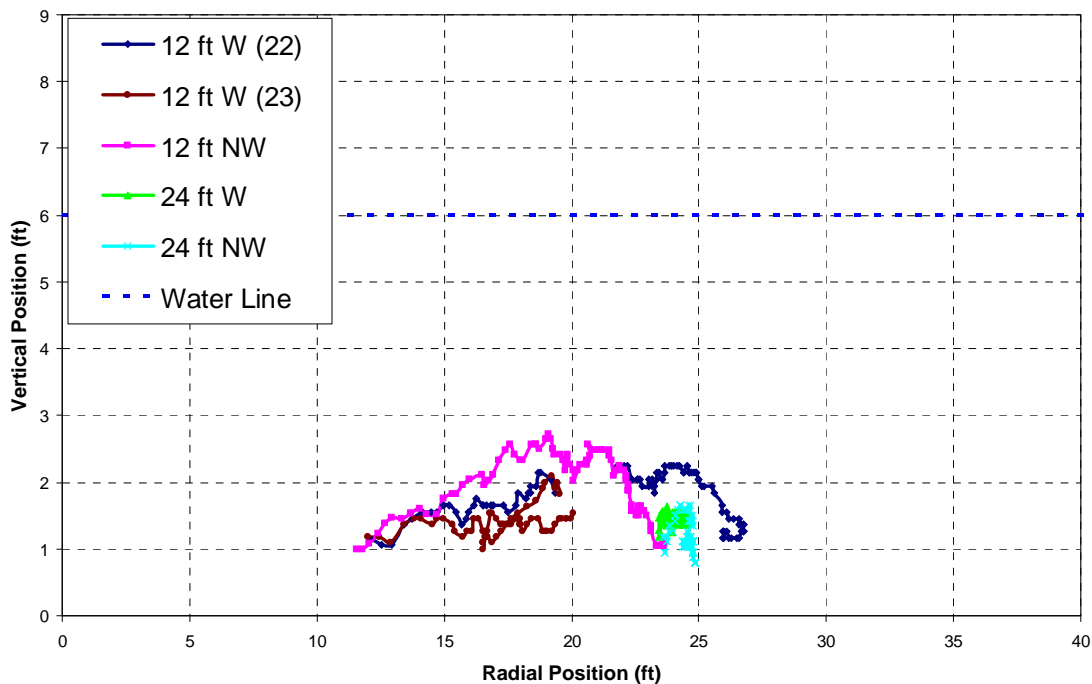
Figure 6.10 - Comparison of Walled and Non-Walled Tetrahedrons for Beta 0 Orientation

Figure 6.11 and Figure 6.12 compare the trajectory of walled tetrahedrons at the Beta 180 orientation to the non-walled tetrahedrons from Tests 11 and 12. The obstacles with greater stand off distances of 18 and 24 feet show similar motion for walled and non-walled tetrahedrons. Walled tetrahedrons at 7 and 12 feet stand off distances had a smaller final radial displacement than their non-walled tetrahedron counterparts.

Trajectory of Walled and Non-Walled Tetrahedron Obstacles
Mk-82 @ 6ft - 7 and 18 SOD - Beta 180
Tests 11+24
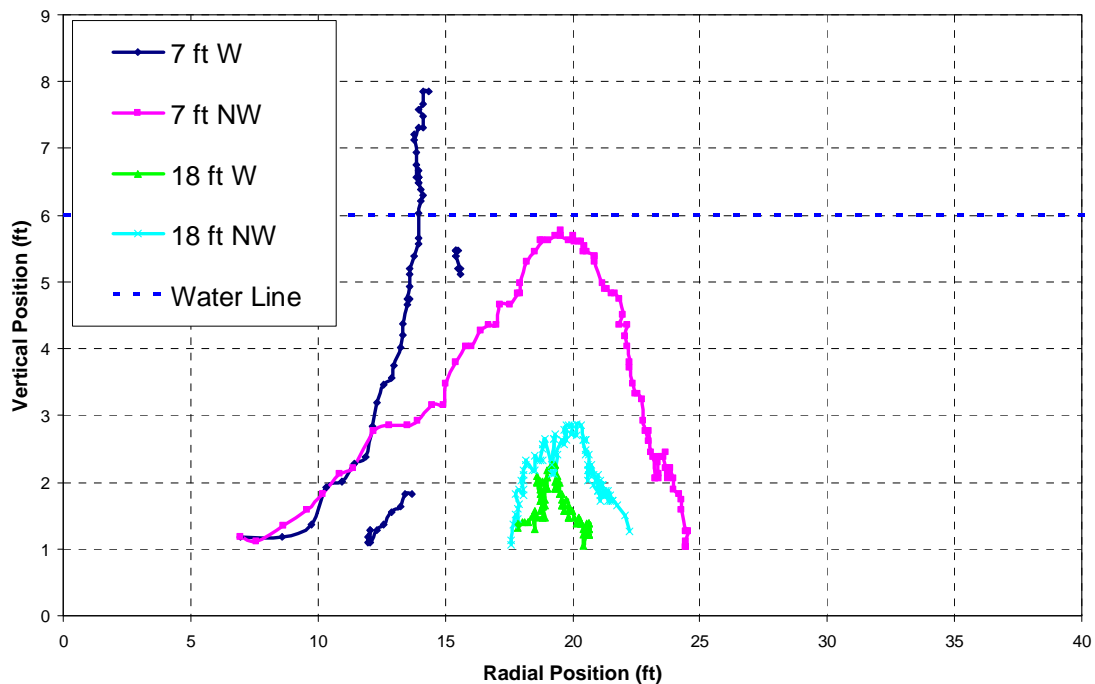
Figure 6.11 - Comparison of Walled and Non-Walled Tetrahedrons for Beta 180 Orientation

Trajectory of Walled and Non-Walled Tetrahedron Obstacles
Mk-82 @ 6ft - 12 and 24 SOD - Beta 180
Tests 12+24
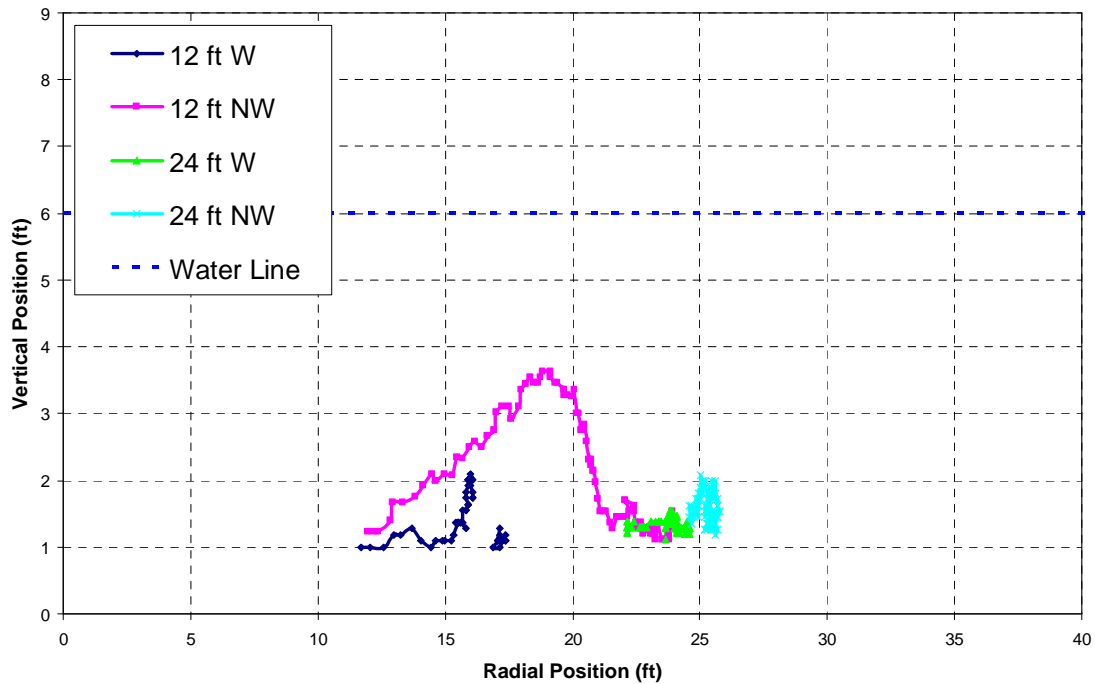
Figure 6.12 - Comparison of Walled and Non-Walled Tetrahedrons for Beta 180 Orientation

6.5   Concrete Blocks

Prior to testing it was hypothesized that the concrete blocks would have little or no motion after an underwater detonation. It seems intuitive that the much heavier obstacles would be more difficult to move. Contrary to the hypothesis, testing showed significant movement of the concrete blocks. The concrete blocks were tested under the MK-82 at 6 feet depth of water condition. Measurements of stand off distance were taken from the charge to the center of mass of the cube, similar to what was done for tetrahedron obstacles. The cubes were oriented so that the face of the cube closest to the charge was perpendicular to the imaginary line connecting the center of the cube and the charge.

Figure 6.13 and Figure 6.14 show the trajectory of concrete blocks and compares it to the trajectory of tetrahedron obstacles at the Beta 0 and Beta 180 orientation for the same test conditions. The block at 7 feet stand off distance moved more in the radial direction than any other obstacle in this study. The block actually hit the wall of the testing container and would have moved further if it had not been for the wall. The block at 18 feet stand off distance moved out slightly in the radial direction and then began moving backwards, stopping at about 15.5 feet radial distance from the charge. The obstacles at 12 and 24 feet stand off distance were also likely affected by backflow. It is not perfectly clear with the block at 12 feet stand off distance since it was lost from view for some time. However, the block was moving outward and upward before being lost from view, and when the block was in view again it was resting on the bottom surface at the same radial distance from the charge as when it was last seen, which suggests it moved out and was then swept back in towards the charge. The block at 24 feet stand off distance did not

move much, approximately one foot out in the radial direction, but was then swept back

towards the charge and ended up at about the same location as it started out.

Trajectory of Concrete Blocks and Tetrahedron Obstacles
Mk-82 @ 6ft - 7 and 18 SOD
Tests 9+11+25
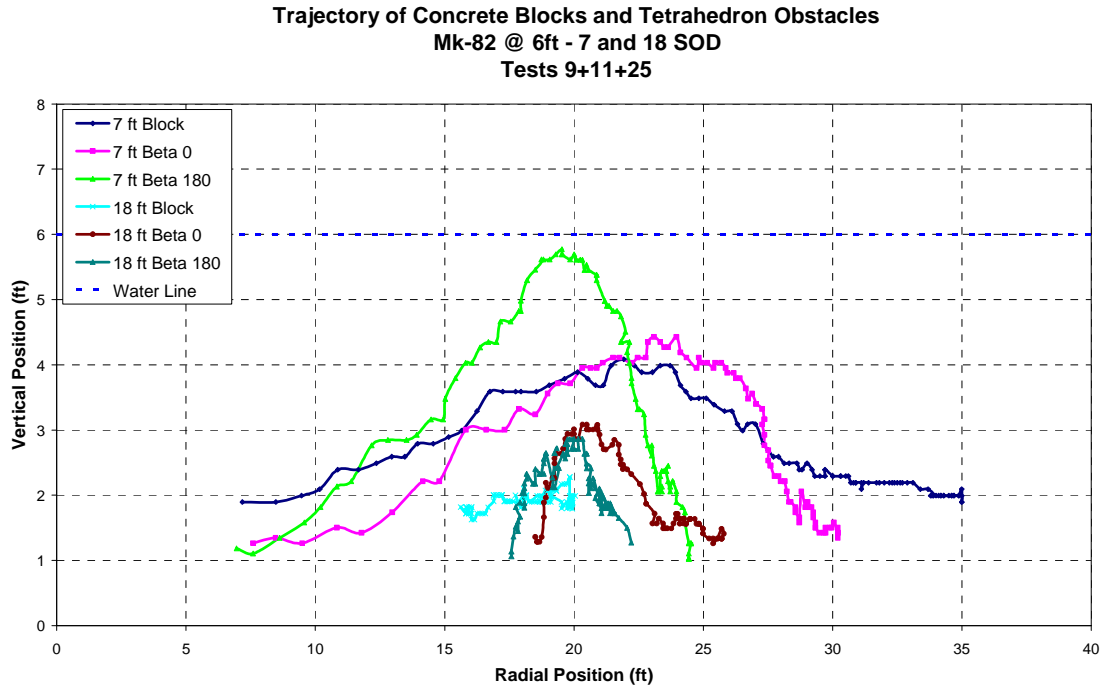
Figure 6.13 - Comparison of Concrete Block Trajectory to Tetrahedron Trajectory

Trajectory of Concrete Blocks and Tetrahedron Obstacles
Mk-82 @ 6ft - 12 and 24 SOD
Tests 10+12+25
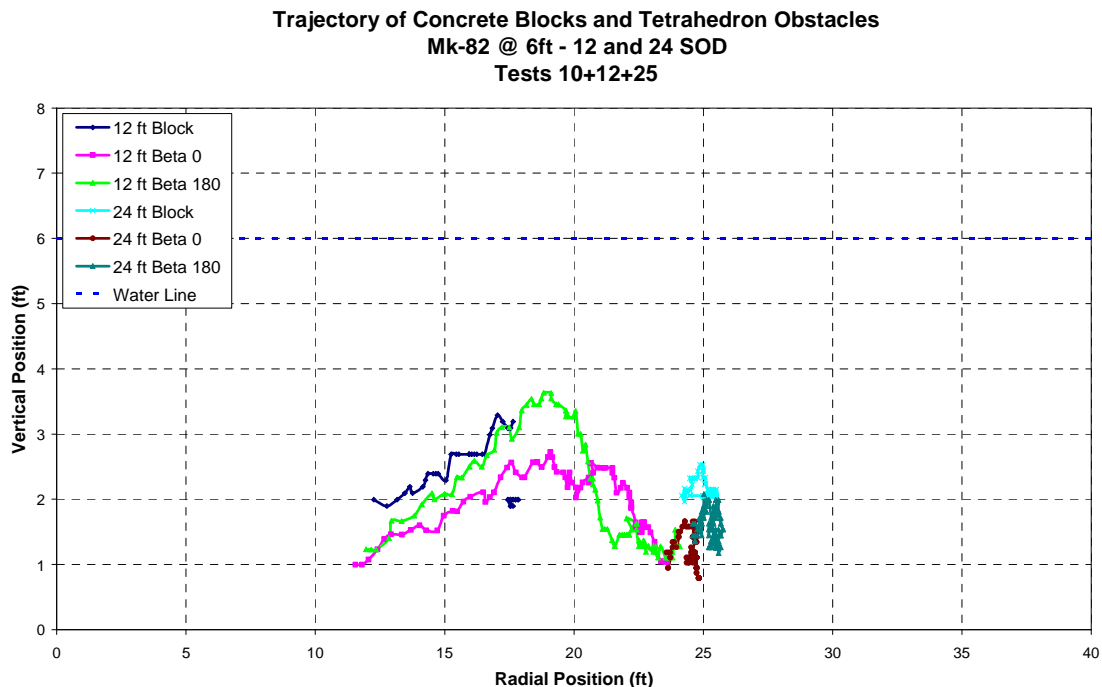
Figure 6.14 - Comparison of Concrete Block Trajectory to Tetrahedron Trajectory

114

6.6 Summary

One common feature of all of the additional obstacles that were tested is that they all had more surface area than the tetrahedrons. Tests conducted with the neutrally buoyant spheres, walled tetrahedrons, and concrete blocks all yielded results where some obstacles had backward radial motion. None of non-walled tetrahedrons had backward motion in Tests 9 through 20. It seems that the obstacles with more surface area are more likely to have backward motion than the tetrahedrons.

Chapter 7 – Conclusion

7.1   Overview

The primary purpose of this study was investigate the validity of the Low Pressure

scaling theory proposed by William McDonald of NSWC, Indian Head. This validation

was accomplished by conducting tests at a small scale, in the range of $1/26^{th}$ to $1/42^{nd}$,

and comparing the data to full scale results and SRI tests results which were conducted at

a $1/12^{th}$ scale. This chapter will summarize those findings and propose suggestions for

future work.

In addition to providing evidence in support of the Low Pressure scaling theory, this

study was also able to examine the effects of certain variables on underwater obstacle

motions. These variables include stand off distance, obstacle orientation, depth of water

and bomb size. A few additional tests were conducted to examine the effects of adding

more surface area to the obstacles or using relatively heavy obstacles. All of these

findings will be summarized in this chapter.

7.2   Summary of Findings

The Low Pressure scaling theory appears to be valid for cases when the obstacles are not

ejected from the water. A comparison of SRI data and data from this study shows that

the trajectories of obstacles match closely when the obstacles are not ejected from the

water. Full scale data was only available in the form of final and initial radial positions

so it is not possible to tell which full scale obstacles were ejected from the water.

116

However, the full scale data for final radial position versus initial stand off distance matches well with the data from this study.

This study examined how variables such as stand off distance, obstacle orientation, depth of water and bomb size affect the trajectory of the obstacles. It was found that obstacles with smaller stand off distances tend to have larger radial displacements than the obstacles with larger stand off distances. In many cases, the obstacles with shorter stand off distances also had a greater maximum vertical displacement than the obstacles with long stand off distances.

Obstacle orientation seems to little or no significant effect on the trajectory and final radial displacements of obstacles. Although the obstacle trajectories did not match perfectly when comparing two obstacles with different orientations, the trajectories were not so different one could conclude that the effect was due to the obstacle orientation.

An investigation of how the depth of water affects the trajectories of the obstacles shows that there was no significant difference in the trajectories due to depth of water for the MK-82 bomb simulations. However, the MK-84 bomb simulations showed that the obstacles with a greater initial stand off distance (18 ft and 24 ft) tend to travel more in the radial direction when the water depth is greater. It is possible that there would be a difference in trajectories due to water depth with the MK-82 bomb, but the tests conducted in this study simulated the MK-82 at only nine feet depth of water while the MK-84 was simulated in twelve feet depth of water.

The bomb size had a clear effect on the trajectory and final radial displacements of the obstacles. As one would expect, the larger bomb produced greater displacements for obstacles when all other factors were held constant.

The additional tests conducted with walled tetrahedrons and concrete blocks were not as thorough as the testing with non-walled tetrahedrons, but there was some useful information obtained from those tests. The walled tetrahedrons were close in weight to the non-walled tetrahedrons, but had more surface area. None of the non-walled tetrahedrons ever moved backwards in the radial direction during a test. The walled tetrahedrons displayed backwards radial movement on several occasions. In some cases, the walled tetrahedrons had smaller final displacements than the non-walled counterparts due to the backward motion. Contrary to what one might expect, the relatively heavy concrete blocks showed significant motion. The concrete block with the shortest stand off distance moved more in the radial direction than any other obstacle with an MK-82 bomb. Some of the concrete blocks had backwards radial movement.

7.3   Suggestions for Future Work

There are many issues which could be investigated in future work. The Navy and SRI have done tests with obstacles other than tetrahedrons such as hedgehog shaped steel structures. The motion of other obstacles could be studied at a small scale with less money using Low Pressure scaling. Also, it seems that Low Pressure scaling does not seem to work in cases where the obstacles are ejected. More testing could be done to verify this claim by creating test conditions to deliberately eject obstacles from the water and studying the trajectory.

Another issue to address is the effect of increased surface area on obstacle motion. A few tests from this study suggest that obstacles with more surface area are more likely to be affected by the backflow of water to fill the gaseous void created by the explosion. The backward movement was also seen in the heavy concrete block obstacles. A more detailed study could investigate the effect of increased surface area.

Finally, there could be more small scale testing performed to investigate the effects of using more than one bomb, as this would be a realistic scenario in a military situation. This kind of testing would provide knowledge that is more directly applicable to actual military scenarios.

Appendix A

Test Number	Depth of Water (inches)	Scale Factor	Number of Obstacles	Stand off Distances (inches)	Orientation
9	2.77	$\frac{1}{26}$	2	3.23, 8.31	Beta 0
10	2.77	$\frac{1}{26}$	2	5.54, 11.08	Beta 0
11	2.77	$\frac{1}{26}$	2	3.23, 8.31	Beta 180
12	2.77	$\frac{1}{26}$	2	5.54, 11.08	Beta 180
13	2.77	$\frac{1}{26}$	4	3.23, 8.31, 3.23, 8.31	Beta 180
14	2.00	$\frac{1}{36}$	4	2.33, 4.0, 6.0, 8.0	Beta 0
15	2.00	$\frac{1}{36}$	4	2.33, 4.0, 6.0, 8.0	Beta 180
16	2.00	$\frac{1}{36}$	1	2.33	Beta 0
17	3.43	$\frac{1}{42}$	4	2.0, 3.43, 5.14, 6.86	Beta 0
18	3.43	$\frac{1}{42}$	4	2.0, 3.43, 5.14, 6.86	Beta 180
19	3.86	$\frac{1}{28}$	4	3.0, 5.14, 7.71, 10.29	Beta 0
20	3.86	$\frac{1}{28}$	4	3.0, 5.14, 7.71, 10.29	Beta 180

Table A.1 – Test Conditions with Small Scale Values for Depth of Water and Stand off Distance

Test Number	Depth of Water (inches)	Scale Factor	Type of Obstacle	Stand off Distances	Orientation
21	2.77	$\frac{1}{26}$	Neutrally Buoyant Spheres	3.23, 5.54, 8.31, 11.08	N/A
22	2.77	$\frac{1}{26}$	Walled Tetrahedrons	3.23, 5.54, 8.31, 11.08	Beta 0
23	2.77	$\frac{1}{26}$	Walled Tetrahedrons	3.23, 5.54, 8.31, 11.08	Beta 0
24	2.77	$\frac{1}{26}$	Walled Tetrahedrons	3.23, 5.54, 8.31, 11.08	Beta 180
25	2.77	$\frac{1}{26}$	Concrete Blocks	3.23, 5.54, 8.31, 11.08	N/A

Table A.2 – Test Conditions with Small Scale Values for Depth of Water and Stand Off Distance

References

[1]   "RP-80 EBW Detonator." Teledyne Technologies, Inc.
        <http://www.teledynerisi.com/products/0products_1ebw_page23.asp>,
        Accessed Oct 9, 2006.

[2]   "FS-17 Firing System." Teledyne Technologies, Inc.
        <http://www.teledynerisi.com/products/0products_2fs_page49.asp>,
        Accessed Oct 9, 2006.

[3]   McDonald, William W. "Scaling of Water Flows and Obstacle Displacements in
        Shallow Underwater Explosion Field Tests." NSWC IHCR 06-94. February 10,
        2006.

[4]   "Tool Design." WiseTool. <http://www.wisetool.com/density.htm>,
        Accessed Oct 9, 2006

[5]   "High Speed Digital Video." Vision Research, Inc.
        <http://www.visionresearch.com/index.cfm?sector=htm/files&page=camera_51_n
        ew>, Accessed Dec 19, 2006.

[6]   Personal communication with Andrew Wardlaw, IHDNSWC, May 30, 2006.

[7]   "Dumb Bombs." Federation of American Scientists: Military Analysis Network.
        <http://www.fas.org/man/dod-101/sys/dumb/index.html>, Accessed Dec 19,
        2006.

[8]   Potter, Merle. Wiggert, David. *Mechanics of Fluids.* Prentice Hall, New Jersey.
        1991.

[9]   Cole, R.H. *Underwater Explosions.* Princeton University Press, 1965 Dover
        Edition, New York. 1948.

[10]   Brennen, Christopher E. *Cavitation and Bubble Dynamics.* Oxford University
        Press, 1995. <http://caltechbook.library.caltech.edu/1/01/cavbubdynam.pdf>,
        Accessed, Dec 18, 2006.

[11]   Josserand, Christophe. "Cavitation induced by explosion in a model of ideal
        fluid." University of Chicago. <http://arxiv.org/PS_cache/cond-
        mat/pdf/9812/9812109.pdf>, Accessed Dec 18, 2006.

[12]   McDonald, William W. "Scaling of Water Flows and Obstacle Displacements in
        Shallow Underwater Explosion Field Tests." In Support of Advanced
        Technology and Research Inc. Contract N00174-04-D-0012/004

[13]   Gefken, Paul. "Characterization of Surf Zone Obstacle Rigid Body Motion for 1/12-Sclale Bombs." NSWC IHCR 06-95. March 10, 2006.

[14]   Personal communication with Amos Dare

[15]   McDonald, W. Wardlaw, A. "Computation-Guided Scaling of Water Flows and Obstacle Displacements in Shallow UNDEX Field Tests." Shock & Vibration Symposium. Monterey, CA. 1 Nov 2006.

[16]   Snay, H. *Model Tests and Scaling,* NOLTR 63-257, DASA 1240-I(3), 1964, (Downgraded to Unclassified 11 Feb 1966).